NASA TECHNICAL NOTE

NASA TN D-3938

GROUND EFFECTS ON A FOUR-PROPELLER TILT-WING CONFIGURATION OVER A FIXED AND A MOVING GROUND PLANE

by Kenneth W. Goodson

Langley Research Center

Langley Station, Hampton, Va.

NATIONAL AERONAUTICS AND SPACE ADMINISTRATION • WASHINGTON, D. C. • MAY 1967

NASA TN D-3938

GROUND EFFECTS ON A FOUR-PROPELLER TILT-WING CONFIGURATION OVER A FIXED AND A MOVING GROUND PLANE

By Kenneth W. Goodson

Langley Research Center
Langley Station, Hampton, Va.

NATIONAL AERONAUTICS AND SPACE ADMINISTRATION

For sale by the Clearinghouse for Federal Scientific and Technical Information
Springfield, Virginia 22151 – CFSTI price $3.00

GROUND EFFECTS ON A FOUR-PROPELLER TILT-WING CONFIGURATION OVER A FIXED AND A MOVING GROUND PLANE

By Kenneth W. Goodson
Langley Research Center

SUMMARY

A wind-tunnel investigation of a four-propeller tilt-wing V/STOL configuration in ground proximity with and without ground-plane boundary layer has been conducted. Tests were made at transition-speed conditions to determine the effect of ground proximity and the effect of ground-plane boundary layer on the measured aerodynamic results.

The investigation showed that considerable reductions in lift and drag coefficients occur for some wing-flap angle combinations when the tilt-wing configuration is moved into ground proximity under near-equilibrium thrust conditions. The adverse effects of the ground on the lift coefficients are intensified under accelerating thrust conditions. Under accelerating conditions, the drag coefficient is also further reduced and this reduction should aid the acceleration.

For high-lift, high-thrust conditions, the presence of a boundary layer on the wind-tunnel ground plane causes a reduction in the lift and drag coefficients in ground effect for the tilt-wing configuration. Effects of ground-plane boundary layer are evident in both the tail-off and tail-on pitching moments. The results show that wind-tunnel ground-effect tests of tilt-wing configurations should be made with ground-plane boundary layer removed if ground-effect aerodynamic characteristics are to be simulated, especially for high-lift, high-thrust conditions.

INTRODUCTION

Investigation of various airplane configurations in ground proximity in wind tunnels (ref. 1) has shown that the measured aerodynamic characteristics for high-lift conditions can be appreciably altered by the boundary layer which exists on a fixed ground-plane. Some test results obtained on a four-propeller tilt-wing V/STOL configuration over a fixed ground plane (ref. 2) showed large reductions in lift and drag at low ground height.

The present investigation conducted in the 17-foot (5.18-meter) test section of the Langley 300-MPH 7- by 10-foot tunnel was undertaken in order to investigate the effects of removing the ground-plane boundary layer through use of the moving-belt ground plane and to obtain ground-effect data with the ground-plane boundary layer removed. Aerodynamic data obtained on other models of the four-propeller tilt-wing V/STOL configuration are presented in references 3, 4, and 5.

SYMBOLS

In order to avoid the problem of conventional coefficients approaching infinity at high thrust coefficients and to make the data compatible with the data of reference 2, the present results are presented in the form of coefficients based on the dynamic pressure in the slipstream. The coefficients based on slipstream dynamic pressure are indicated by the subscript s. The slipstream coefficients can be converted to conventional coefficients by dividing by $\left(1 - C_{T,s}\right)$; that is,

$$C_L = \frac{C_{L,s}}{\left(1 - C_{T,s}\right)}$$

The positive directions of forces, moments, and angles are indicated in figure 1. Data for the complete model are presented about the stability axes with moments presented about the center of gravity, as shown in figures 1(a) and 2.

Measurements for this investigation were taken in the U.S. Customary System of Units. Equivalent values are indicated herein in the International System of Units (SI) in the interest of promoting use of this system in future NASA reports. Details concerning the use of SI, together with physical constants and conversions, are given in reference 6. (Also, see the appendix.)

b wing span, ft (meters)

c wing chord, ft (meters)

$\bar{c}$ mean wing geometric chord, ft (meters)

$C_{D,s}$ drag coefficient based on slipstream, $\frac{\text{Drag}}{q_s S}$

C_L lift coefficient based on free stream, $\frac{\text{Lift}}{qS}$

$C_{L,s}$ lift coefficient based on slipstream, $\frac{\text{Lift}}{q_s S}$

$(C_{L,s})_\infty$ slipstream lift coefficient at $h/\bar{c} = \infty$

$C_{m,s}$ pitching-moment coefficient based on slipstream, $\frac{\text{Pitching moment}}{q_s S \bar{c}}$

$C_{T,s}$ average slipstream thrust coefficient based on slipstream and total thrust of all propellers, $\frac{\text{Thrust}}{q_s N\left(\frac{\pi D^2}{4}\right)}$

$(C_{T,s})_{nominal}$ nominal thrust coefficient used to identify curves, usually $C_{T,s}$ at $\alpha = 0^o$

D propeller diameter, ft (meters)

h height of fuselage bottom above ground, ft (meters)

$h/\bar{c}$ ratio of fuselage height to wing mean geometric chord

i_t horizontal-tail incidence angle with respect to the fuselage reference line, deg

i_w wing-incidence angle with respect to the fuselage reference line, deg

M airplane pitching moment, ft-lbf (meter-newtons)

N number of propellers

q free-stream dynamic pressure, $\frac{1}{2}\rho V_\infty^2$, lbf/ft^2 (newtons/meter^2)

q_s slipstream dynamic pressure, $q + \frac{T}{N\left(\frac{\pi D^2}{4}\right)}$, lbf/ft^2 (newtons/meter^2)

r propeller radius to any section, ft (meters)

R maximum radius of propeller, ft (meters)

S wing area, ft^2 (meters^2)

T total thrust of all propellers, lbf (newtons)

V local-stream velocity, ft/sec or knots (meters/second)

V_∞ free-stream velocity, ft/sec or knots (meters/second)

W airplane weight, lbf (newtons)

α angle of attack of fuselage reference line, deg

β angle of sideslip, deg

δ_f flap deflection, deg

δ_v vane deflection, deg

Δ incremental change between in-ground proximity and out-of-ground proximity (see fig. 28)

ρ mass density of air, slugs/ft^3 (kilograms/meter^3)

Subscripts:

corr corrected

D=0 zero drag

eq equilibrium condition

max maximum

meas measured

MODEL AND APPARATUS

The present investigation utilizes the 1/11-scale model of reference 2. A drawing of the complete model showing the important dimensions and other physical characteristics is presented in figure 2. The drawing shows the wing at zero and 90° incidence. The wing-incidence angle could be changed remotely through a range from 0° to 90°. The wing construction consisted of an aluminum box spar covered with mahogany to obtain the airfoil contours. The wing was fitted with a double-slotted flap. (See fig. 3.) When the double-slotted flap was deflected 30° and 40°, the flap vane angle was 20° and 30°,

respectively. Figure 4 shows details of the leading-edge slat used on the model in conjunction with the double-slotted flap.

The fuselage was constructed with an aluminum strong back covered with mahogany panels. A sketch showing the fuselage cross sections is presented in figure 5. Wing-fuselage ramps used to improve the airflow in the center section are shown in figure 6. The all-movable horizontal tail (shown in fig. 2) could be set at various angles with respect to the fuselage reference line.

The geometric characteristics of the propellers are shown in figure 7. The four-blade propellers were constructed of resin-bonded glass fibers over a balsa-wood core and were mounted 5.6 percent propeller diameter below the wing-section chord line. The propellers were driven by four variable-frequency $7\frac{1}{2}$- horsepower electric motors. The directions of rotation are shown in figure 2. Each electric motor was instrumented to record the propeller thrust.

The investigation of ground effects was conducted in the 17-foot (5.18-meter) test section (located in the effuser, see appendix of ref. 7) of the Langley 300-MPH 7- by 10-foot tunnel. Photographs of the sting-supported model mounted on an electrical strain-gage balance in the test section are shown in figure 8.

A discussion of the moving-belt ground-plane equipment is given in references 1 and 8. Figure 9 shows a sketch of the moving ground plane consisting of a fabric belt between two rollers driven by an electric motor. The ground plane was 144 inches (366 cm) wide by 121 inches (307 cm) long. The boundary layer ahead of the belt was removed with a suction slot just upstream of the moving ground plane. Boundary-layer buildup on the moving ground plane could be prevented by operating the belt at approximately free-stream velocity. The effect of the moving belt on the boundary-layer profile is shown in figure 10.

TESTS AND CORRECTIONS

The thrust coefficients presented in this report are based on the total propeller thrust measured for each test point. The propeller blade angle at the 3/4-radius station was equal to 12° for all tests. The propeller rotational speed was held constant (7000 rpm) for all tests. The tunnel velocity was predetermined for each test to obtain the nominal thrust coefficient for the fuselage level condition ($\alpha = 0^{\circ}$). The thrust coefficient established at zero angle of attack, however, did not remain constant with change in angle of attack because of the change in propeller characteristics with change in angle of attack, as seen in the various data figures. The present power-on tests were made over a range of slipstream thrust coefficients from 0.6 to 0.9 at a slipstream dynamic pressure of about 10 lbf/ft^2 (478.8 N/m^2). The Reynolds number based on this

slipstream dynamic pressure and wing mean aerodynamic chord of 8.8 inches (22.35 cm) was about 0.51×10^6.

For most of the tests, the wing was tilted 20°, the flap was deflected 60°, and the leading-edge slat was on. This configuration was tested at nominal ratios of ground height to chord length of 0.40, 1.09, 1.70, and 9.20 (measured from bottom of fuselage to ground plane at $\alpha = 0^\circ$ with power off) for nominal slipstream thrust coefficients of 0.6, 0.8, and 0.9 throughout an angle-of-attack range from approximately -8° to as high as 24°. Some tests were made at zero angle of attack over a thrust-coefficient range and height range for various wing-tilt angles with the flaps deflected 40° and 60° and with the leading-edge slat on.

It should be noted that the heights presented are nominal values obtained at $\alpha = 0^\circ$ with power off. With power on, the lifting model deflects the sting support, and an incremental change in height results. The height also changes with angle of attack because the sting-support mechanism rotates about a point other than the height reference point on the model fuselage. The data presented herein have not been corrected for these incremental changes in nominal height since they are small. (For example, $\Delta h = 0.34$ inch (0.86 cm) for $i_w = 20^\circ$ and $\delta_f = 60^\circ$ based on $(C_{L,s})_{max}$ at $h/\bar{c} = 0.40$ and $(C_{T,s})_{nominal} \approx 0.67$.) The relative changes between the aerodynamic data for the belt fixed and for the belt moving would not significantly affect the intended comparisons; however, the corrected heights with respect to the fuselage bottom can be obtained by use of the following equation:

$$h_{corr} = 38.4(1 - \cos \alpha) + (h_{meas})_{\alpha=0^\circ} \cos \alpha + 0.004(C_{L,s} \cos \alpha + C_{D,s} \sin \alpha) q_s S \cos \alpha$$

where $q_s \approx 10$ lbf/ft^2 (478.8 N/m^2) for the model tests.

A study (ref. 9) of the effects of tunnel walls on the aerodynamic characteristics of V/STOL configurations, which uses the method of reference 10, shows that for small ratios of model size to tunnel size, the corrections to lift and drag are small. In view of these findings and the relatively small size of the present model, wall corrections have not been applied to the results of this study.

PRESENTATION OF RESULTS

The aerodynamic characteristics of a four-propeller tilt-wing configuration obtained from this investigation are presented in the following figures.

The results obtained with this basic wing-flap configuration (tail off) at various thrust coefficients and ground heights for both a stopped and a moving ground-plane belt are presented in figures 11 and 12. These data have been cross plotted to compare directly results at various ground heights, as shown in figures 13 and 14. The basic data have also been combined in figures 15 to 17 in such a manner as to compare directly the results obtained with the ground-plane belt stopped and moving at given ground heights.

A limited amount of data obtained as a function of slipstream thrust coefficient for several other wing-tilt angles and flap angles at $\alpha = 0^{\circ}$ is shown in figures 18 to 20. Some additional data were obtained at various horizontal-tail incidence angles to study the effects of ground-plane boundary layer with the horizontal tail on (figs. 21 to 27). Results of the investigation are summarized in figures 28 to 35.

DISCUSSION

Ground Effects

The following discussion of ground effects will be made by comparing out-of-ground-effect data with in-ground-effect data obtained with the moving ground belt (ground-plane boundary layer removed).

Lift and drag characteristics.- The limited ground-effects data of reference 2 showed reductions in lift and drag coefficients for tests made in the presence of a ground-plane boundary layer. Similar results (tail-off configuration) were obtained in the present investigation with the boundary layer removed, as can be seen in figures 15, 16, 17, and 28. Figure 28 shows approximately a 15-percent lift loss at $h/\bar{c} = 0.40$ for $(C_{T,s})_{nominal} \approx 0.67$, with larger losses being incurred at higher thrust coefficients. Note that $(C_{T,s})_{nominal} \approx 0.67$ more nearly represents the equilibrium condition $(C_{D,s} \approx 0$ at $\alpha = 0^{\circ})$ than do the higher thrust coefficients. (See fig. 17.) Under accelerating thrust conditions, the drag coefficient is also further reduced and this reduction should aid the acceleration. The effects of ground proximity for other wing-tilt angles obtained by cross plotting data of figures 19 and 20 are shown in figure 29. (Note that the wing-incidence angle shown represents the actual angle of attack of the wing since the fuselage is held at $\alpha = 0^{\circ}$.) This figure shows that reductions in lift and drag coefficients due to ground proximity (belt moving) are also experienced at other wing-tilt angles ($i_W = 20^{\circ}$ to 56°) for the flaps deflected either 40° or 60°, especially at the higher thrust coefficients. These results, however, show the ground effect to be more severe than would probably be encountered by the airplane in its operating range, since they do not represent thrust-drag equilibrium. Comparison of the results of figures 29 and 30 at a given wing-tilt angle (for example, $i_W = 40^{\circ}$) shows that the ground-effect

increment is considerably smaller under equilibrium conditions (fig. 30; $C_{D,s} = 0$ at $\alpha = 0^o$, tail-off configuration) than would be surmised from figure 29.

Figure 30 shows that under equilibrium conditions ($C_{D,s} = 0$ at $\alpha = 0^o$), the main effect of ground proximity is the reduction in slipstream thrust coefficient required, especially at the higher wing-tilt angles. To understand better what this means as far as the airplane is concerned, the data of figure 30 have been converted to thrust-weight ratios and equilibrium velocities for a wing loading of 70 lbf/ft^2 (3350 N/m^2). (See fig. 31.) Figure 31 shows that airplane response to ground effect is an increase in speed (approximately 37- to 59-percent increase at $i_w = 40^o$) and some reduction in thrust-weight ratio (approximately 10- to 13-percent reduction at $i_w = 40^o$) with the flaps deflected 40^o and 60^o. The magnitude of these effects will be altered somewhat by use of the programed wing-flap combination and by addition of the tail surfaces. The magnitudes will also be different under accelerating and decelerating conditions. At wing-tilt angles from 0^o to 20^o, ground effects tend to be small.

The data of figures 24 and 27 (belt moving) for $h/\bar{c} = 0.40$ with $i_t = 10^o$ and data of figure 21 for $h/\bar{c} = 9.20 \approx \infty$ have been combined as figure 32 in order to show directly the effect of ground proximity on the model with the horizontal tail on. Comparison of lift data from figures 21, 24, 27, and 17 shows that addition of the horizontal tail to the model reduced the lift coefficient somewhat out of ground effect ($h/\bar{c} \approx \infty$), but did not alter the lift in ground effect at $h/\bar{c} = 0.40$. The drag characteristics were not appreciably affected at either ground height shown ($h/\bar{c} \approx \infty$ or $h/\bar{c} = 0.40$). The effect of horizontal-tail incidence angles on the lift and drag ground-effect increments is shown in figure 33.

Pitching-moment characteristics.- Figure 29 indicates that ground proximity (belt moving) can appreciably affect the pitching-moment coefficients, especially at the higher thrust coefficients. It is felt that these large values are misleading since these results are not in thrust-drag equilibrium. To substantiate this observation, the data of figures 19 and 20 have been cross plotted at $C_{D,s} = 0$ to show actual tail-off equilibrium results. (See fig. 30.) Figure 30 shows the equilibrium pitching-moment increments on the wing-flap-body combination to be very small, as is also shown by the scaled-up pitching-moment ratios (for $W/S = 70$ lbf/ft^2 (3350 N/m^2)) of figure 31. With the horizontal tail on, however, there are significant changes in pitching-moment coefficients both in and out of ground effect (compare figs. 17 and 32), primarily caused by the downwash at the tail. The main effect of the ground on the pitching moments (nose-down changes in moments) occurs with the tail on and is due to the ground-imposed changes in the downwash at the tail.

The data of figure 29 show that for accelerating thrust conditions $\left((C_{T,s})_{nominal} \approx 0.80 \text{ and } 0.90\right)$, fairly large nose-down pitching-moment increments

are produced in ground proximity at the higher wing-tilt angles (tail-off configuration). It should be noted that similar nose-down pitching-moment characteristics are obtained for $i_w = 20^o$ and $\delta_f = 60^o$ for angles of attack above $(C_{L,s})_{max}$. (See figs. 16 and 17.) The downwash associated with this change in pitching moment (and lift) would be expected to alter the tail-on characteristics. The effect of horizontal-tail incidence angles on pitching moment is shown in figure 33.

To give a clearer picture of the effects of ground height on pitching moment for the model with the horizontal tail on, the pitching-moment data of figures 21, 25, 26, and 27 ($i_t = 10^o$) are presented in figure 34. This figure shows that for $i_w = 20^o$ and $i_t = 10^o$, the ground-effect increment in pitching moment varies considerably with change in angle of attack of the configuration.

Effect of Ground-Plane Boundary Layer

As shown in reference 1, the aerodynamic characteristics of high-lift configurations tested in wind tunnels can be appreciably altered by boundary-layer buildup on a fixed ground plane when in close proximity to the ground. The high-energy deflected flow of high-lift configurations can penetrate forward beneath the low-energy boundary layer of a fixed (stopped belt) ground plane and thereby alter the flow around the model and hence its aerodynamic characteristics. This section deals with comparison of data obtained on the present tilt-wing configuration in ground proximity with the ground belt stopped and moving (with and without boundary layer). The basic data showing the effects of ground-plane boundary-layer buildup on the aerodynamic characteristics of the present tilt-wing model are shown in figures 15 to 17.

Lift and drag characteristics.- The preceding section entitled "Ground Effects" showed that ground proximity (with ground-plane boundary layer removed – belt moving) had considerable effect on the lift and drag characteristics of the present tilt-wing configuration. The effect of not removing the ground-plane boundary layer on the ground effects can be seen from figures 15 to 17 and 28 to 33 by comparing the ground-belt-stopped data with the ground-belt-moving data. These results show that for $i_w = 20^o$ and $\delta_f = 60^o$ and for near-equilibrium thrust conditions $\left(C_{D,s} \approx 0 \text{ at } (C_{T,s})_{nominal} \approx 0.67\right)$, the effect of stopping the ground belt is relatively small. However, when the thrust level is increased to $(C_{T,s})_{nominal} \approx 0.82$ and 0.91 (accelerating values), the effect of the ground-plane boundary layer on the ground-effect increment becomes considerably larger at the lowest ground height. (See fig. 28.) These lift characteristics have also been plotted in conventional coefficients to show more graphically the effects of increasing the thrust level at a given wing incidence. (See fig. 35.) These figures show that for some conditions, reductions in lift and drag caused by the boundary layer become

larger at higher angles of attack especially for angles above $(C_{L,s})_{max}$. Figure 29 shows that the effects of ground-plane boundary layer are also dependent upon the flap angle. Similar boundary-layer effects are observed with the horizontal tail on.

These results indicate that wind-tunnel tests of tilt-wing configurations should be made with the ground-plane boundary layer removed if ground-effect aerodynamic characteristics are to be simulated, especially for high-lift, high-thrust conditions.

Pitching-moment characteristics.- The data of figures 15, 16, 17, 28, and 29 show that the pitching moment (tail-off configuration) is affected by the ground-plane boundary layer primarily at high-thrust conditions and at high angles of attack, especially angles above maximum lift coefficient. Similar effects of ground-plane boundary layer were obtained with the horizontal tail on the model. (See figs. 32, 33, and 34.) A comparison of the tail-off pitching-moment data of figures 15, 16, and 17 with the tail-on pitching-moment data of figure 34 shows that ground-plane boundary layer primarily affects the wing-flap combination with only secondary effects being associated with the tail.

CONCLUDING REMARKS

A wind-tunnel investigation of a four-propeller tilt-wing V/STOL configuration in ground proximity with and without ground-plane boundary layer has indicated the following conclusions: Tests of the tilt wing over a moving ground plane (which simulates still free-air conditions – no boundary layer on the ground) has shown that considerable reductions in lift and drag coefficients are experienced as the model moves into ground proximity for near-equilibrium thrust conditions. For higher thrust conditions (acceleration values), the losses are larger. Under accelerating thrust conditions, the drag coefficient is also further reduced and this reduction should aid the acceleration. The results indicate that ground proximity does not appreciably affect the tail-off pitching moments for any of the wing-tilt angles of the investigation. With the horizontal tail on, however, the ground-induced change in downwash at the tail does affect the tail-on pitching moments. The magnitude of the ground effects is dependent upon the wing-tilt angle, the flap angle, and the thrust condition.

Comparison of wind-tunnel data obtained over a moving ground plane (boundary layer removed) with that of a fixed ground plane (with surface boundary layer) shows that under high-lift, high-thrust conditions the ground-plane boundary layer causes a reduction in the lift and drag coefficients for the model in close ground proximity. The results show that wind-tunnel tests of tilt-wing configurations should be made with

the ground-plane boundary layer removed if ground-effect aerodynamic characteristics are to be simulated, especially for high-lift, high-thrust conditions.

Langley Research Center,
National Aeronautics and Space Administration,
Langley Station, Hampton, Va., January 16, 1967,
721-01-00-17-23.

APPENDIX

CONVERSION TO INTERNATIONAL SYSTEM OF UNITS (SI)

Factors required for converting the U.S. Customary Units used herein to the International System of Units (SI) are given in the following table:

Physical quantity	U.S. Customary Unit	Conversion factor (*)	SI Unit
Area	ft^2	0.0929	meters^2 (m^2)
Density	slugs/ft^3	515.379	kilograms/meter^3 (kg/m^3)
Force	lbf	4.4482	newtons (N)
Length	in.	0.0254	meters (m)
	ft	0.3048	meters (m)
Moment	ft-lbf	1.3558	meter-newtons (m-N)
Pressure	lbf/ft^2	47.8803	newtons/meter^2 (N/m^2)
Velocity	ft/sec	0.3048	meters/second (m/sec)
	knots (international)	0.51444	meters/second (m/sec)

*Multiply value given in U.S. Customary Unit by conversion factor to obtain equivalent value in SI Unit.

REFERENCES

1. Turner, Thomas R.: Endless-Belt Technique for Ground Simulation. Conference on V/STOL and STOL Aircraft, NASA SP-116, 1966, pp. 435-446.

2. Goodson, Kenneth W.: Longitudinal Aerodynamic Characteristics of a Flapped Tilt-Wing Four-Propeller V/STOL Transport Model. NASA TN D-3217, 1966.

3. Newsom, William A., Jr.; and Kirby, Robert H.: Flight Investigation of Stability and Control Characteristics of a 1/9-Scale Model of a Four-Propeller Tilt-Wing V/STOL Transport. NASA TN D-2443, 1964.

4. Deckert, Wallace H.; Page, V. Robert; and Dickinson, Stanley O.: Large-Scale Wind-Tunnel Tests of Descent Performance of an Airplane Model With a Tilt Wing and Differential Propeller Thrust. NASA TN D-1857, 1964.

5. Goodson, Kenneth W.: Comparison of Wind-Tunnel and Flight Results on a Four-Propeller Tilt-Wing Configuration. Conference on V/STOL and STOL Aircraft, NASA SP-116, 1966, pp. 51-62.

6. Mechtly, E. A.: The International System of Units – Physical Constants and Conversion Factors. NASA SP-7012, 1964.

7. Kuhn, Richard E.; and Hayes, William C., Jr.: Wind-Tunnel Investigation of Longitudinal Aerodynamic Characteristics of Three Propeller-Driven VTOL Configurations in the Transition Speed Range, Including Effects of Ground Proximity. NASA TN D-55, 1960.

8. Vogler, Raymond D.: Ground Effects on Single- and Multiple-Jet VTOL Models at Transition Speeds Over Stationary and Moving Ground Planes. NASA TN D-3213, 1966.

9. Staff of Powered-Lift Aerodynamics Section, NASA Langley Res. Center: Wall Effects and Scale Effects in V/STOL Model Testing. AIAA Aerodynamic Testing Conference, Mar. 1964, pp. 8-16.

10. Heyson, Harry H.: Linearized Theory of Wind-Tunnel Jet-Boundary Corrections and Ground Effect for VTOL-STOL Aircraft. NASA TR R-124, 1962.

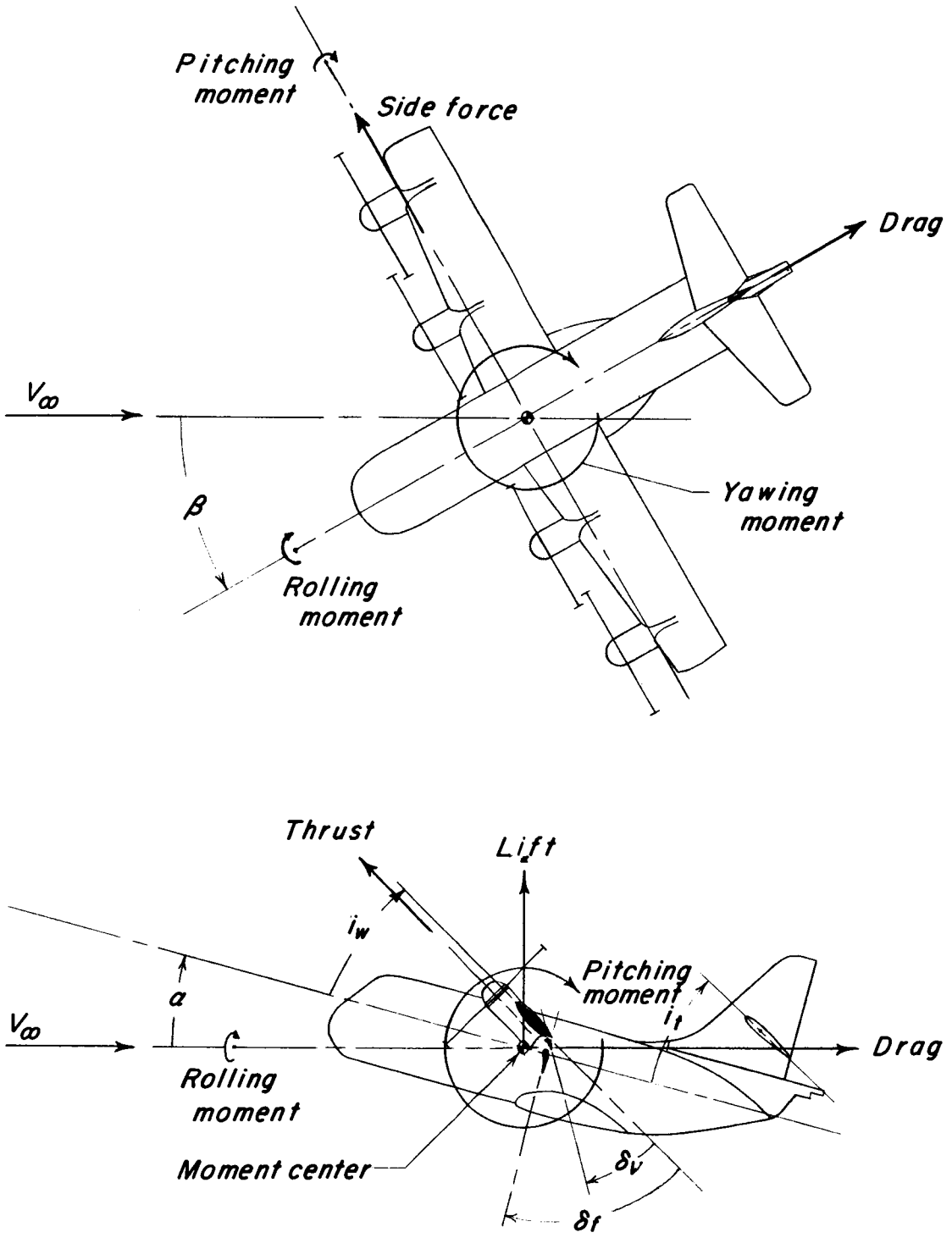

(a) Complete model.

Figure 1.- System of axes. Positive directions of forces, moments, and angles are indicated by arrows.

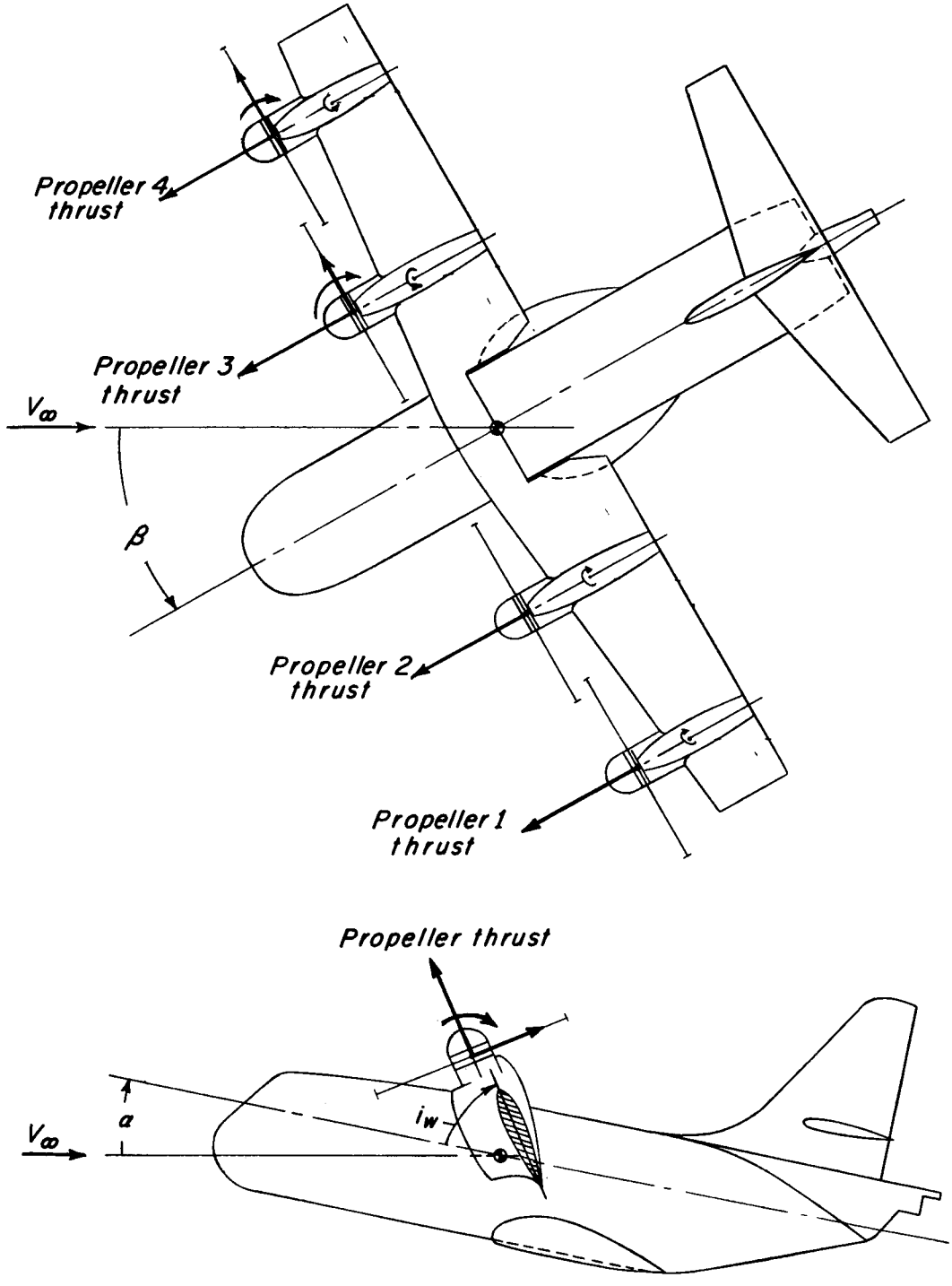

(b) Propellers.

Figure 1.- Concluded.

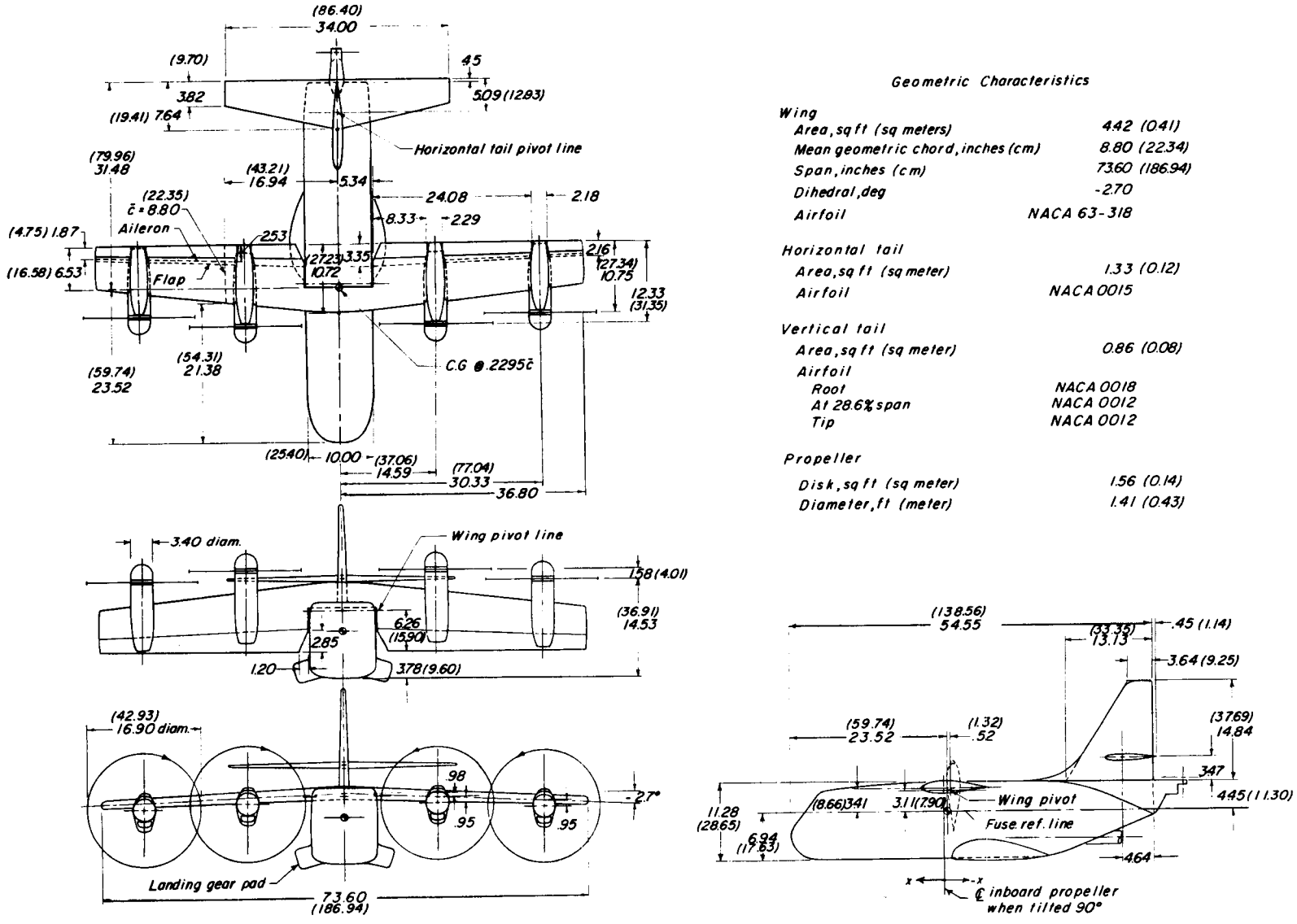

Geometric Characteristics

Wing	
Area, sq ft (sq meters)	4.42 (0.41)
Mean geometric chord, inches (cm)	8.80 (22.34)
Span, inches (cm)	73.60 (186.94)
Dihedral, deg	-2.70
Airfoil	NACA 63-318
Horizontal tail	
Area, sq ft (sq meter)	1.33 (0.12)
Airfoil	NACA 0015
Vertical tail	
Area, sq ft (sq meter)	0.86 (0.08)
Airfoil	
Root	NACA 0018
At 28.6% span	NACA 0012
Tip	NACA 0012
Propeller	
Disk, sq ft (sq meter)	1.56 (0.14)
Diameter, ft (meter)	1.41 (0.43)

Figure 2.- Geometric characteristics of a 1/11-scale four-propeller tilt-wing VTOL model. Dimensions are given in inches and parenthetically in centimeters; because of space limitations conversion to the International System of Units is not given for all dimensions.

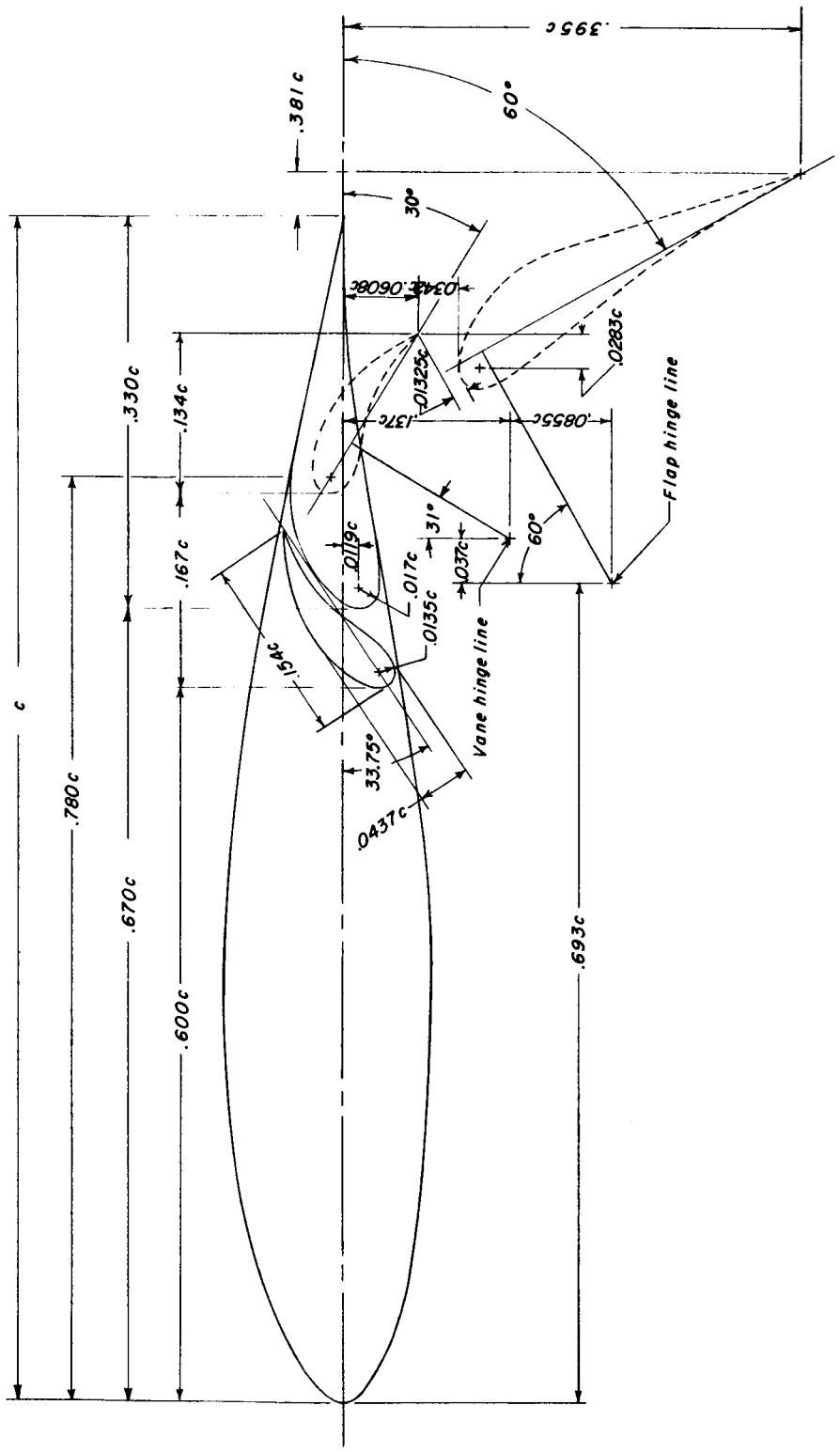

Figure 3.- Details of the flap system of the 1/11-scale tilt-wing VTOL model.

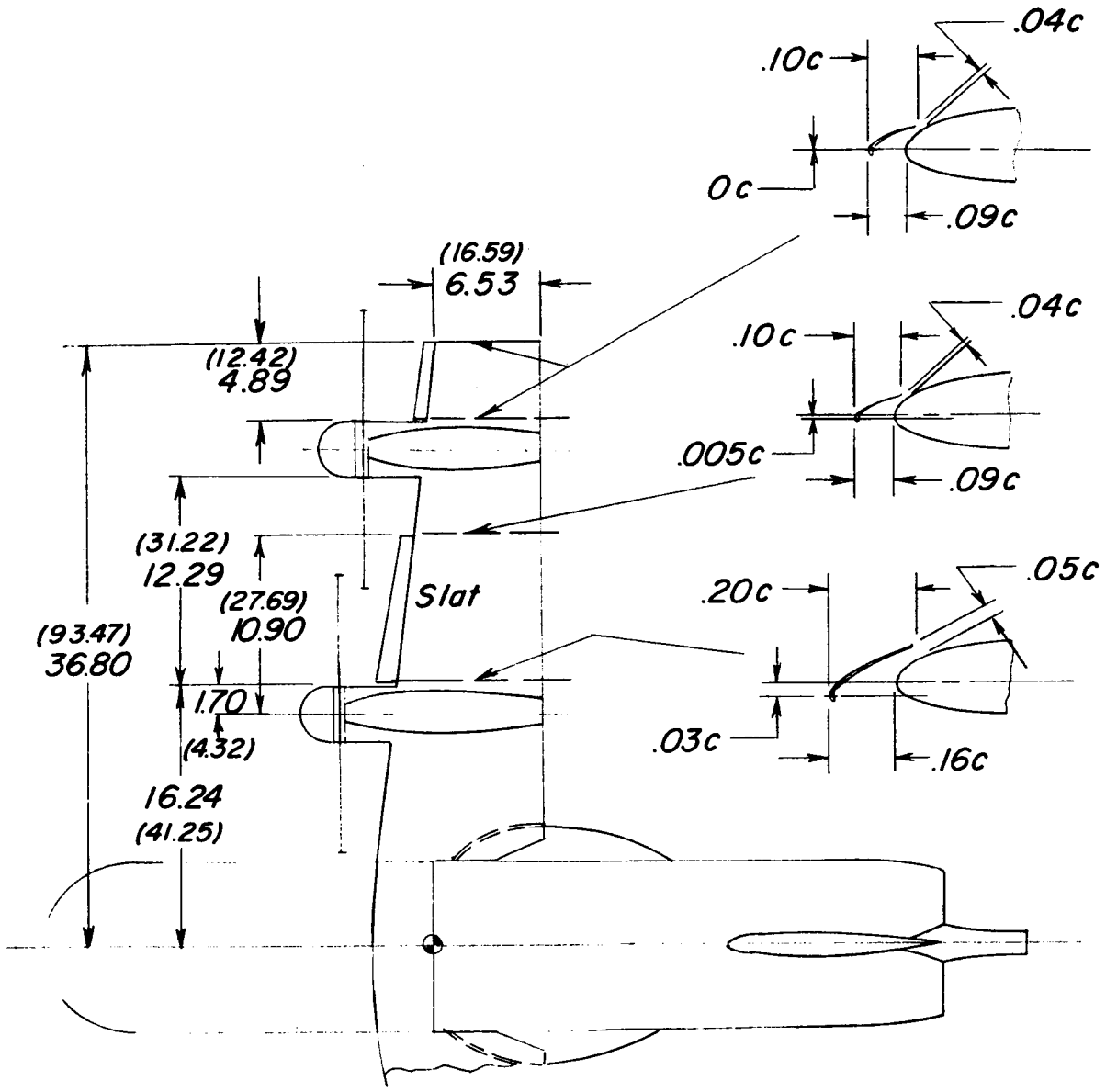

Figure 4.- Details of the wing leading-edge slats of the 1/11-scale tilt-wing VTOL model. Dimensions are given in inches and parenthetically in centimeters.

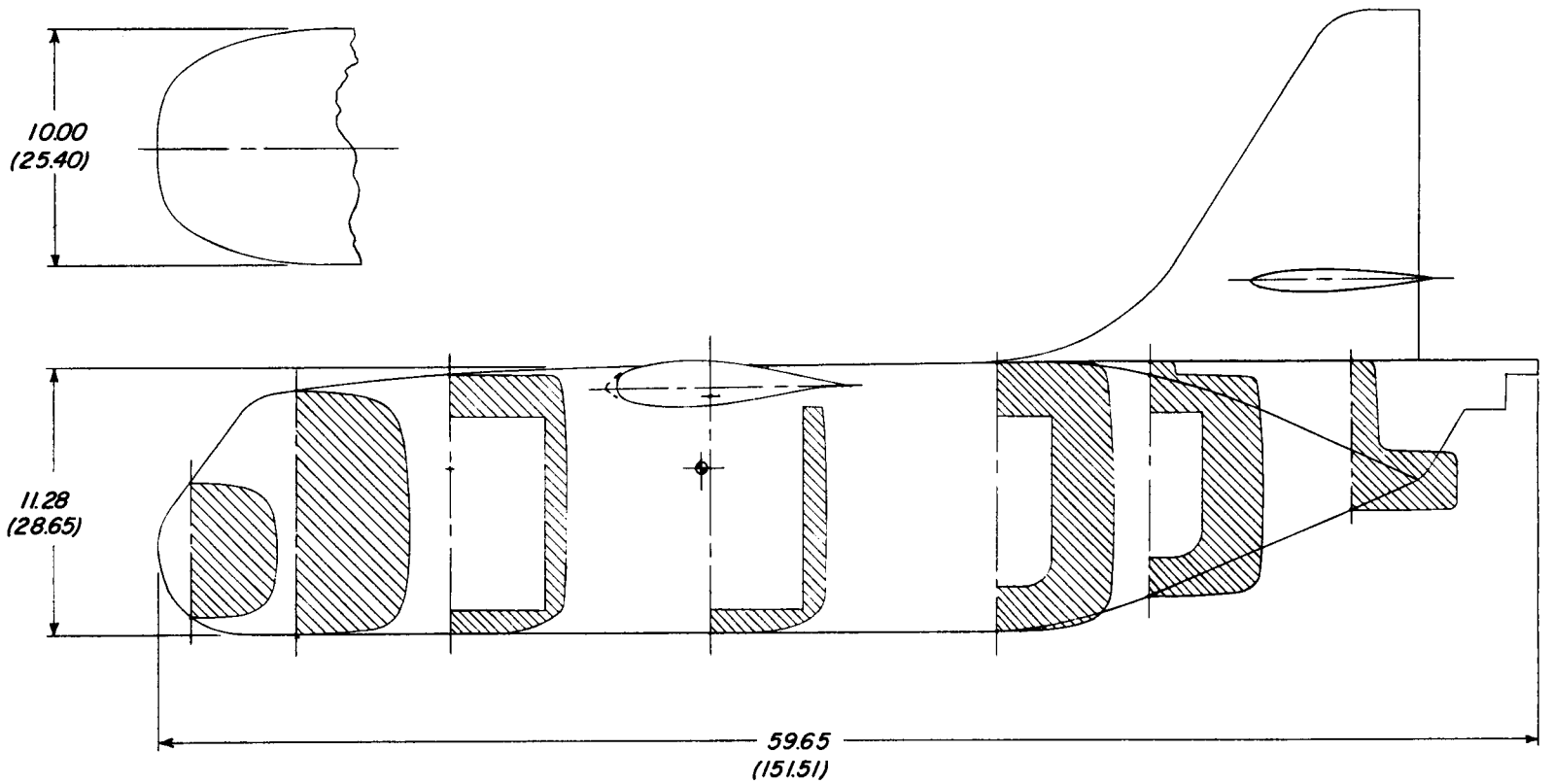

Figure 5.- Fuselage cross sections of a 1/11-scale tilt-wing VTOL model. All dimensions are given in inches and parenthetically in centimeters.

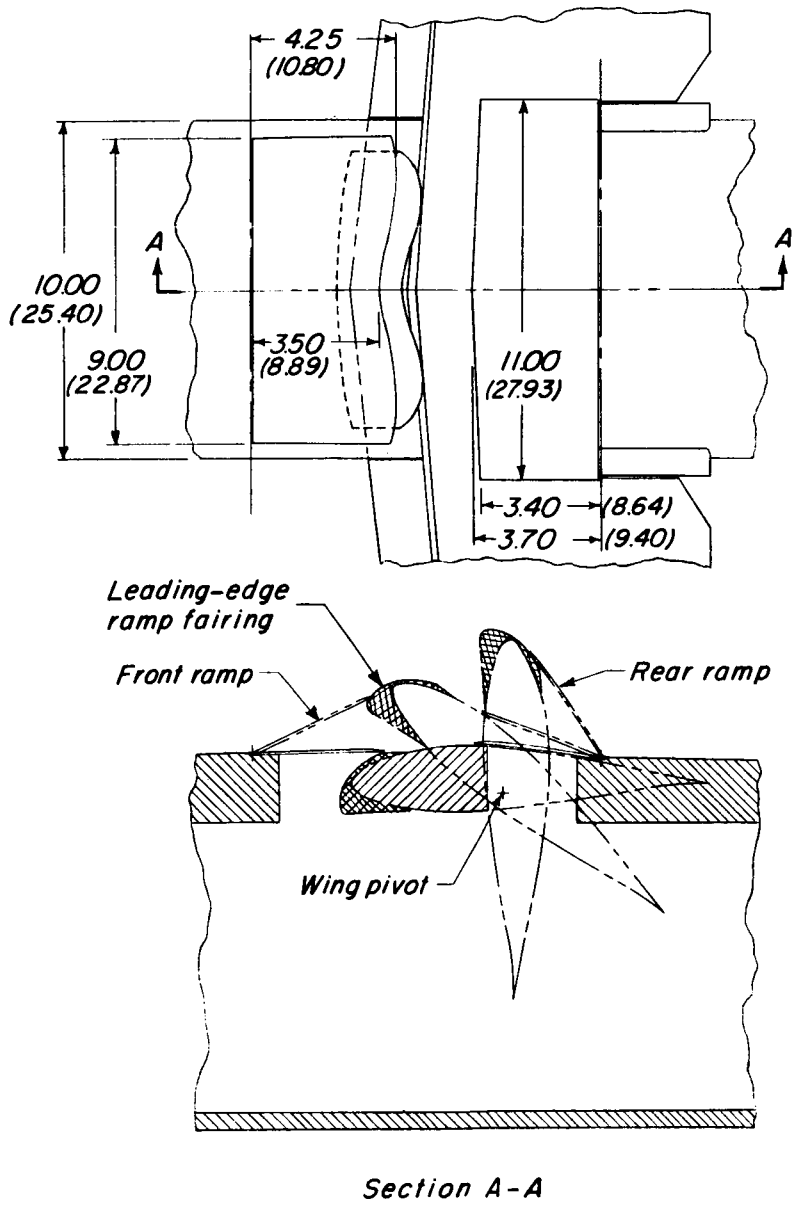

Figure 6.- Wing-fuselage ramps of the 1/11-scale tilt-wing VTOL model. All dimensions are given in inches and parenthetically in centimeters.

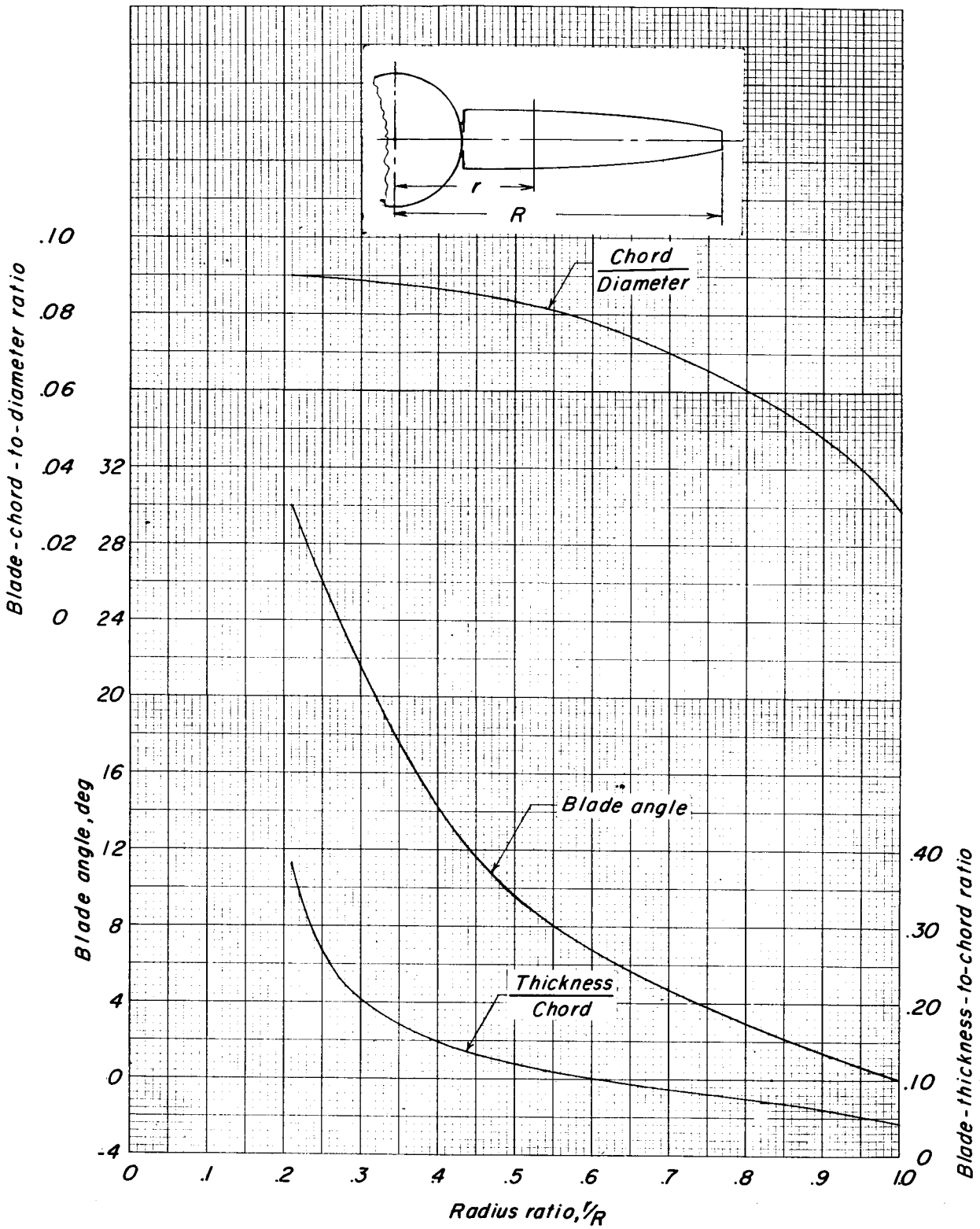

Figure 7.- Geometric characteristics of a propeller blade of a 1/11-scale tilt-wing VTOL model.

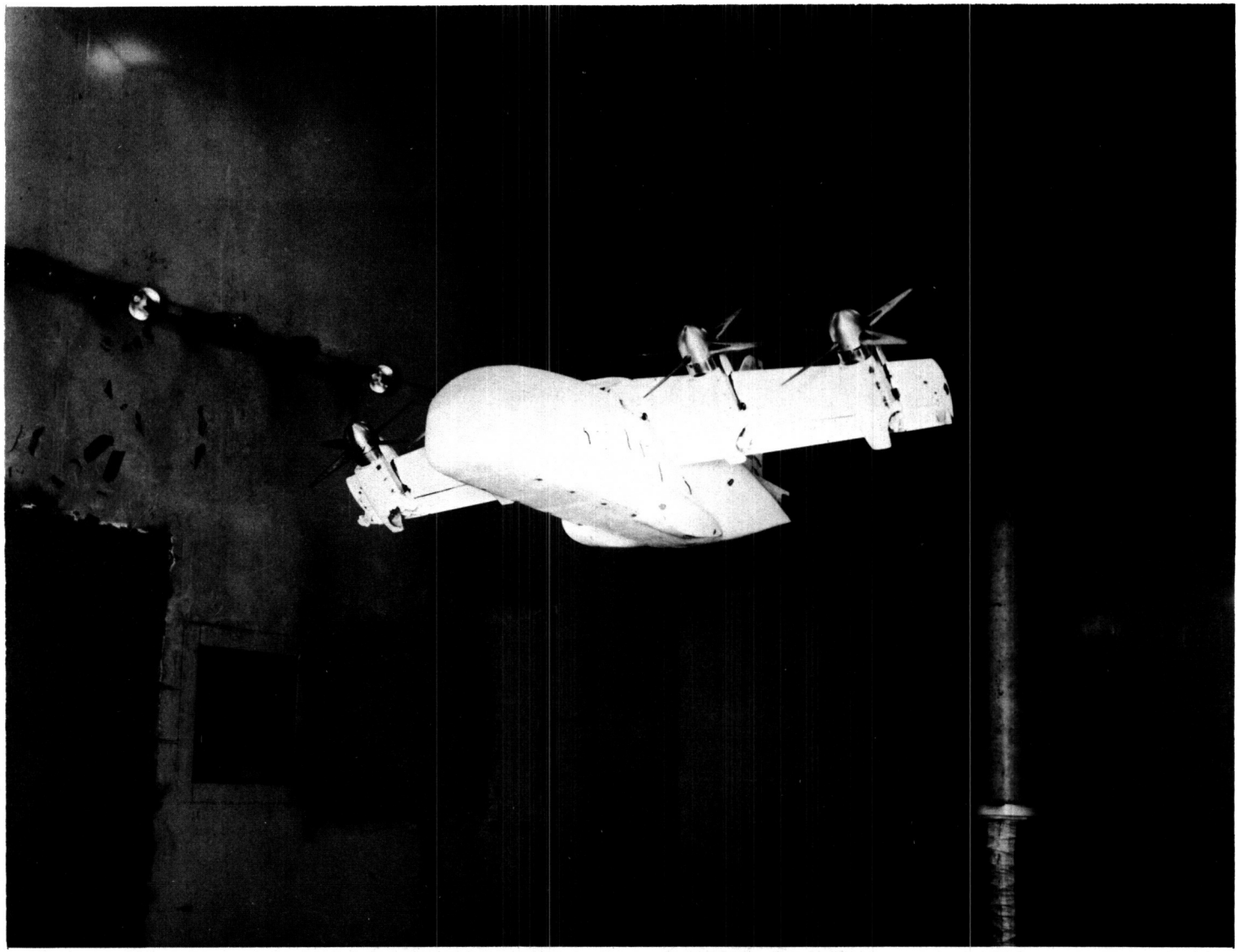

(a) On tunnel center line. L-64-9853

Figure 8.- Photographs of the model in the 17-foot (5.18-meter) test section.

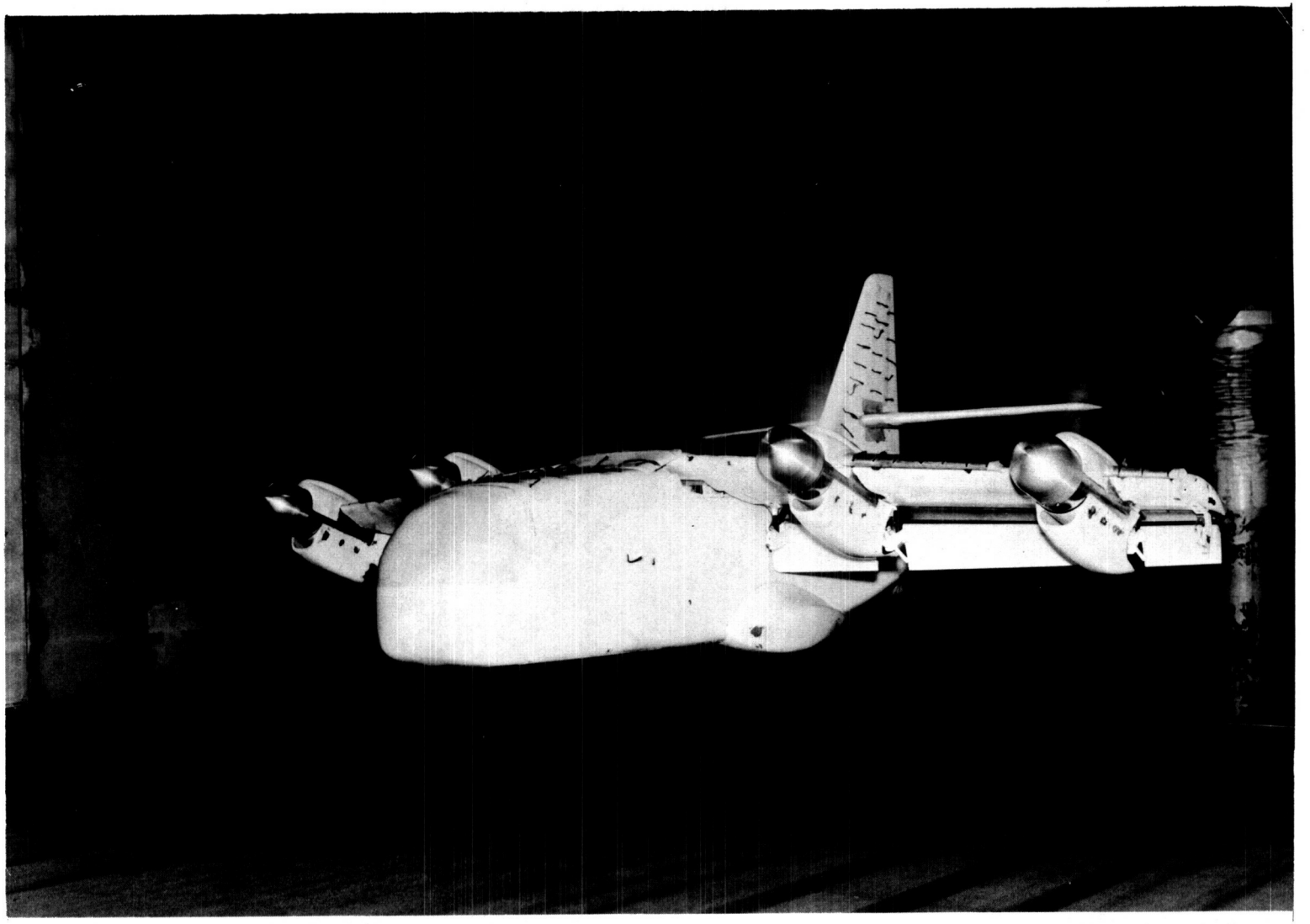

(b) Over the moving ground plane; front view. L-64-10,166

Figure 8.- Continued.

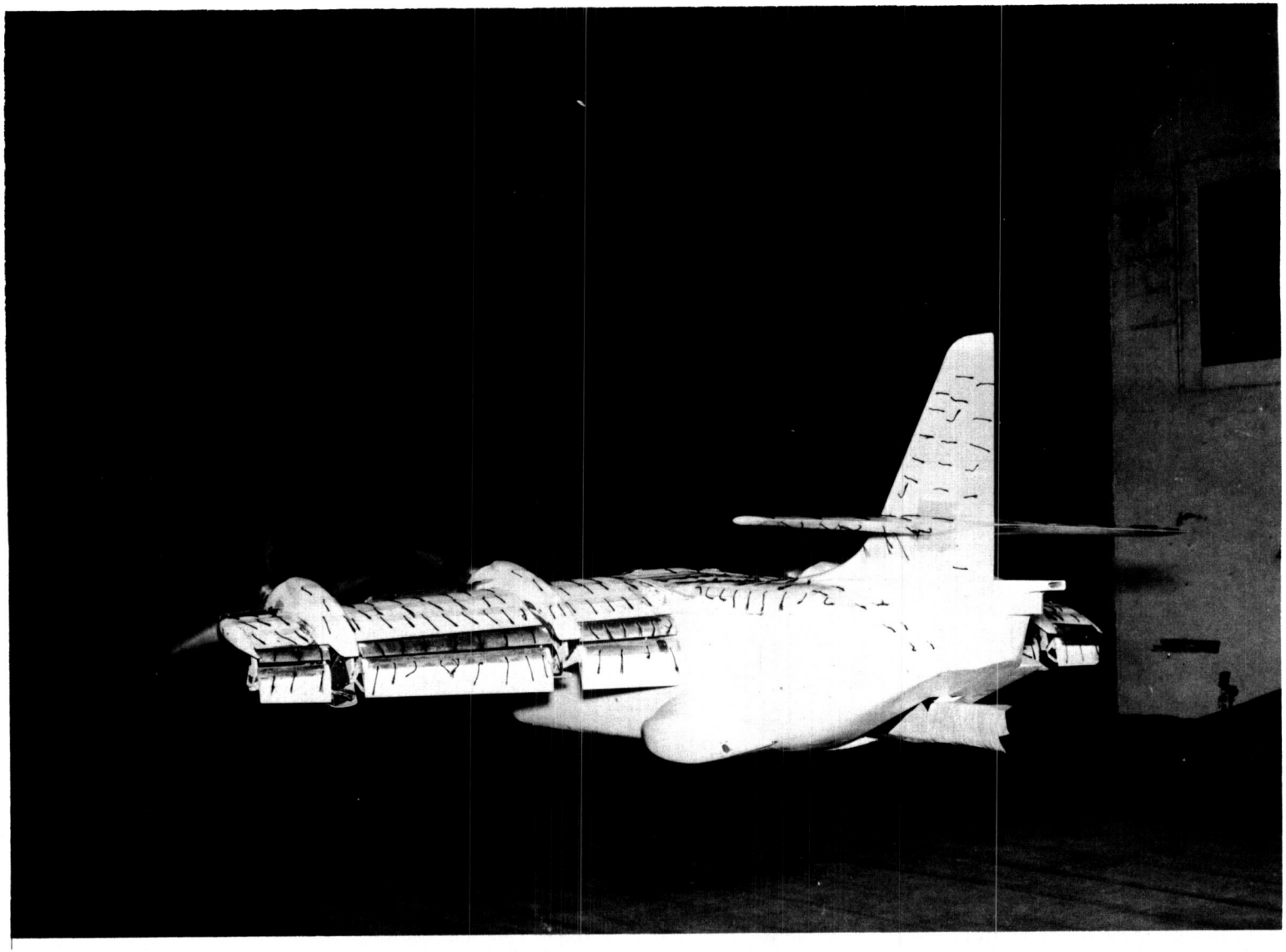

(c) Over moving ground plane; rear view. L-64-10,165

Figure 8.- Concluded.

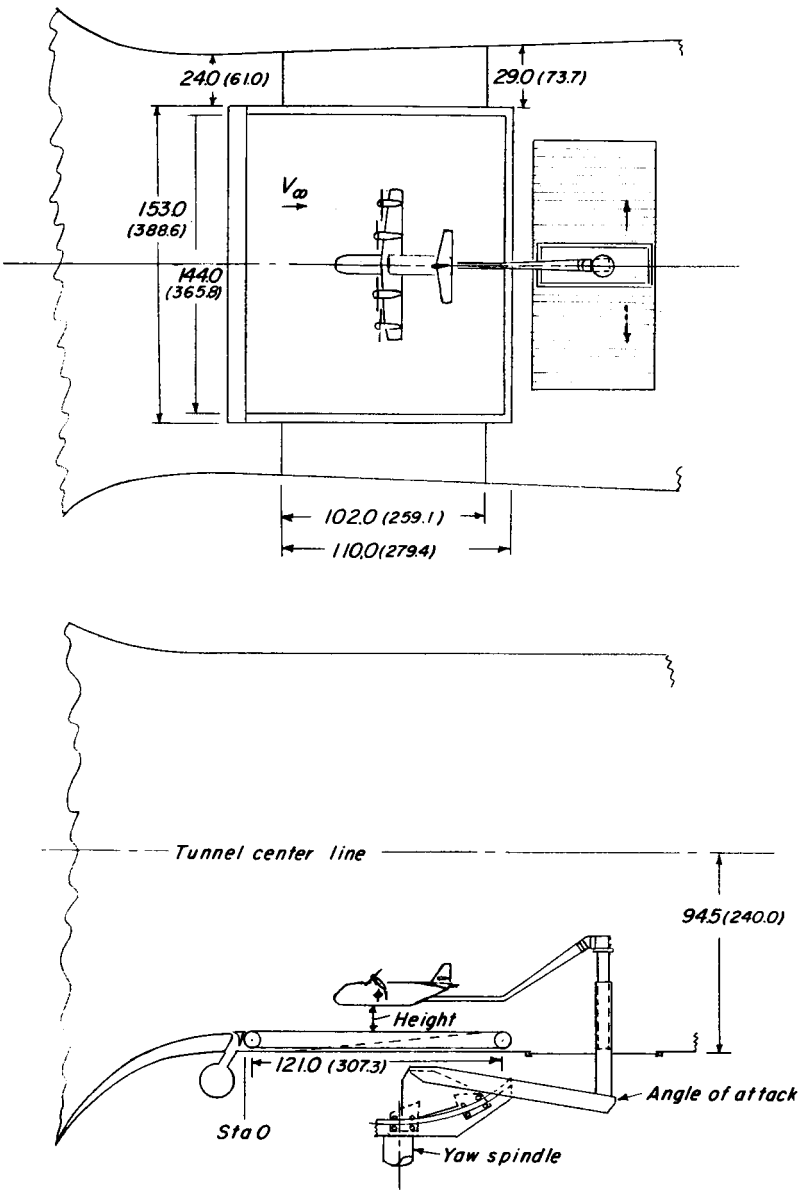

Figure 9.- Sketch of moving-belt ground-plane setup. Dimensions are given in inches and parenthetically in centimeters.

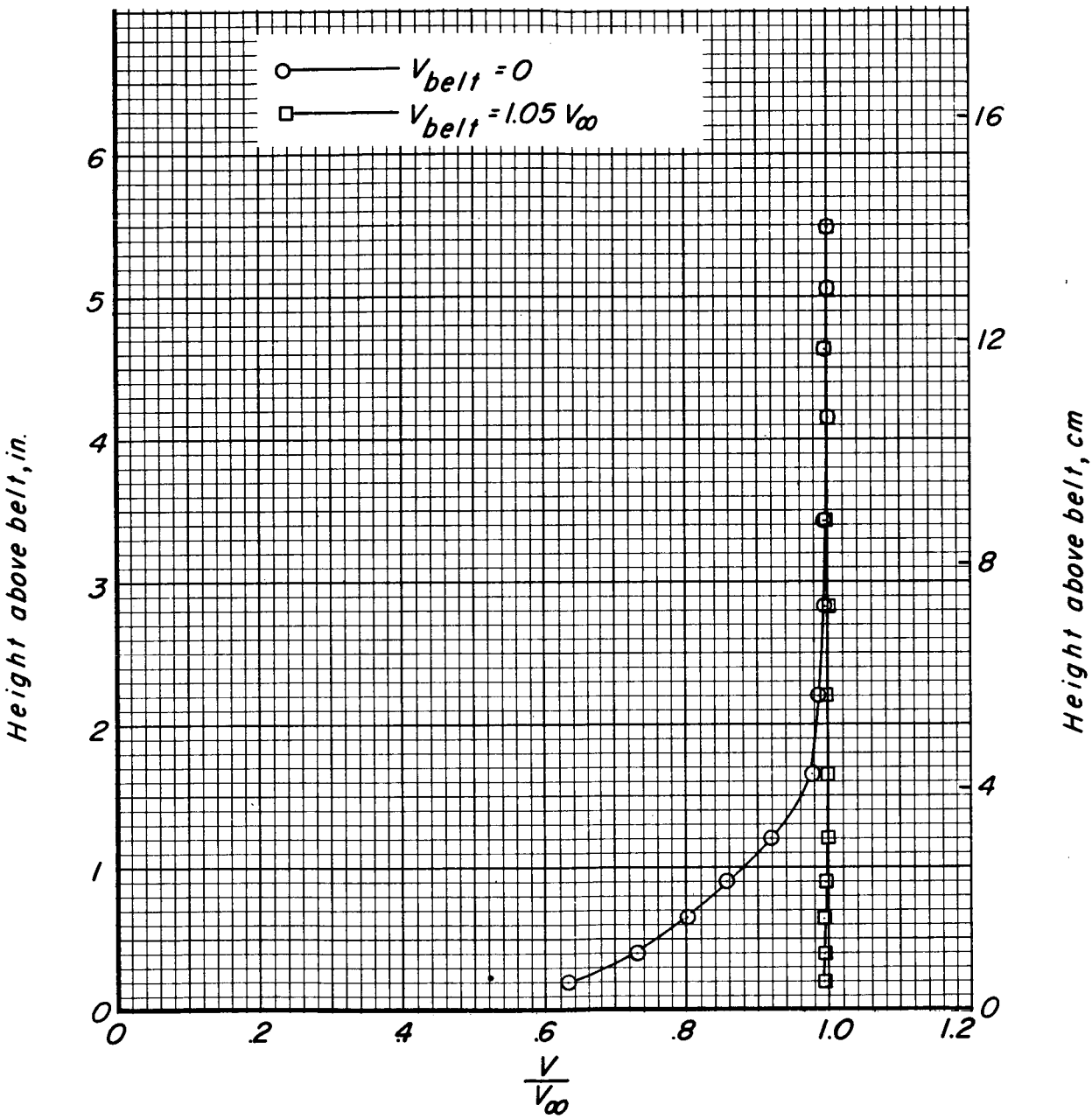

Figure 10.- Effect of moving belt on boundary-layer profile of ground plane at model moment center. V is velocity in boundary layer; V_{belt} is velocity of moving belt; V_∞ = 8.25 ft/sec (25.14 m/sec).

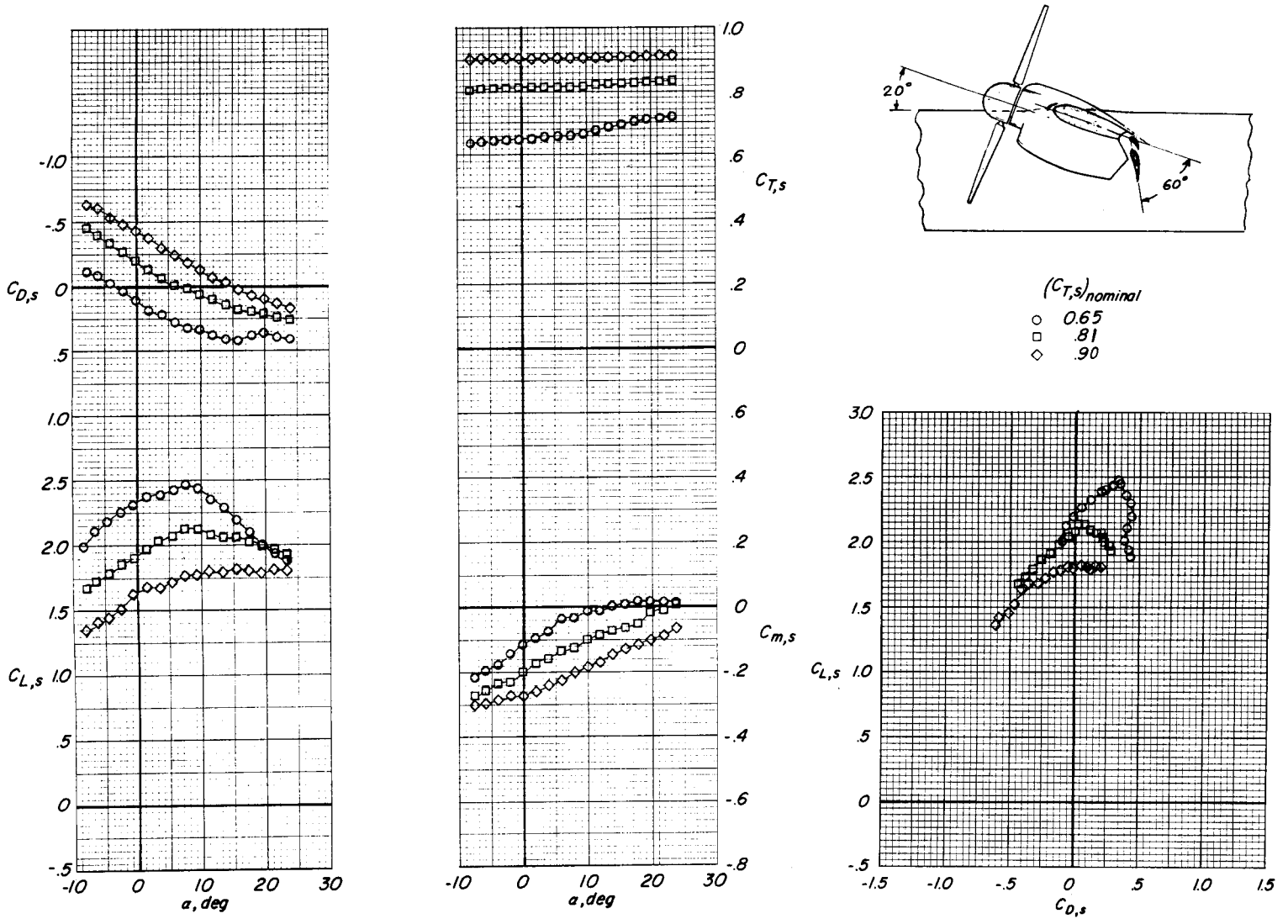

(a) $h/\bar{c} = 9.20 \approx \infty$.

Figure 11.- Effect of thrust coefficient on the aerodynamic characteristics. Ground belt stopped; $i_w = 20^0$; $\delta_f = 60^0$; horizontal tail off; slat on.

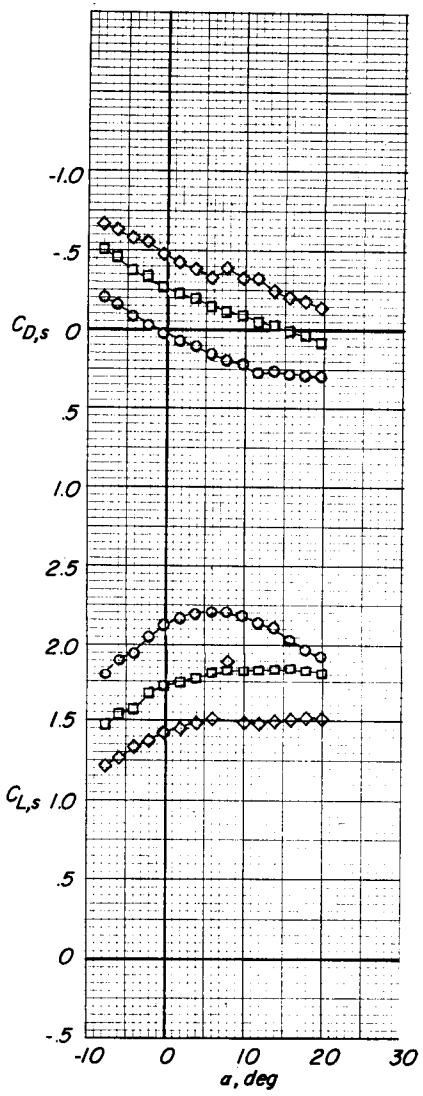

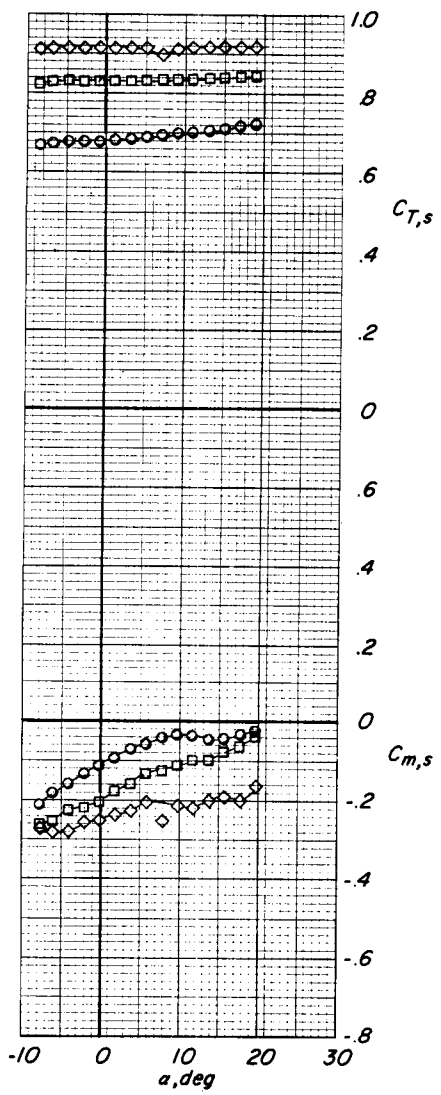

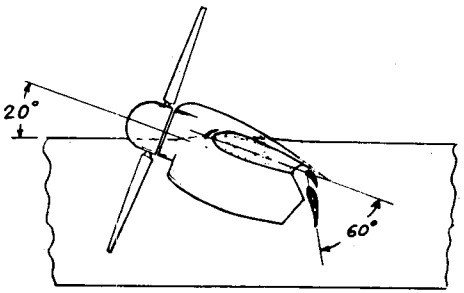

$(C_{T,s})_{nominal}$
○ 0.68
□ .83
◇ .92

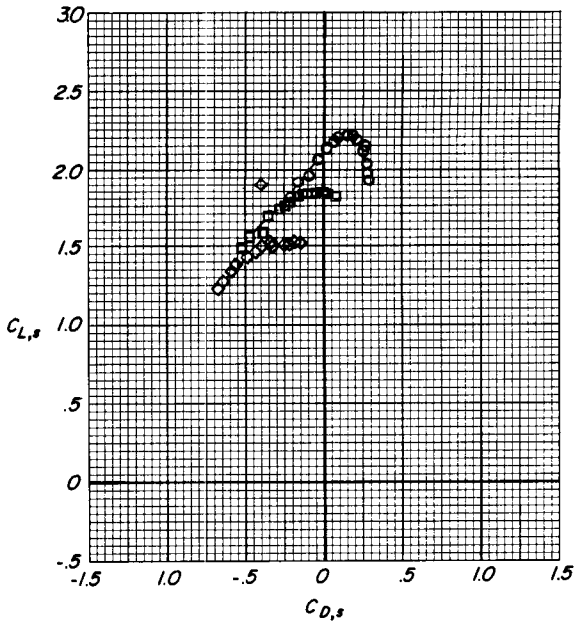

(b) h/c̄ = 1.70.

Figure 11.- Continued.

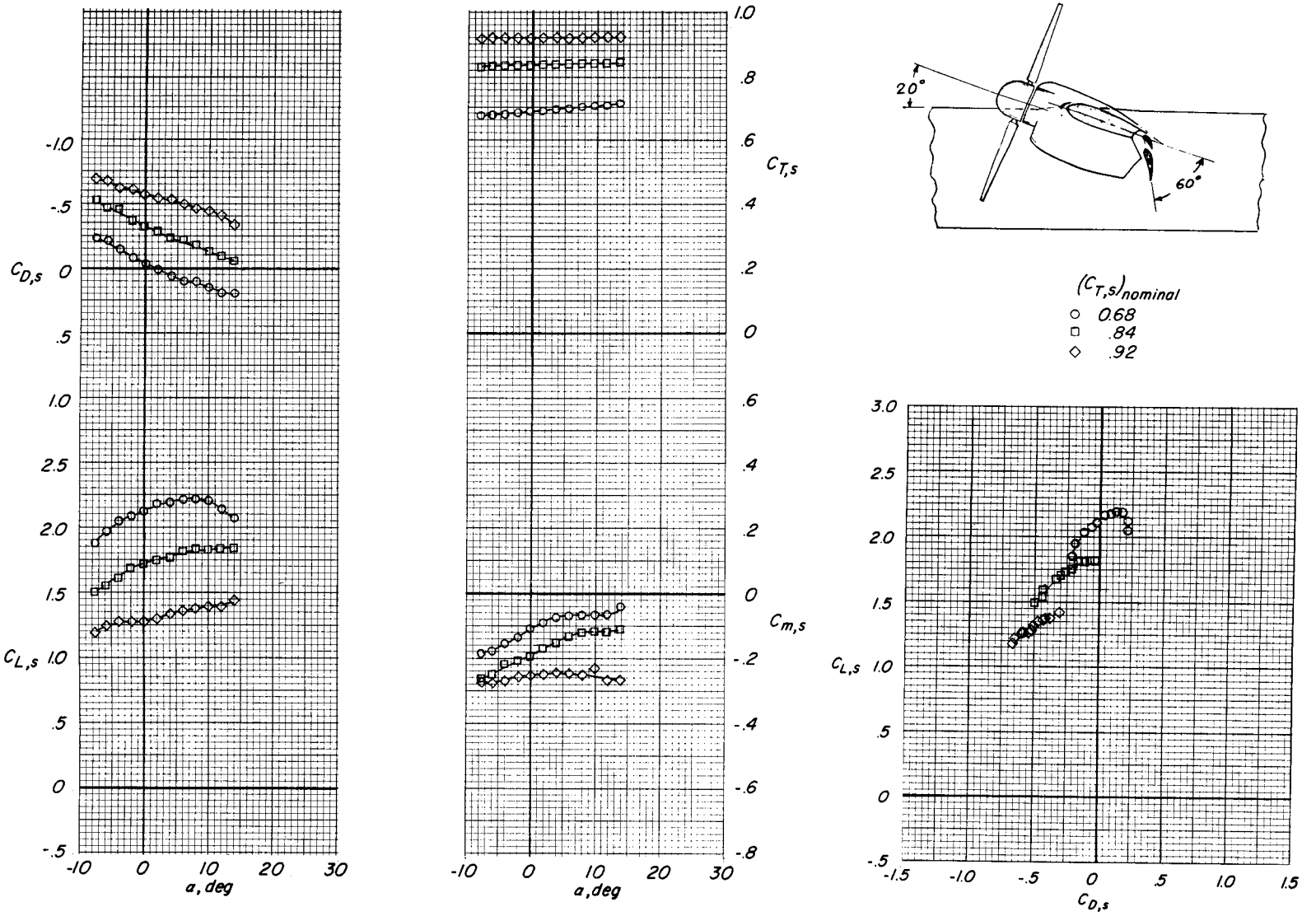

(c) $h/\bar{c} = 1.09$.

Figure 11.- Continued.

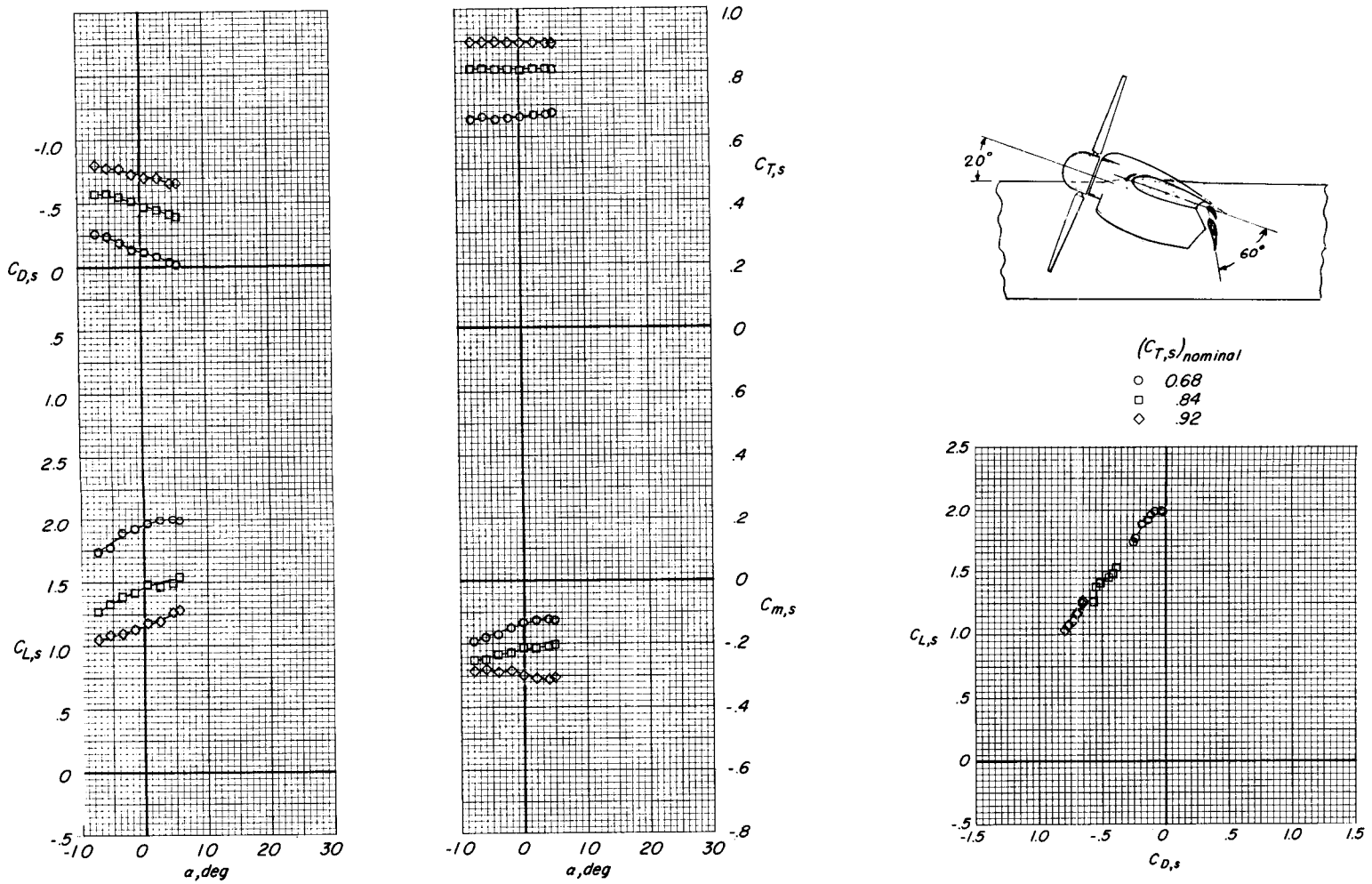

(d) $h/\bar{c} = 0.40$.

Figure 11.- Concluded.

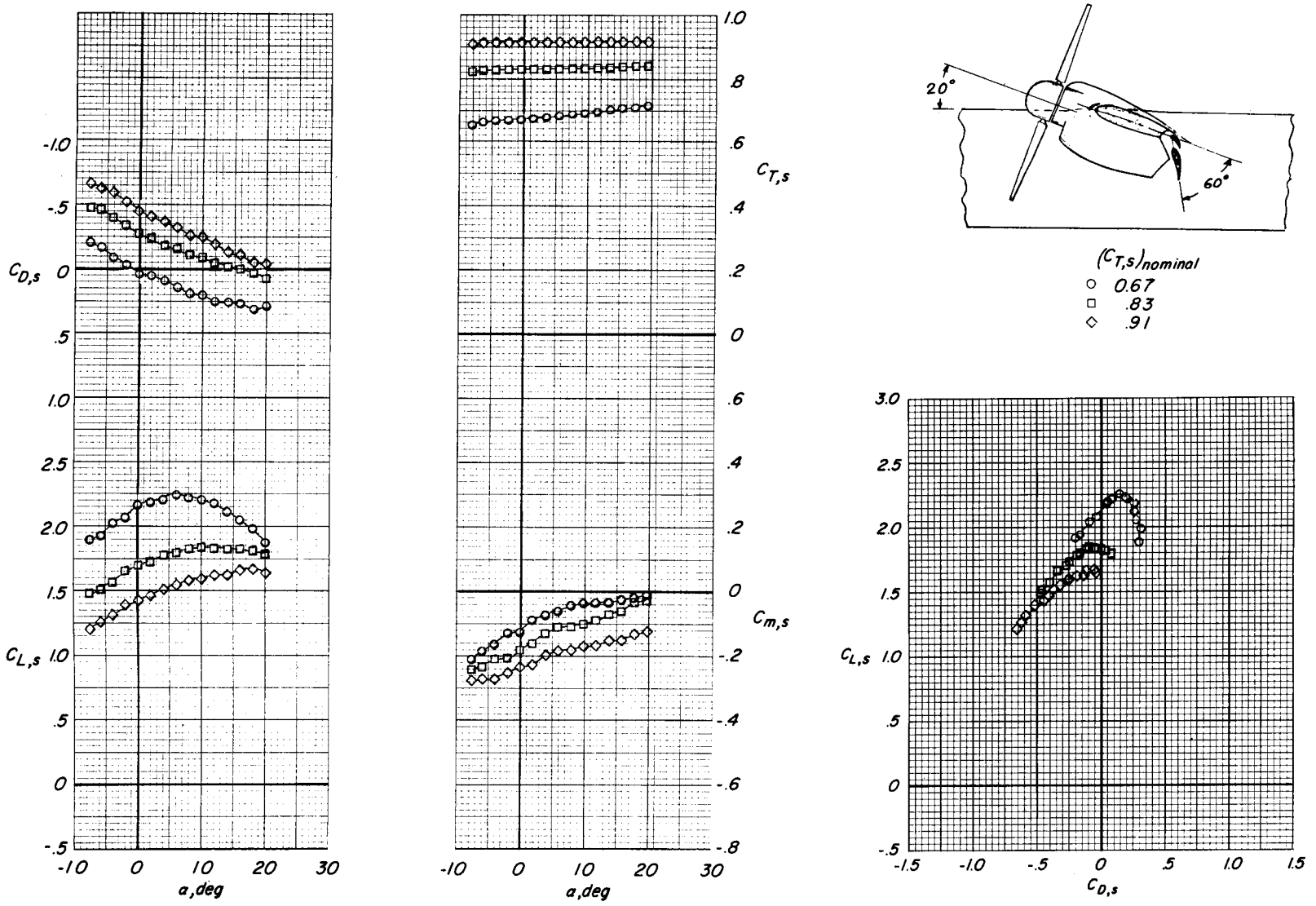

(a) $h/\bar{c} = 1.70$.

Figure 12.- Effect of thrust coefficient on the aerodynamic characteristics. Ground belt moving; $i_w = 20^0$; $\delta_f = 60^0$; horizontal tail off; slat on.

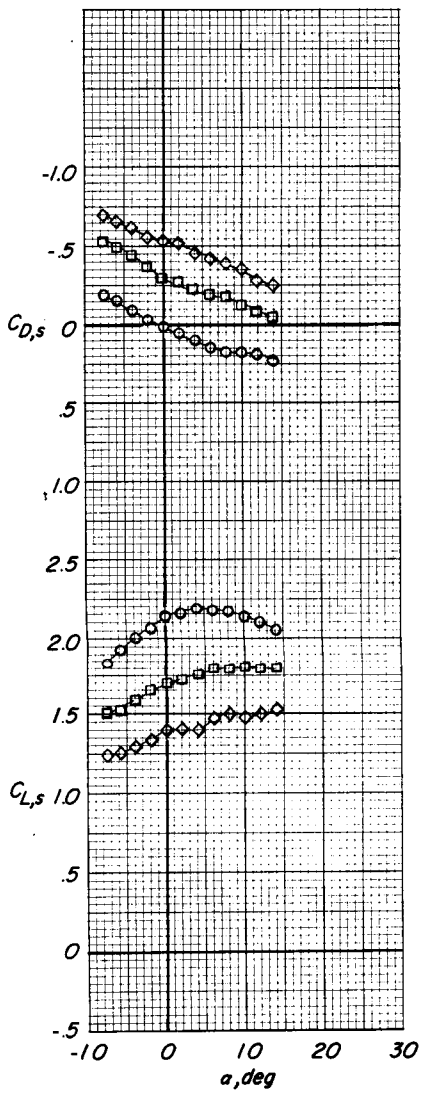

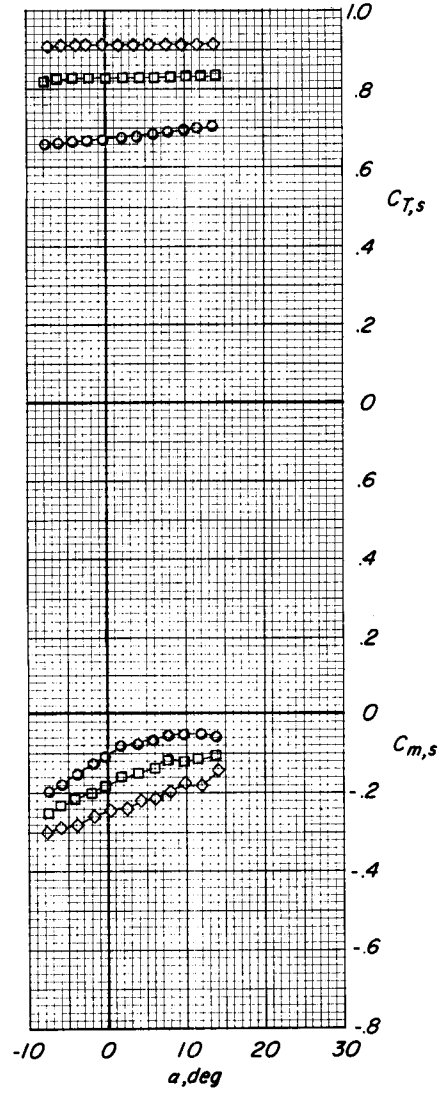

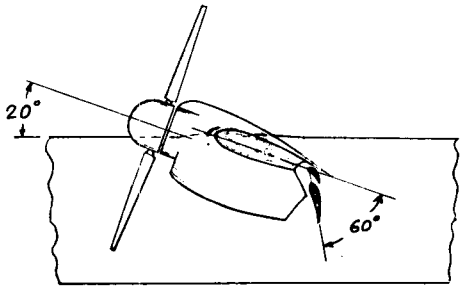

$(C_{T,s})_{nominal}$
○ 0.67
□ .83
◇ .91

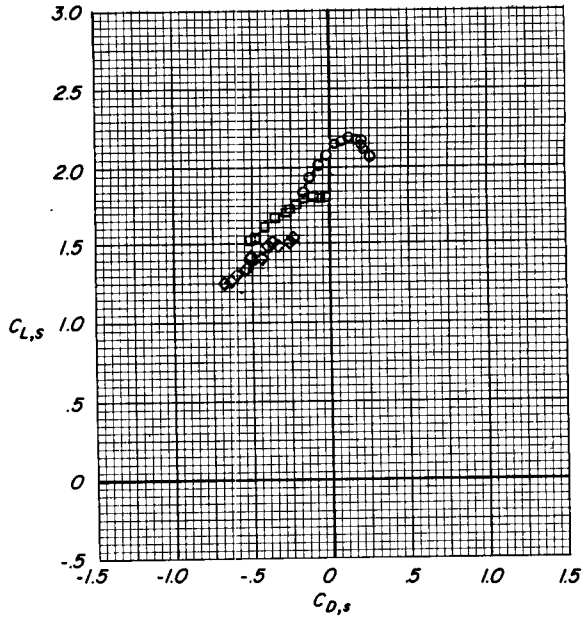

(b) $h/\bar{c}$ = 1.09.

Figure 12.- Continued.

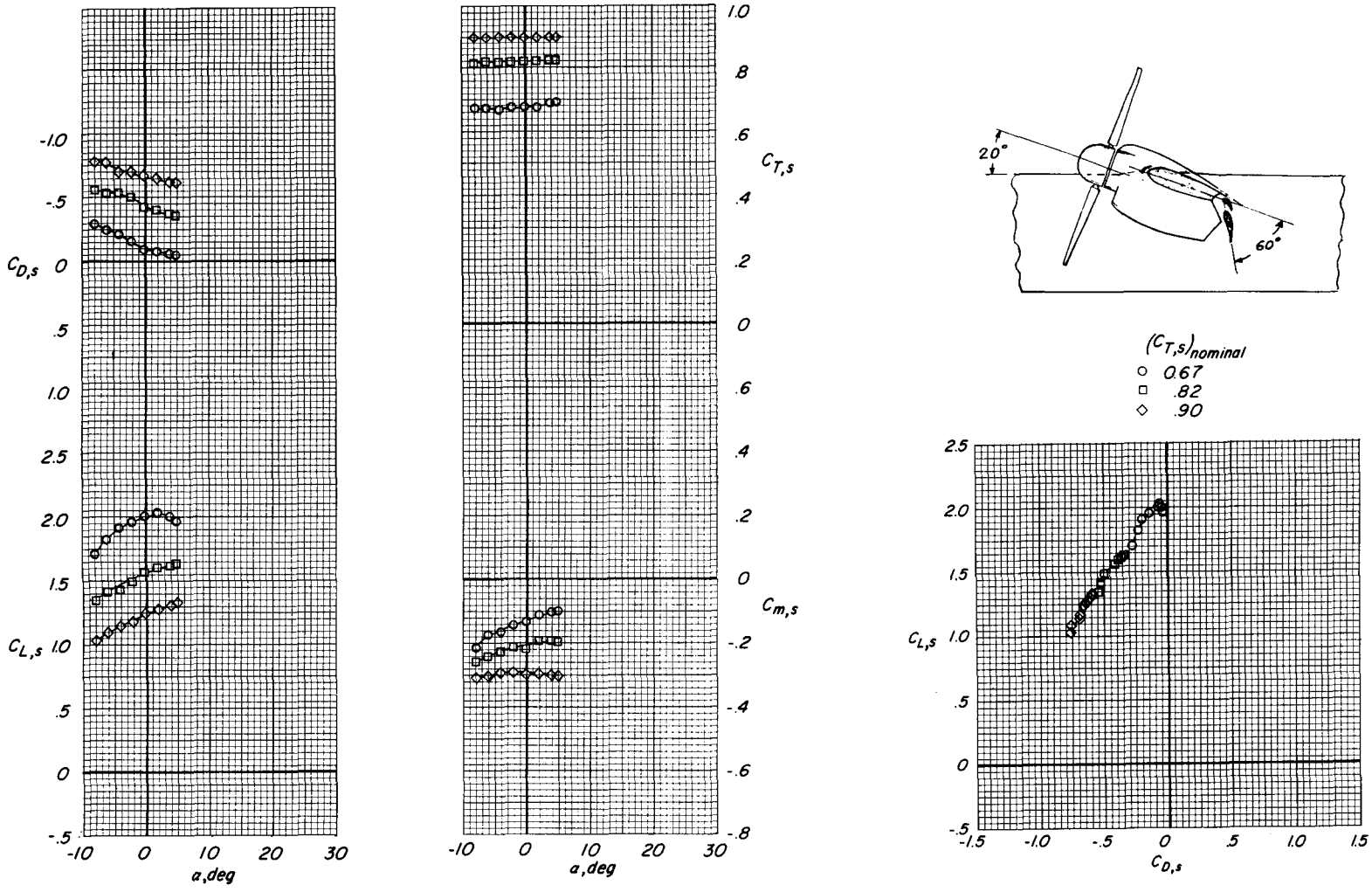

(c) $h/\bar{c} = 0.40$.

Figure 12.- Concluded.

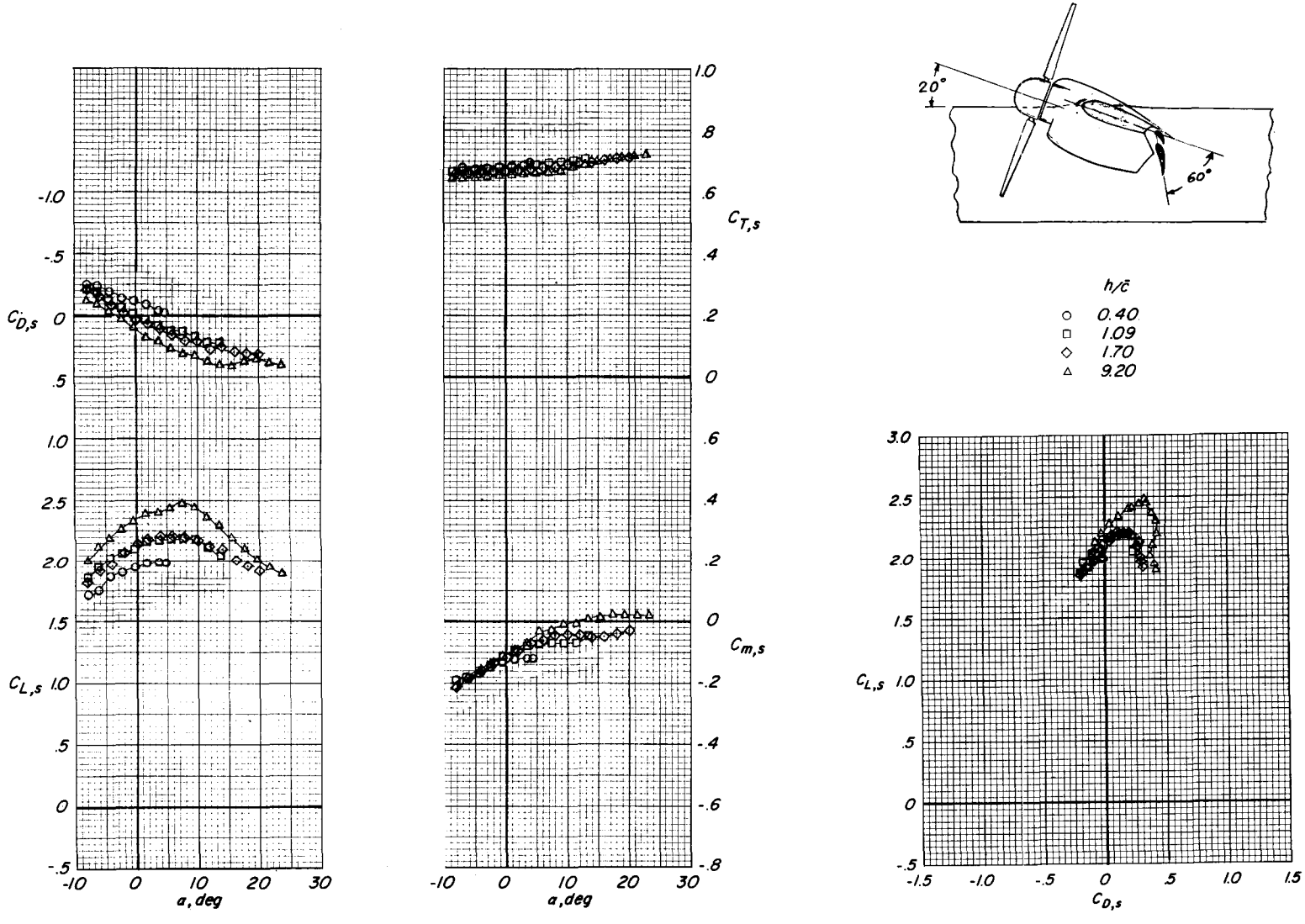

(a) $(C_{T,s})_{nominal} \approx 0.68$.

Figure 13.- Effect of ground height on aerodynamic characteristics. Ground belt stopped; $i_w = 20^0$; $\delta_f = 60^0$; horizontal tail off; slat on.

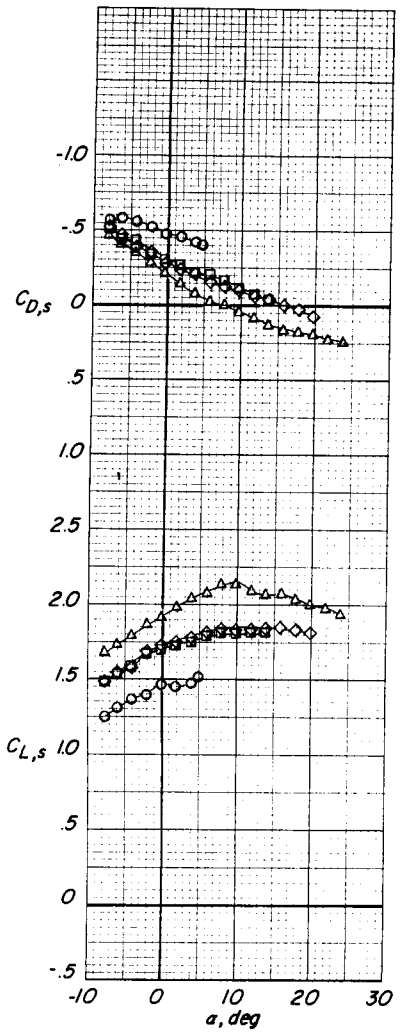

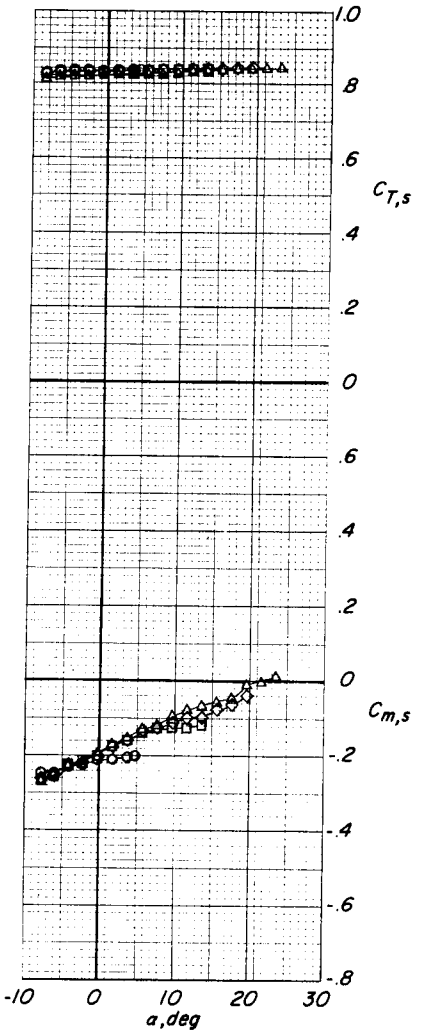

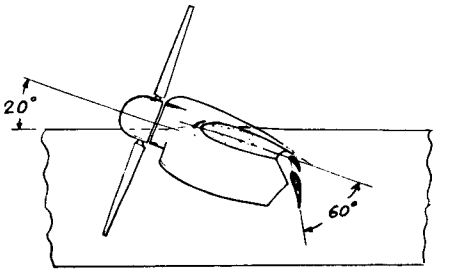

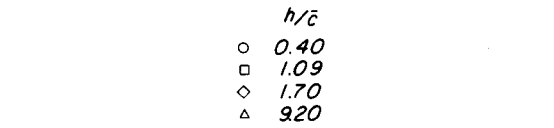

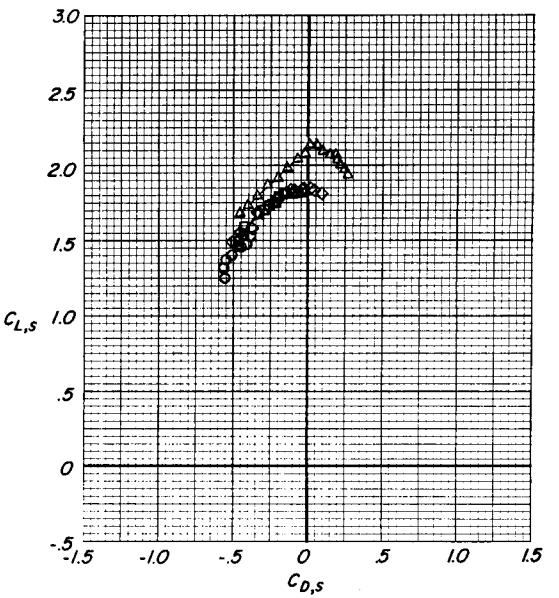

(b) $(C_{T,s})_{nominal} \approx 0.84$.

Figure 13.- Continued.

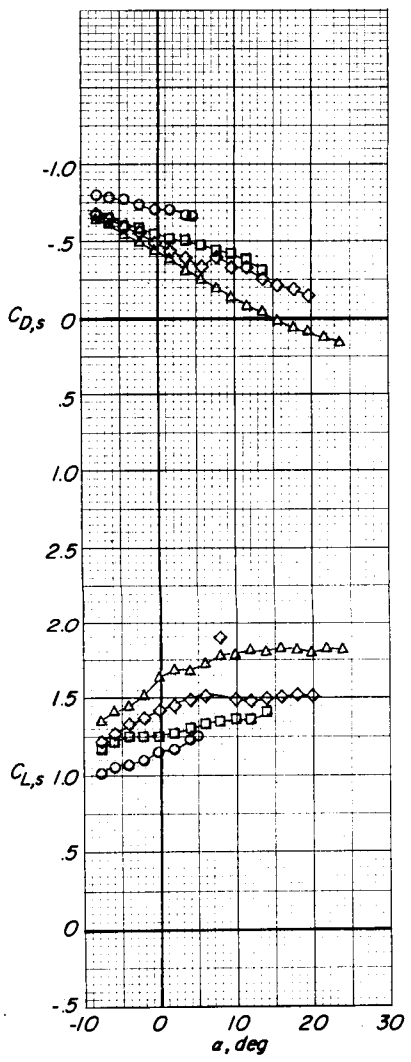

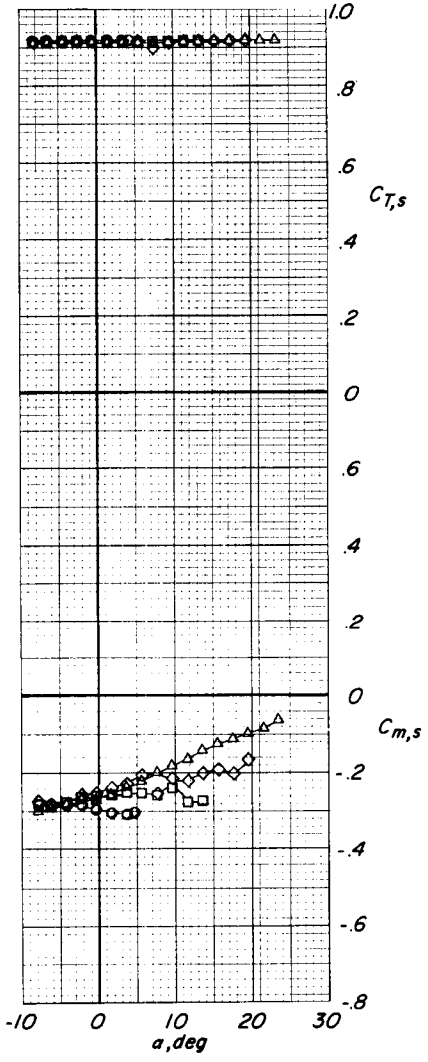

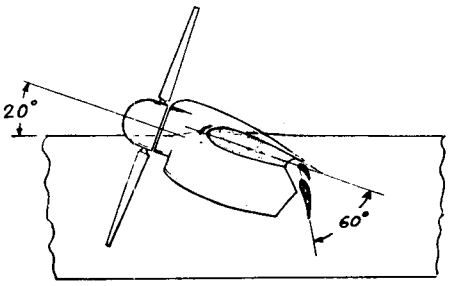

h/c̄
○ 0.40
□ 1.09
◇ 1.70
△ 9.20

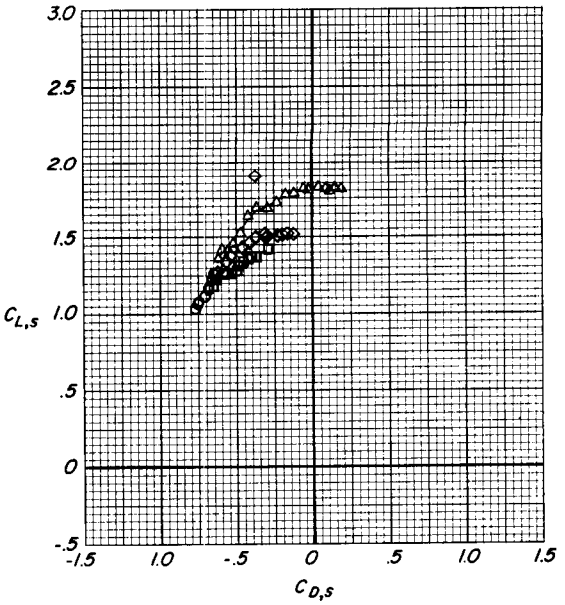

(c) $(C_{T,s})_{nominal} \approx 0.92$.

Figure 13.- Concluded.

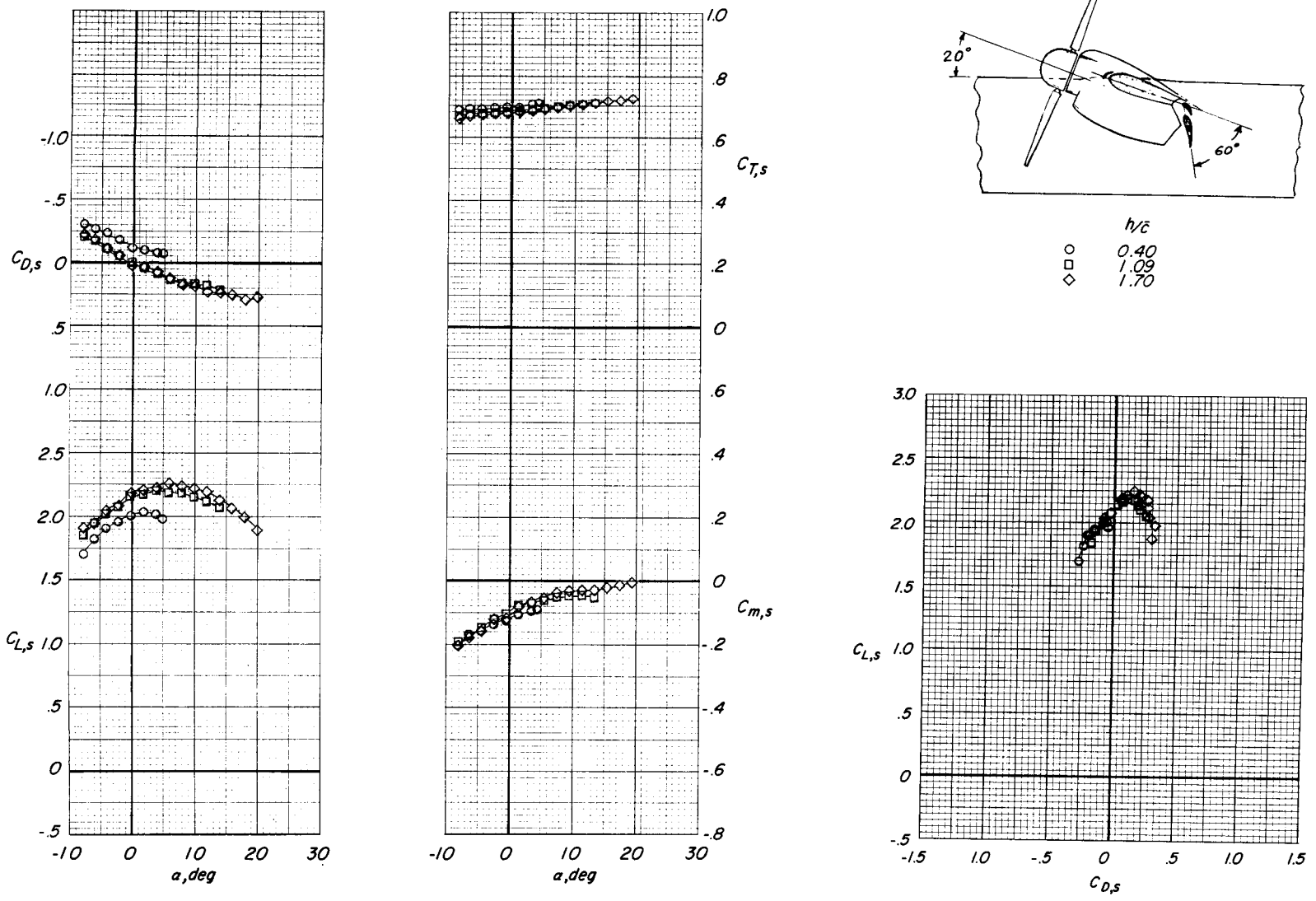

(a) $(C_{T,s})_{nominal} \approx 0.68$.

Figure 14.- Effect of ground height on aerodynamic characteristics. Ground belt moving; $i_w = 20^0$; $\delta_f = 60^0$; horizontal tail off; slat on.

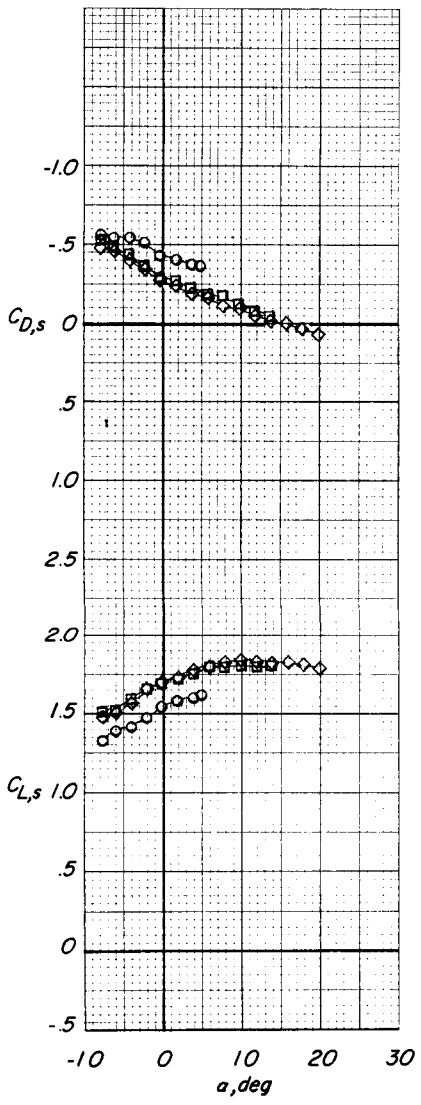

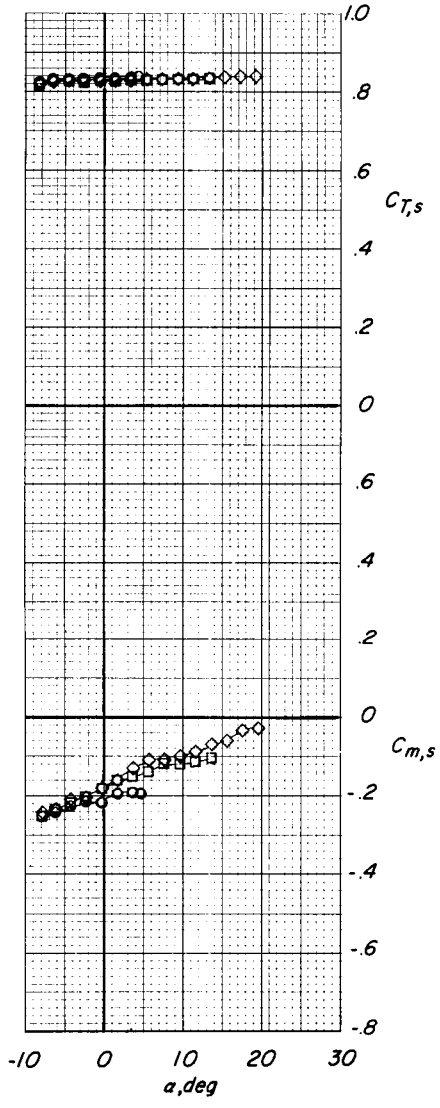

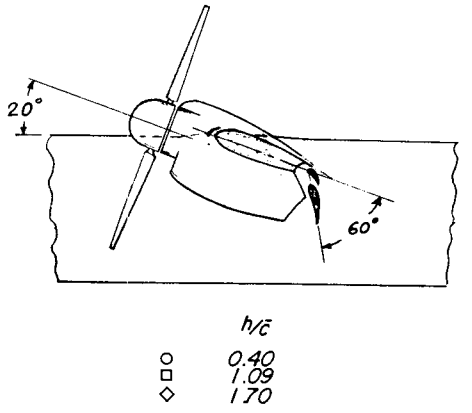

h/c̄
○ 0.40
□ 1.09
◇ 1.70

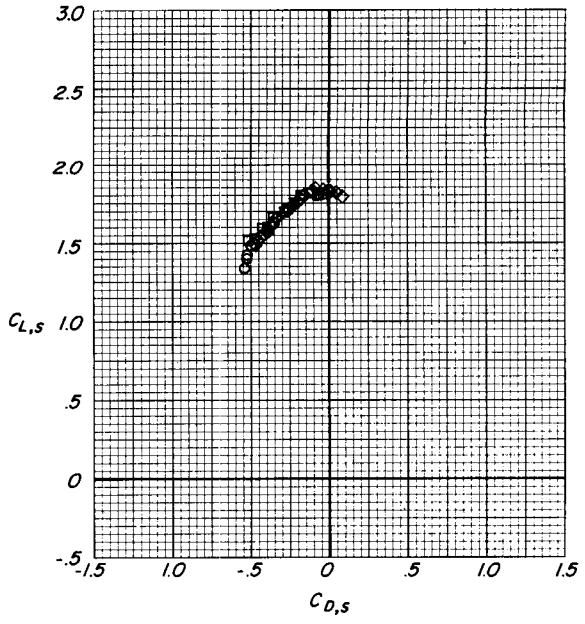

(b) $(C_{T,s})_{nominal} \approx 0.84$.

Figure 14.- Continued.

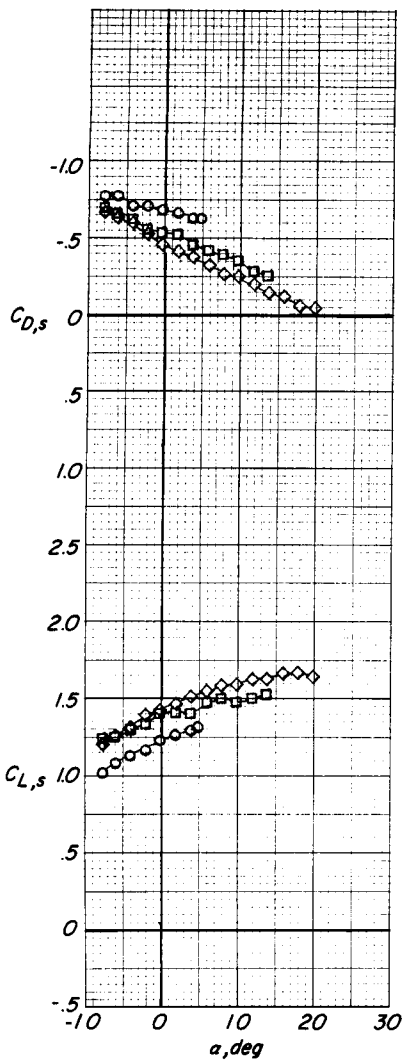

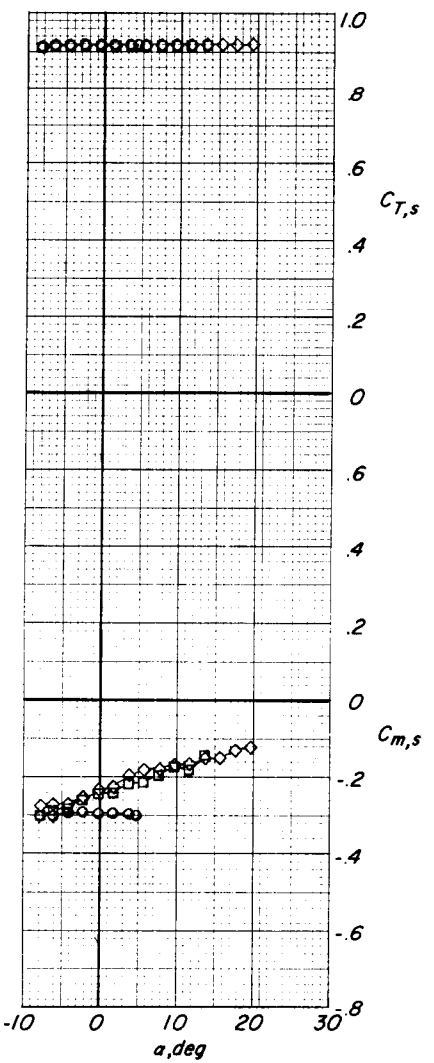

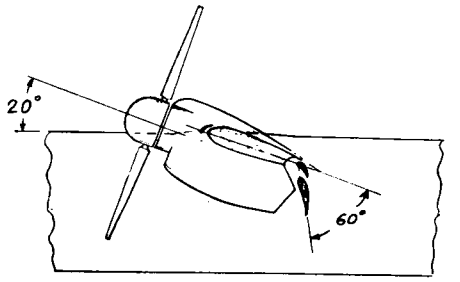

h/c̄
○ 0.40
□ 1.09
◇ 1.70

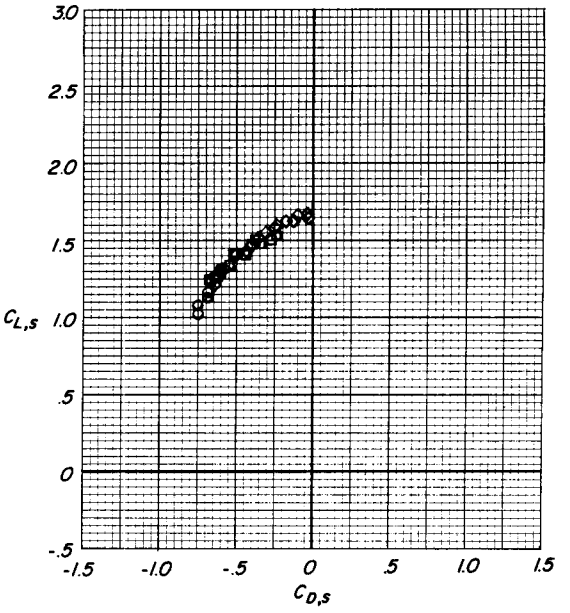

(c) $(C_{T,s})_{nominal} \approx 0.92$.

Figure 14.- Concluded.

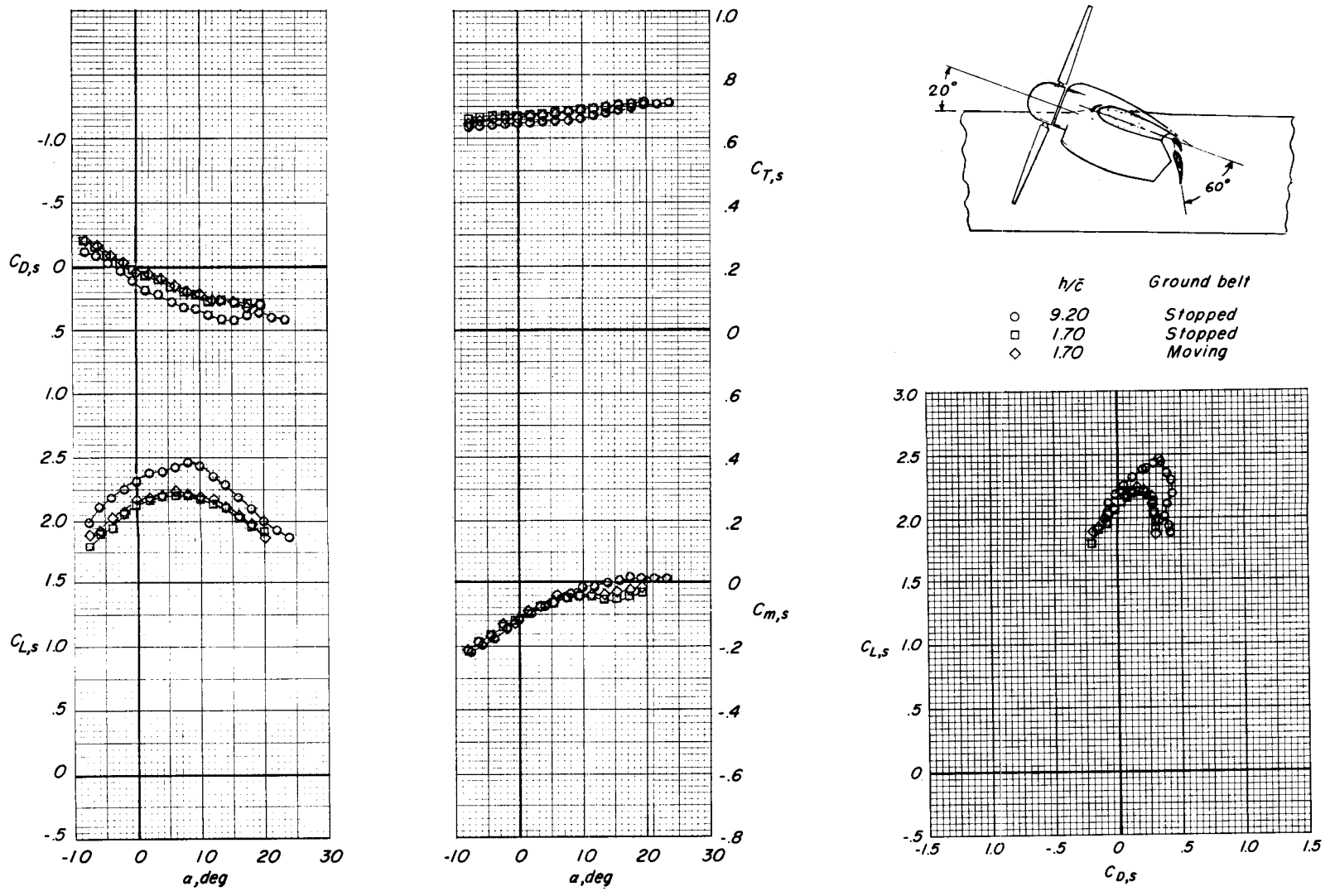

(a) $(C_{T,s})_{nominal} \approx 0.66$.

Figure 15.- Ground effect and effect of ground belt on the aerodynamic characteristics. $h/\bar{c} = 1.70$; $i_w = 20^0$; $\delta_f = 60^0$; horizontal tail off; slat on.

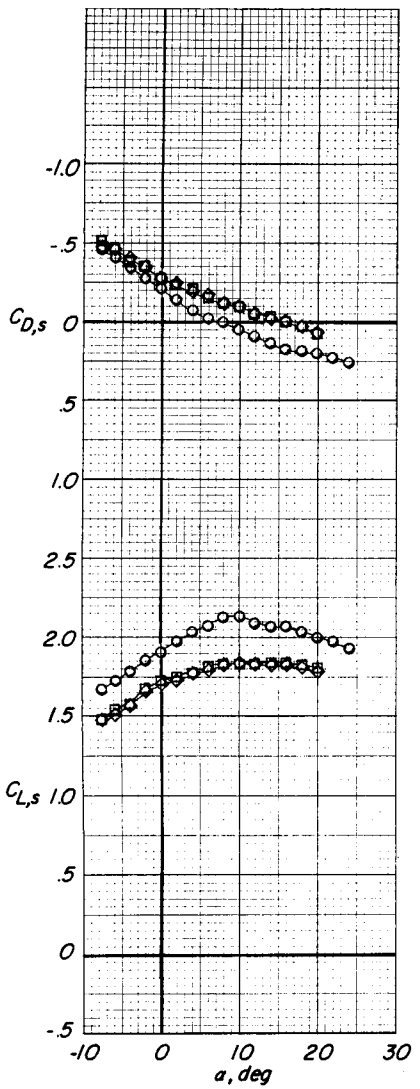

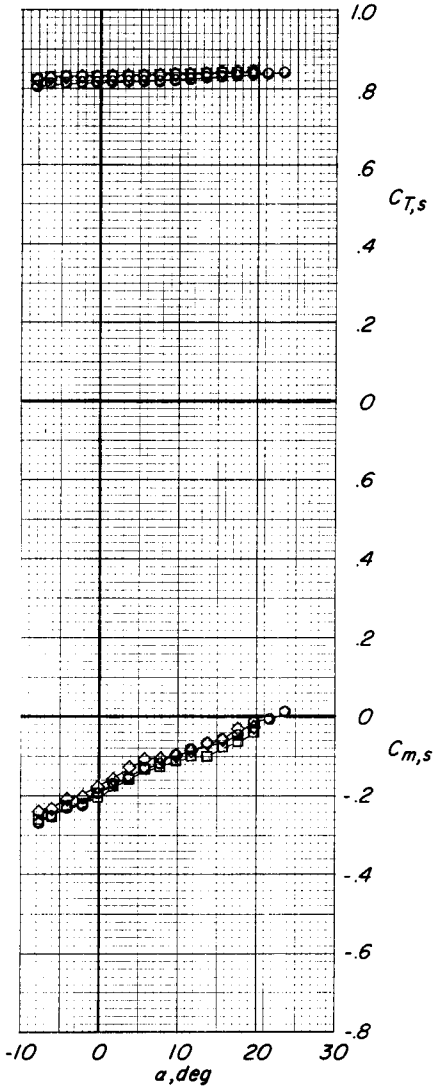

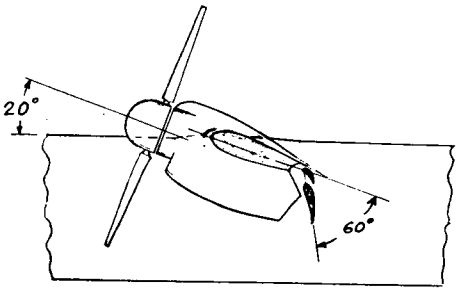

	h/c	Ground belt
○	9.20	Stopped
□	1.70	Stopped
◇	1.70	Moving

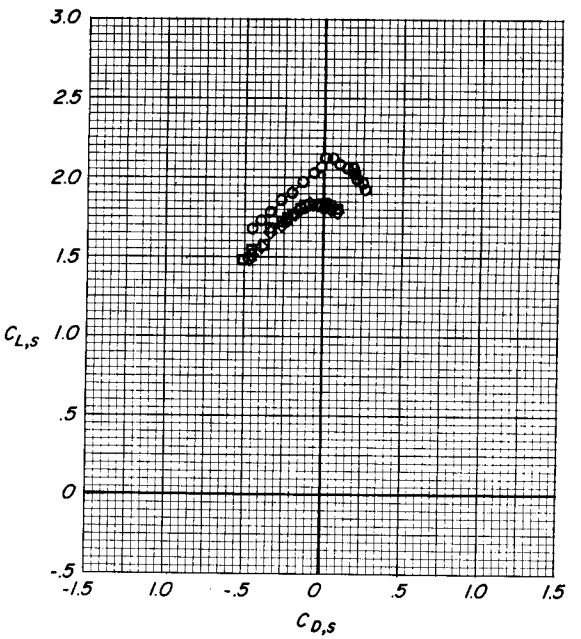

(b) $(C_{T,s})_{nominal} \approx 0.84$.

Figure 15.- Continued.

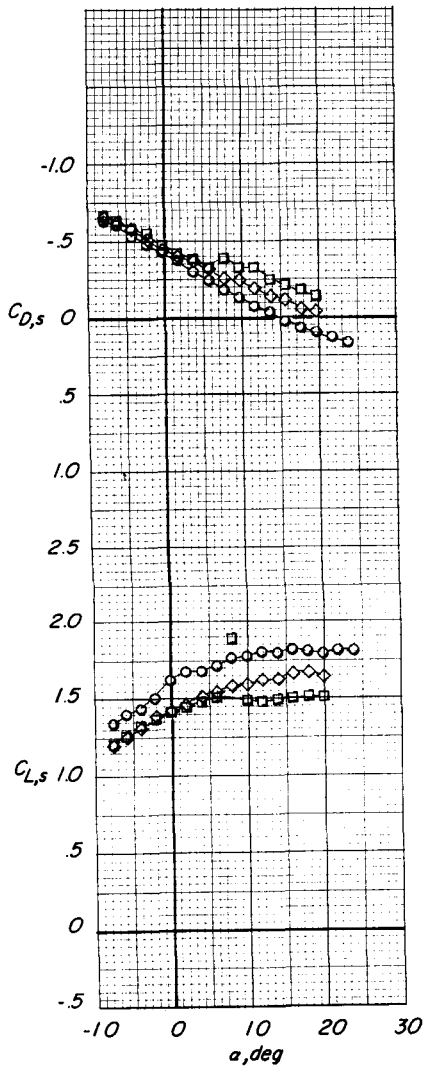

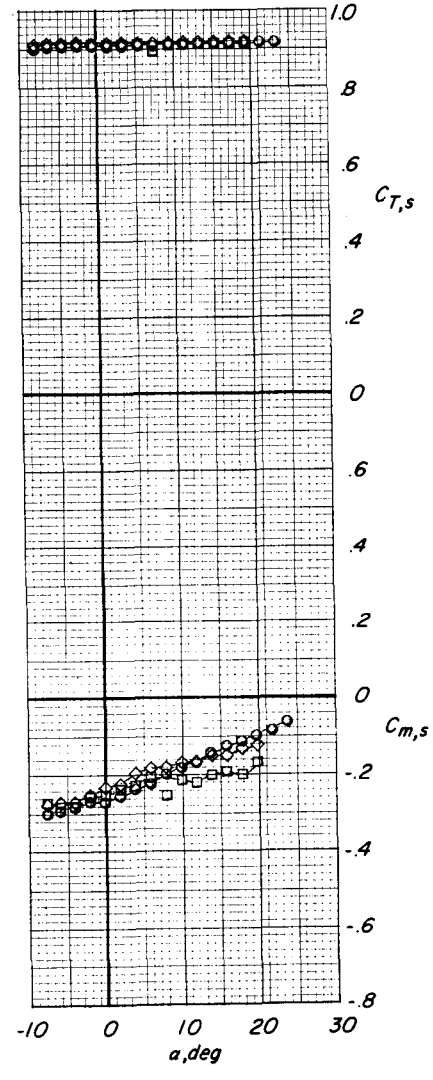

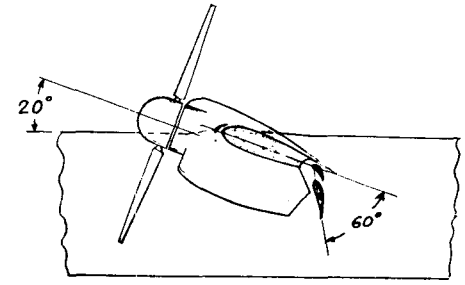

	h/c̄	Ground belt
○	9.20	Stopped
□	1.70	Stopped
◇	1.70	Moving

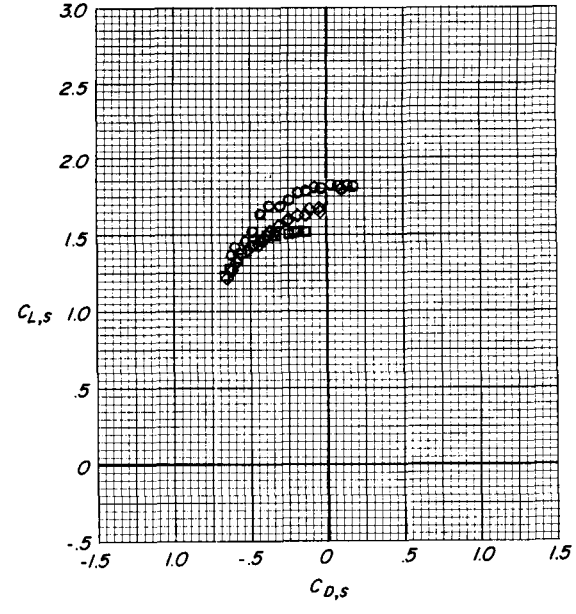

(c) $(C_{T,s})_{nominal} \approx 0.91$.

Figure 15.- Concluded.

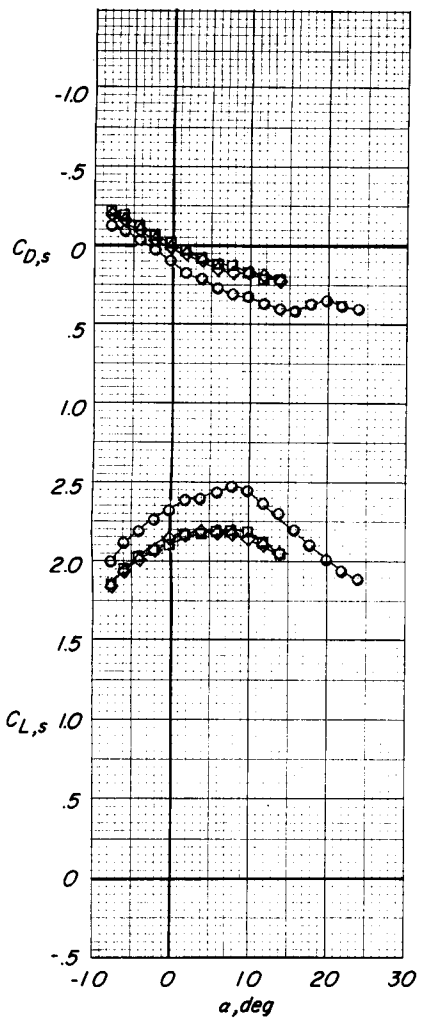

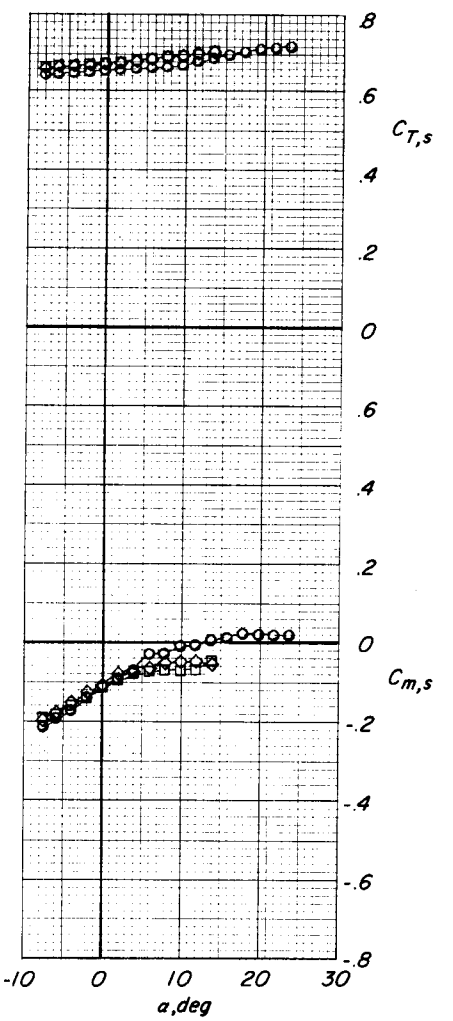

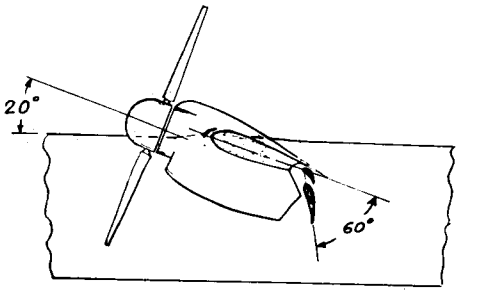

	h/c̄	Ground belt
○	9.20	Stopped
□	1.09	Stopped
◇	1.09	Moving

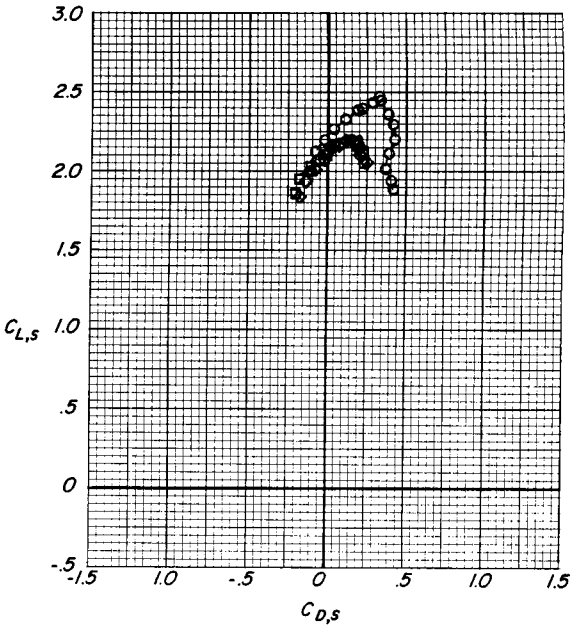

(a) $(C_{T,s})_{nominal} \approx 0.67$.

Figure 16.- Ground effect and effect of ground belt on the aerodynamic characteristics. $h/\bar{c} = 1.09$; $i_w = 20^0$; $\delta_f = 60^0$; horizontal tail off; slat on.

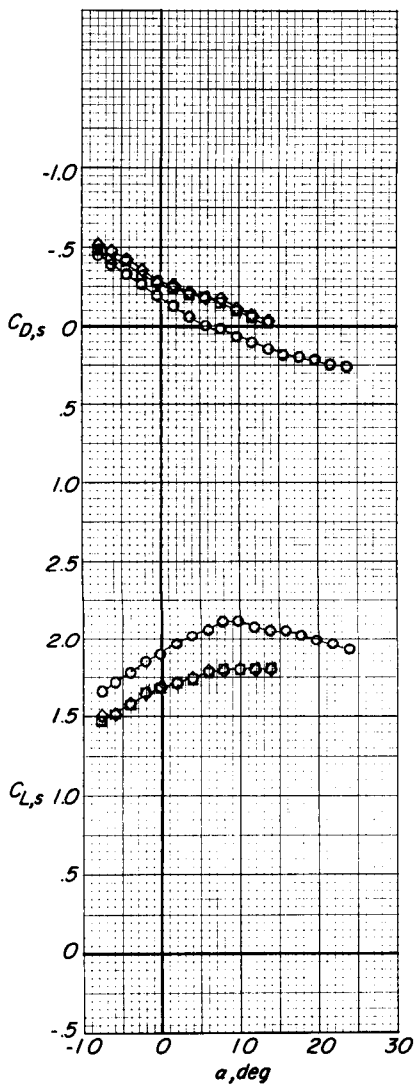

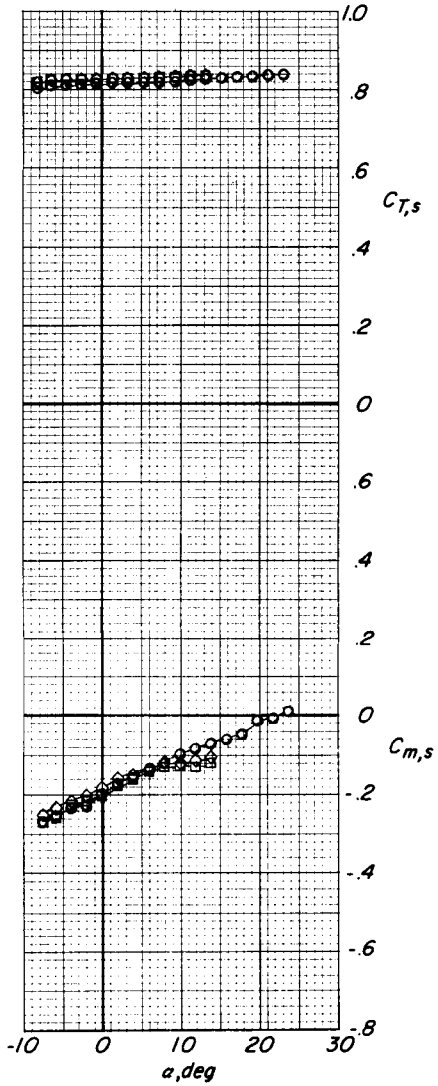

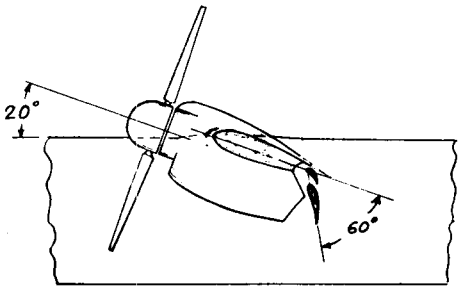

$h/\bar{c}$	Ground belt
○ 9.20	Stopped
□ 1.09	Stopped
◇ 1.09	Moving

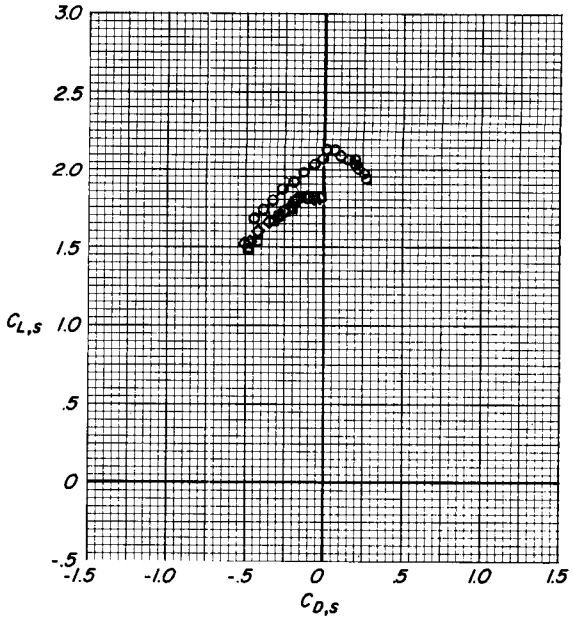

(b) $(C_{T,s})_{nominal} \approx 0.82$.

Figure 16.- Continued.

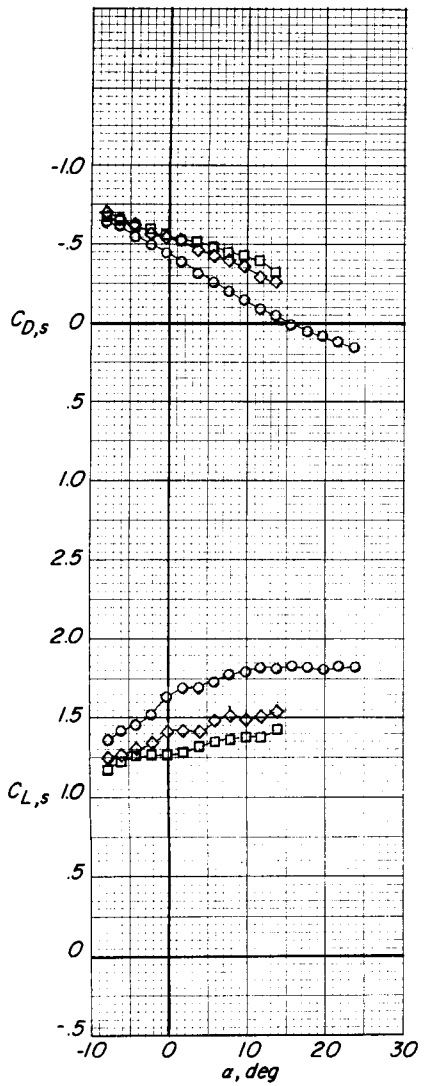

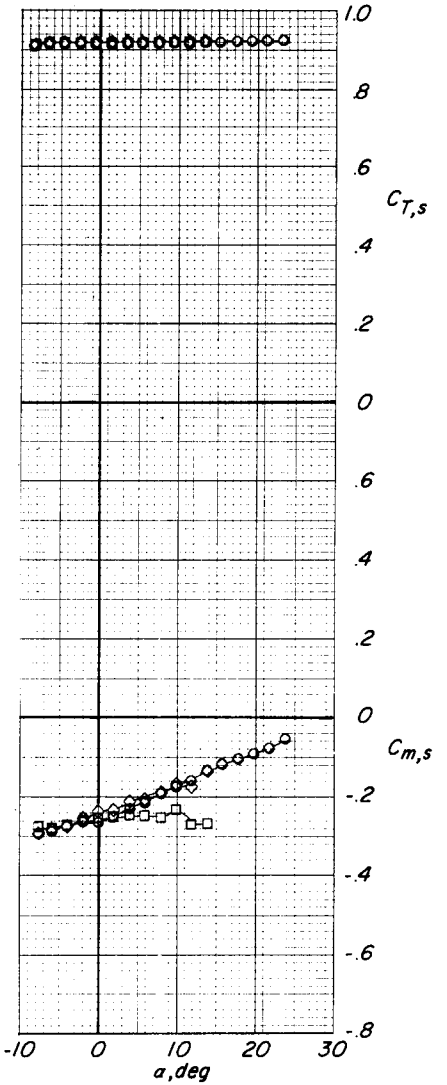

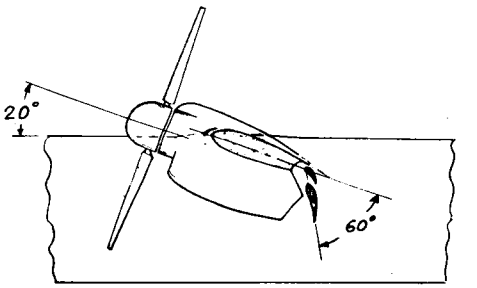

$h/\bar{c}$	Ground belt
○ 9.20	Stopped
□ 1.09	Stopped
◇ 1.09	Moving

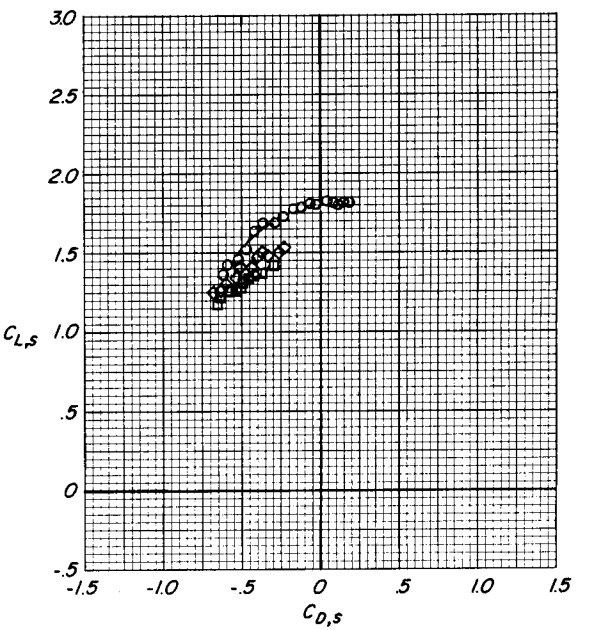

(c) $(C_{T,s})_{nominal} \approx 0.91$.

Figure 16.- Concluded.

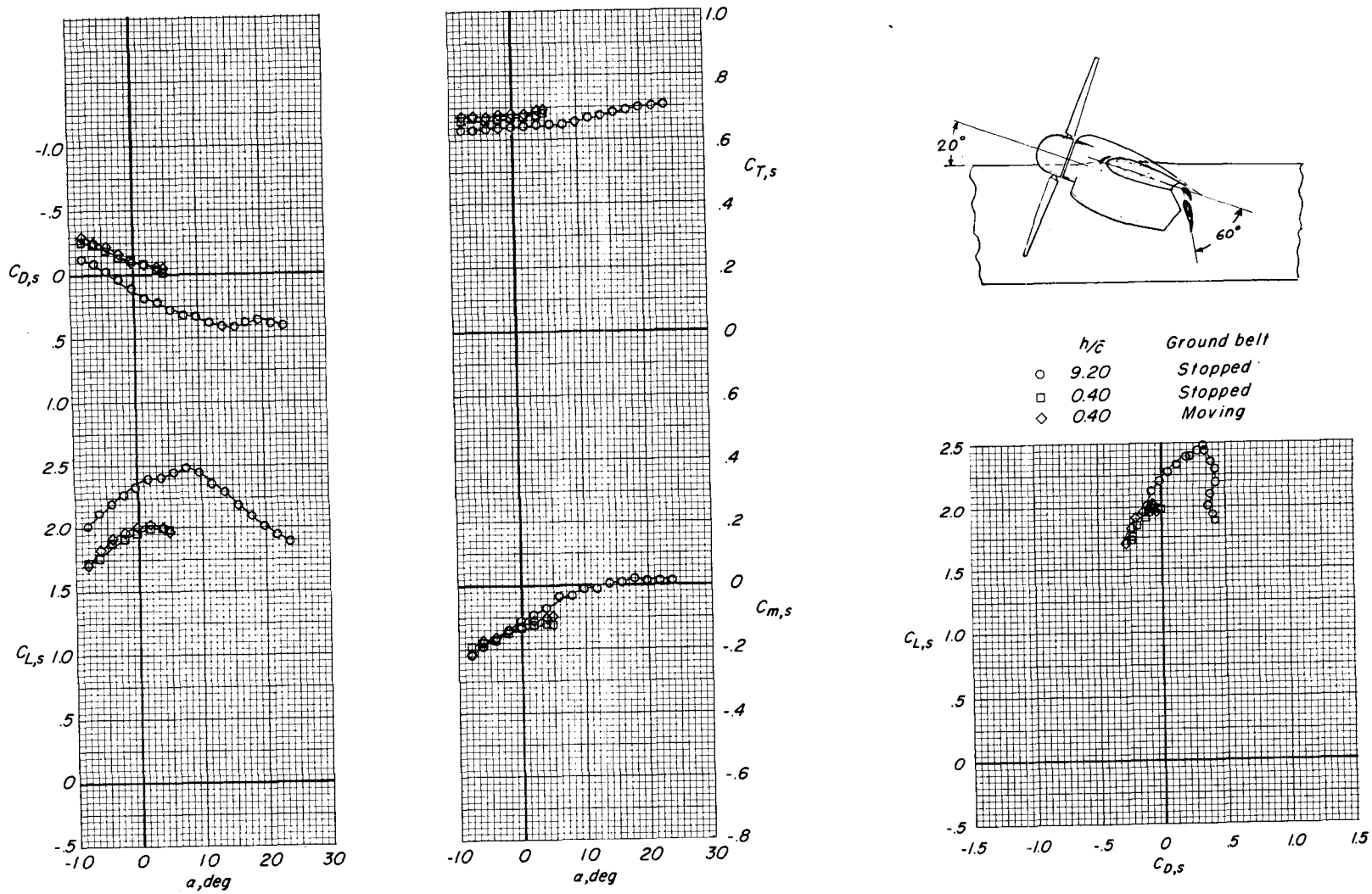

(a) $(C_{T,s})_{nominal} \approx 0.67$.

Figure 17.- Ground effect and effect of ground belt on the aerodynamic characteristics. $h/\bar{c} = 0.40$; $i_w = 20^0$; $\delta_f = 60^0$; horizontal tail off; slat on.

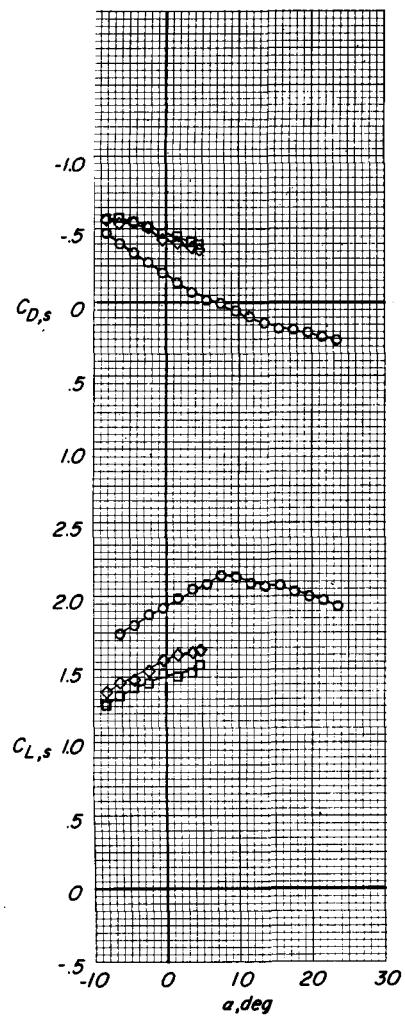

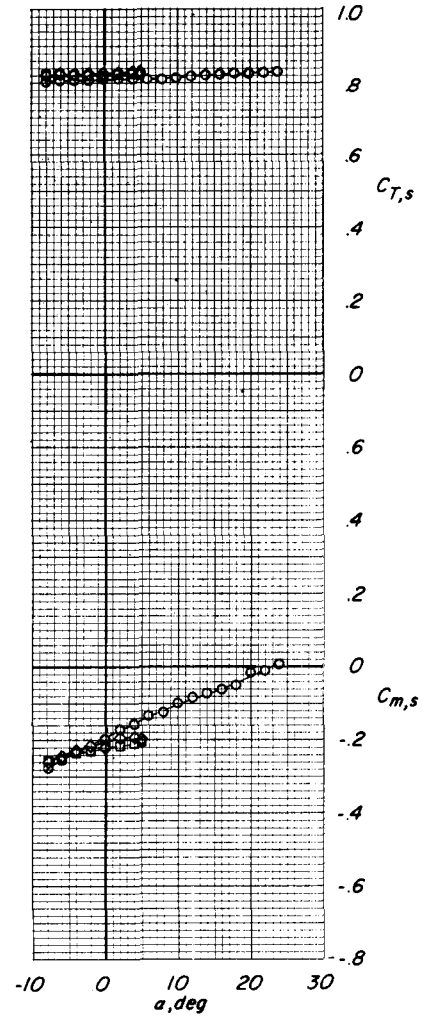

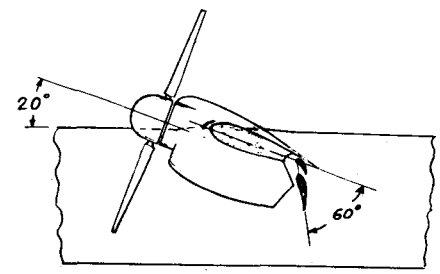

$h/\bar{c}$	Ground belt
○ 9.20	Stopped
□ 0.40	Stopped
◇ 0.40	Moving

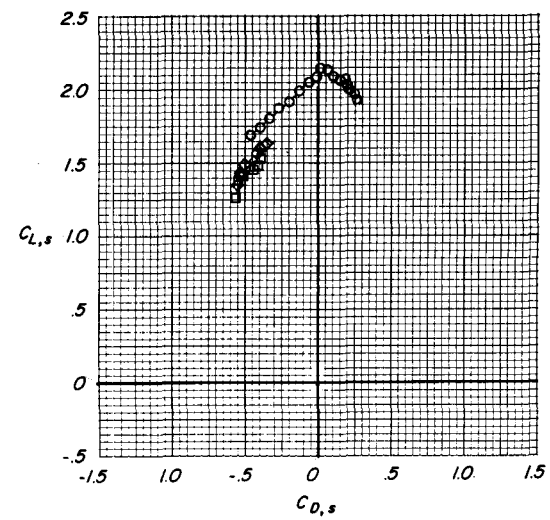

(b) $(C_{T,s})_{nominal} \approx 0.82$.

Figure 17.- Continued.

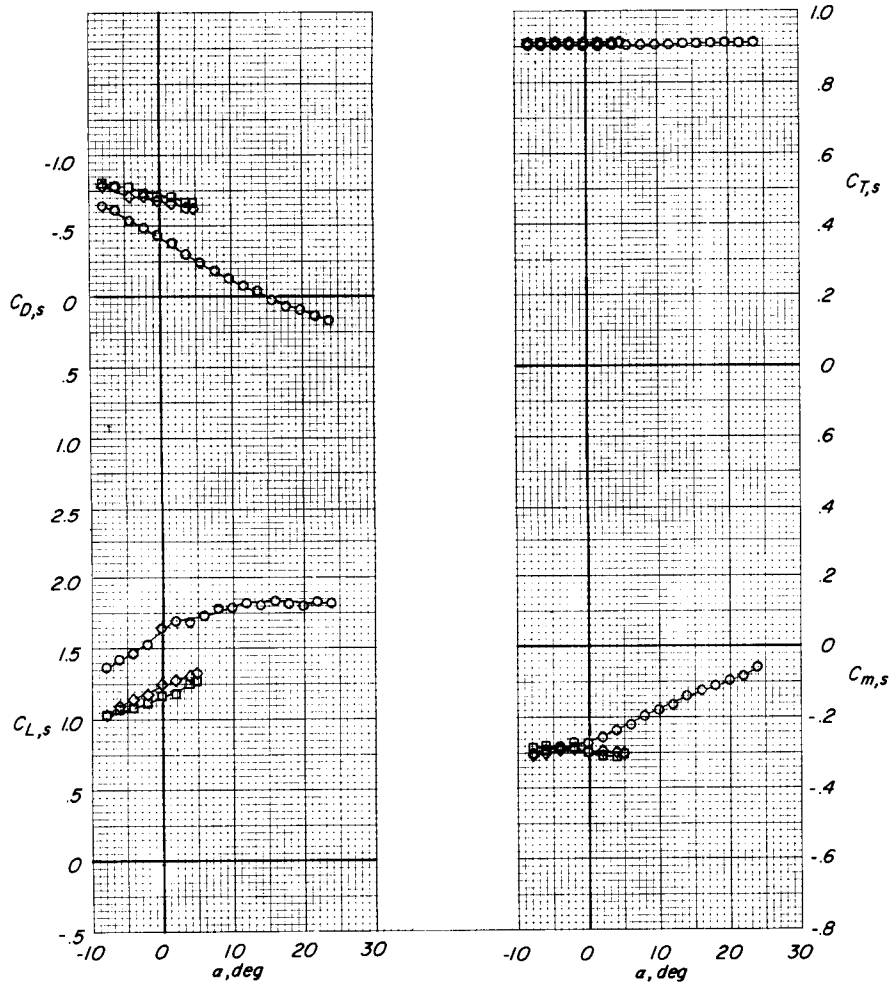

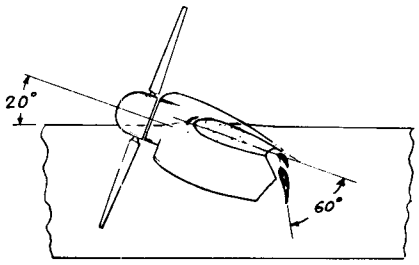

h/c	Ground belt
○ 9.20	Stopped
□ 0.40	Stopped
◇ 0.40	Moving

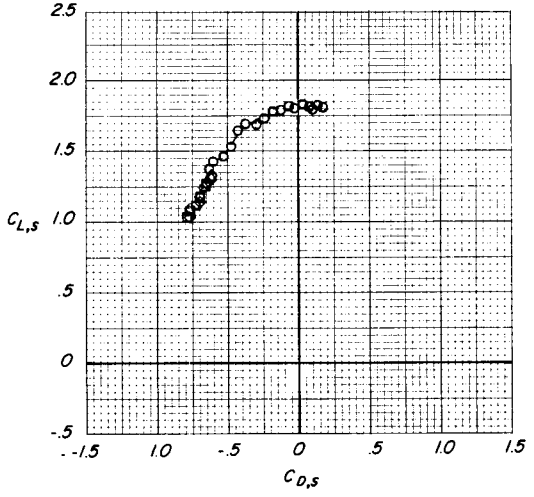

(c) $(C_{T,s})_{nominal} \approx 0.91$.

Figure 17.- Concluded.

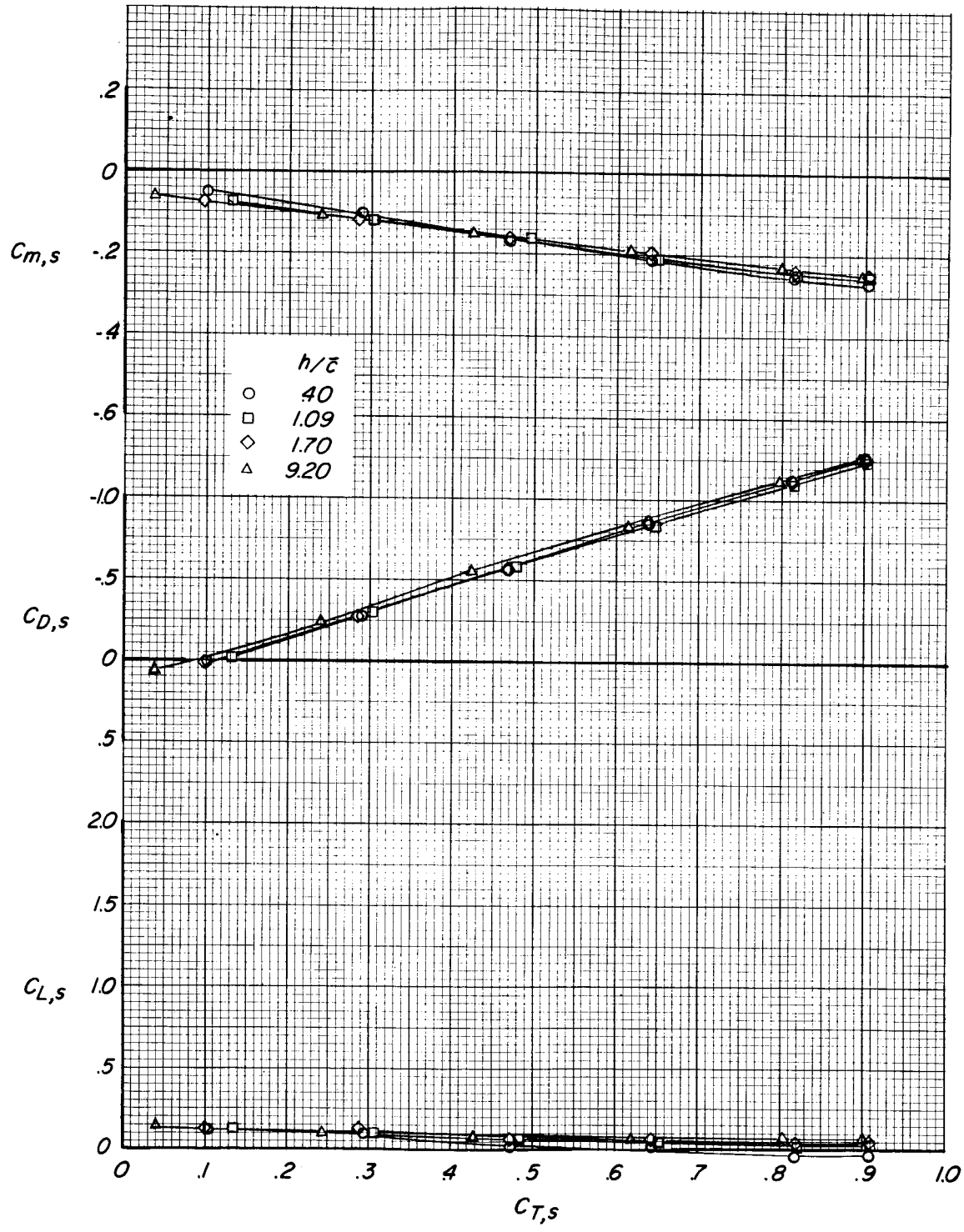

(a) Ground belt stopped.

Figure 18.- Effect of ground height on the aerodynamic coefficients for a range of thrust coefficients. $i_w = 0^0$; $\delta_f = 0^0$; horizontal tail off; $\alpha = 0^0$; slat off.

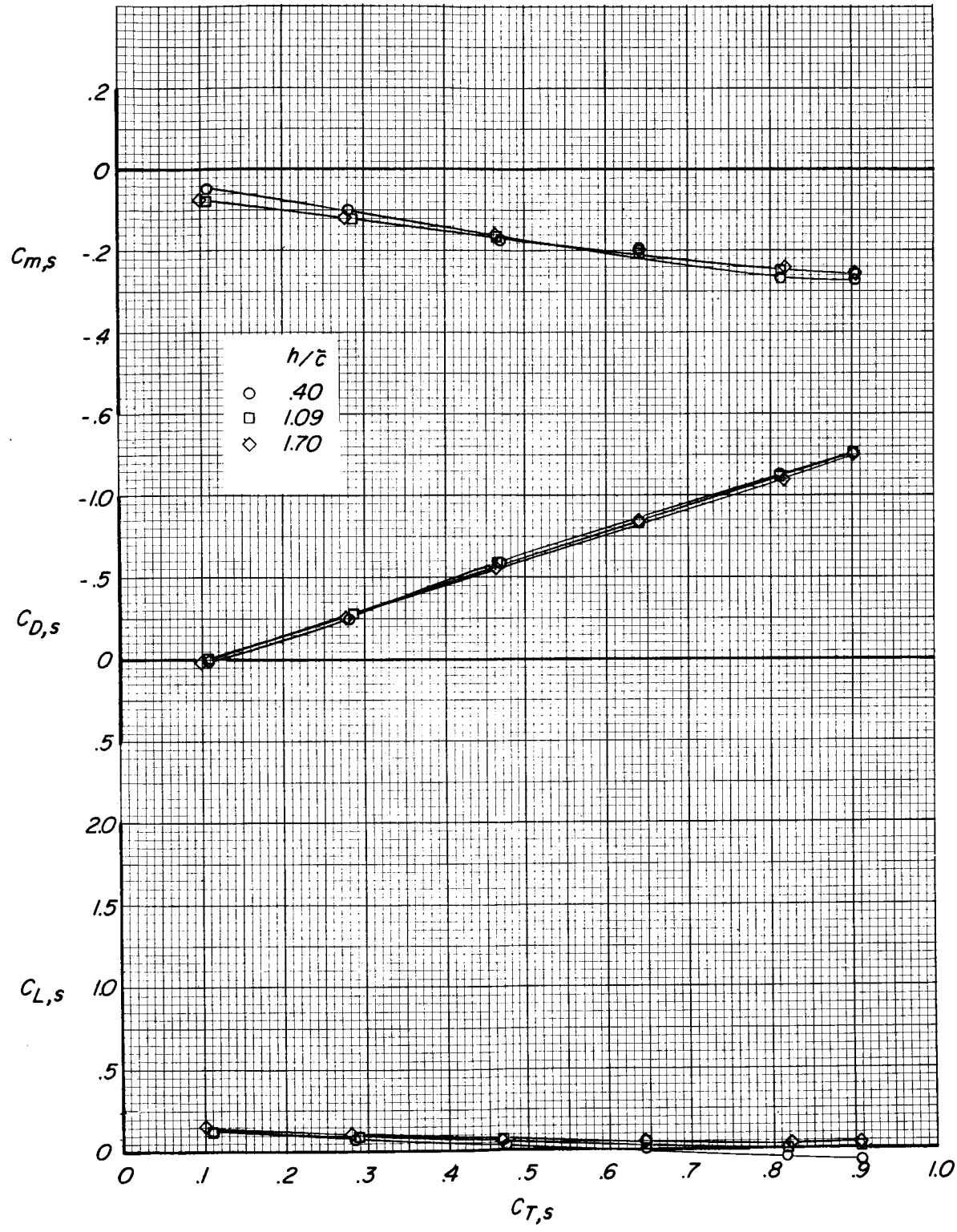

(b) Ground belt moving.

Figure 18.- Concluded.

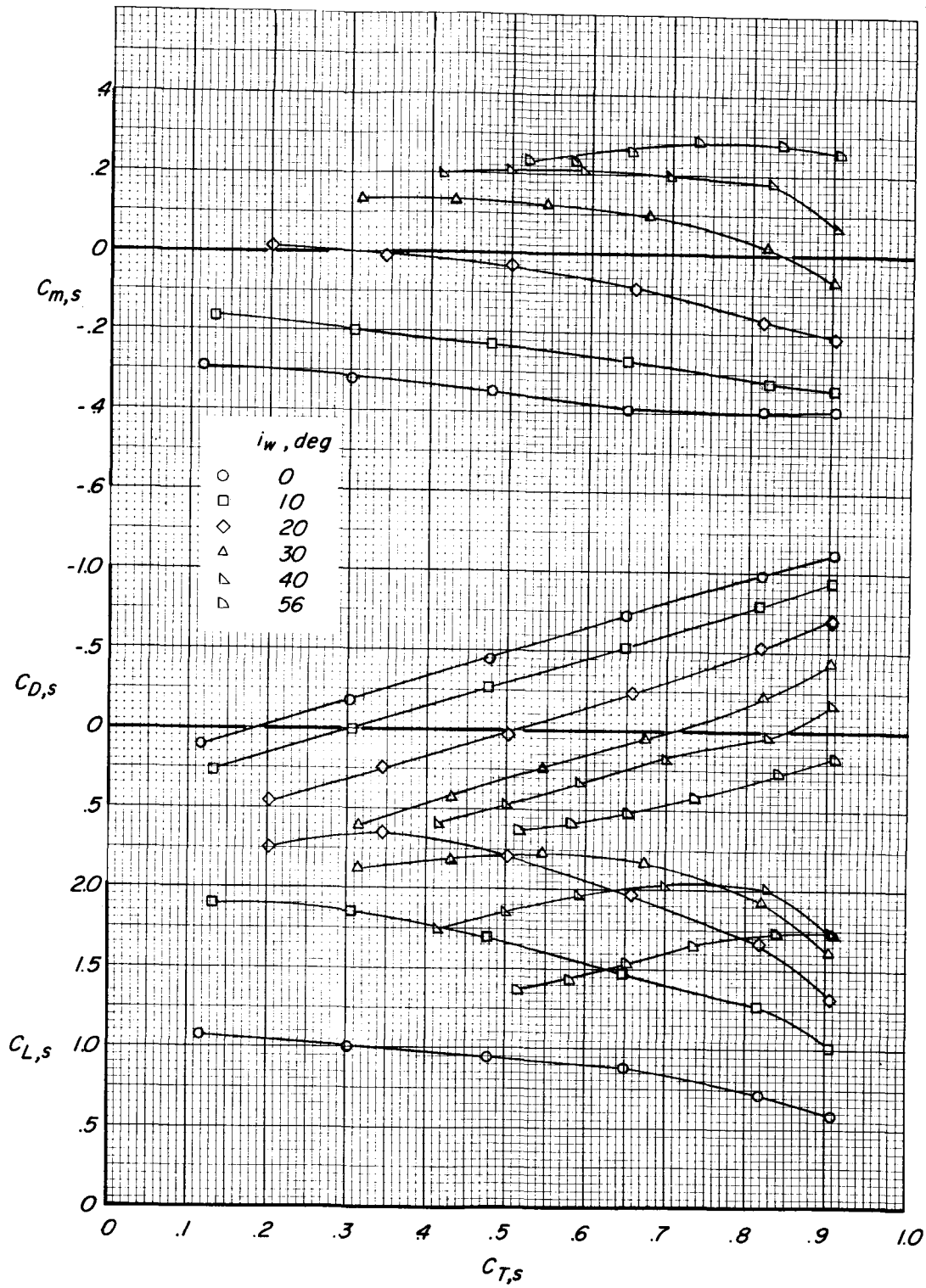

(a) $h/\bar{c}$ = 9.20; ground belt stopped.

Figure 19.- Effect of wing incidence on the aerodynamic coefficients for a range of thrust coefficients. $\delta_f = 40^0$; $\alpha = 0^0$; horizontal tail off; slat on.

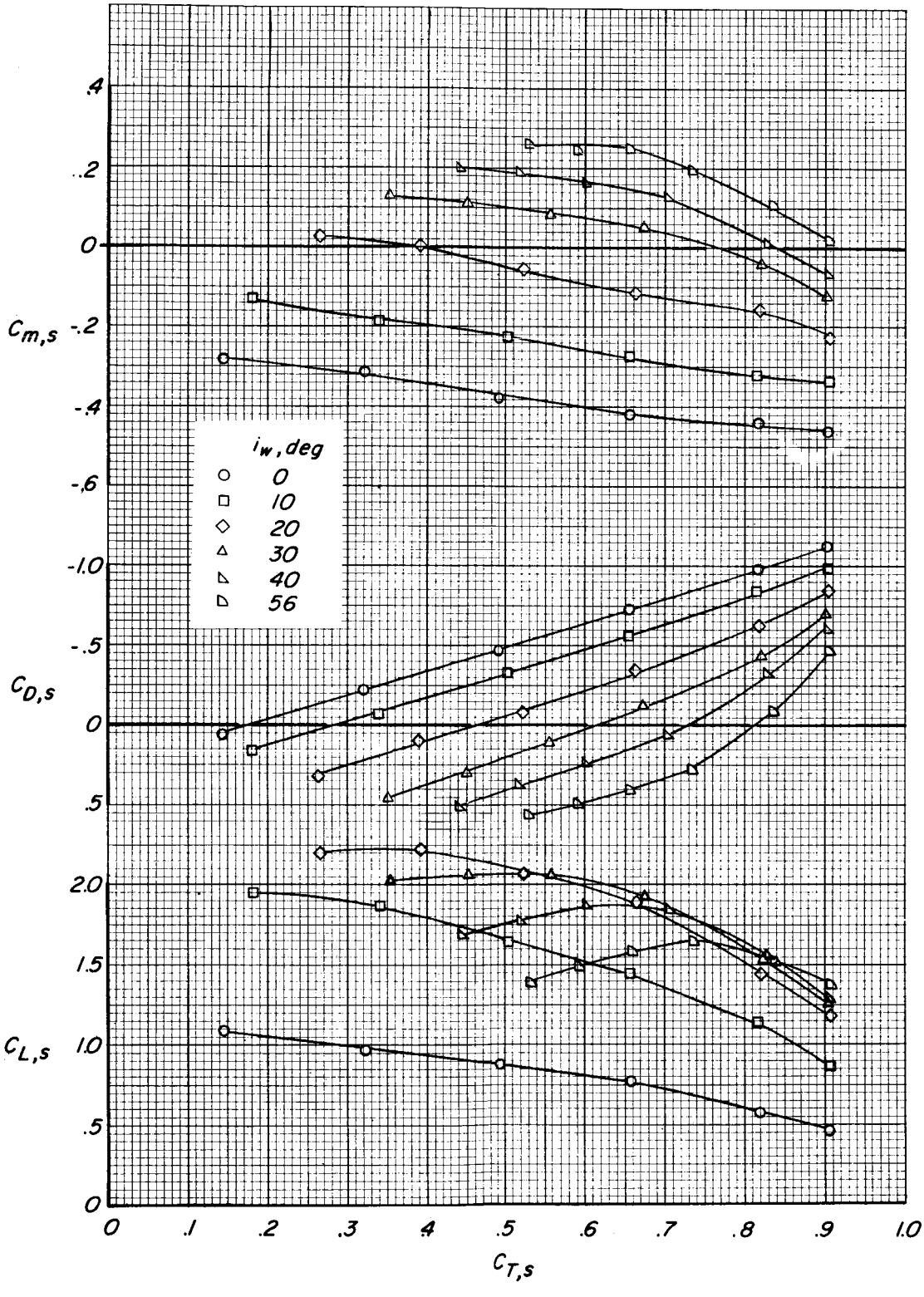

(b) $h/\bar{c}$ = 0.40; ground belt stopped.

Figure 19.- Continued.

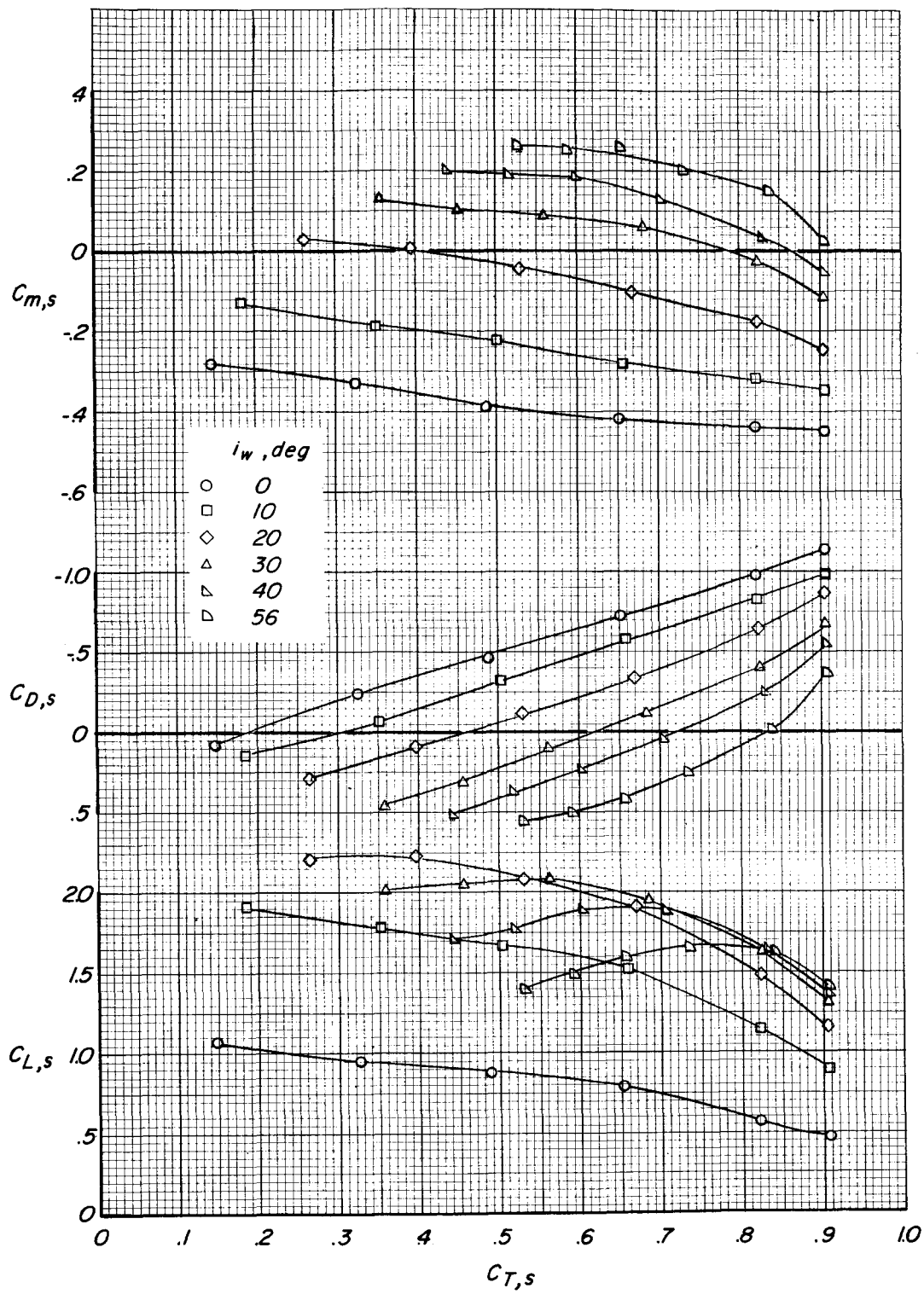

(c) $h/\bar{c}$ = 0.40; ground belt moving.

Figure 19.- Concluded.

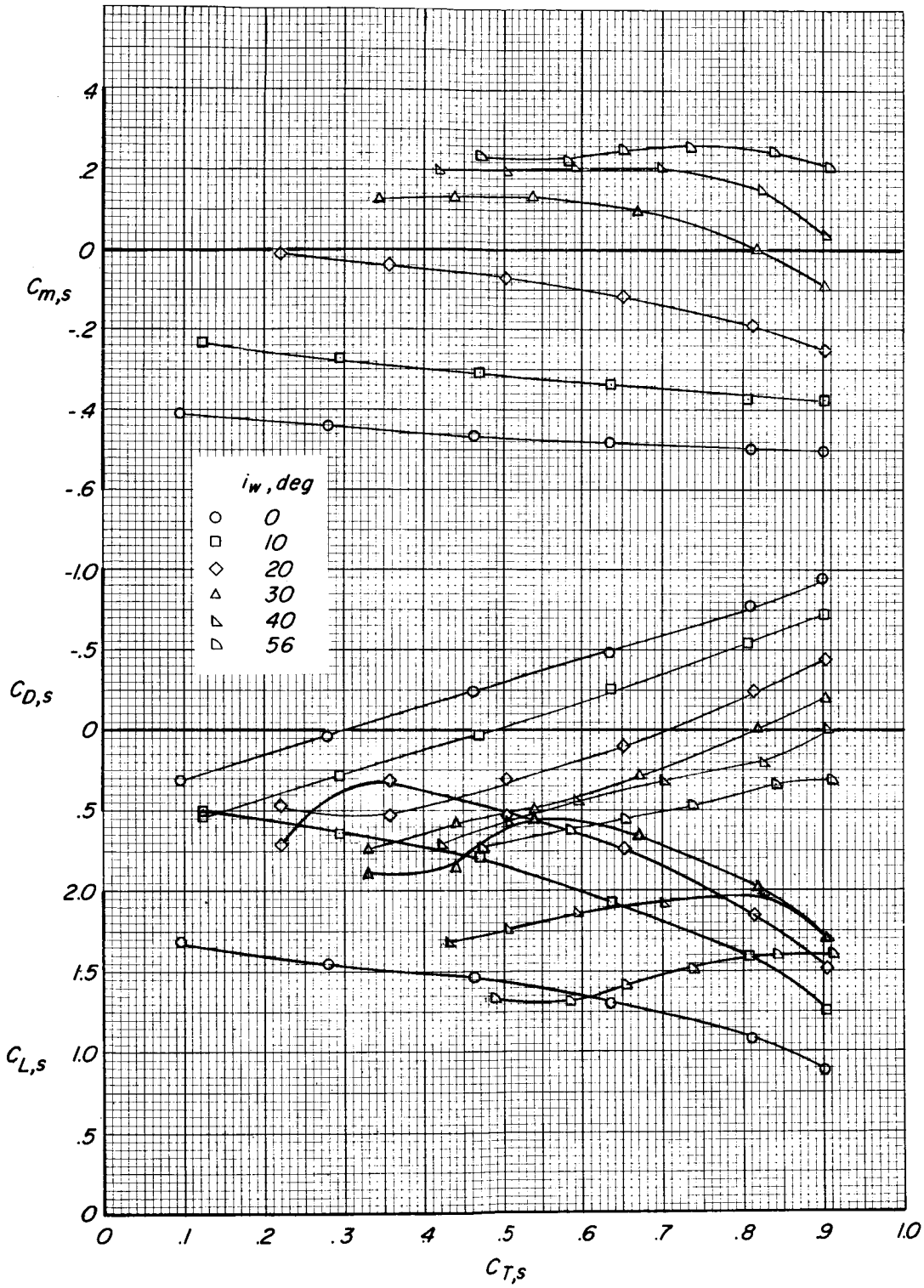

(a) $h/\bar{c}$ = 9.20; ground belt stopped.

Figure 20.- Effect of wing incidence on the aerodynamic coefficients for a range of thrust coefficients. $\delta_f = 60^0$; $\alpha = 0^0$; horizontal tail off; slat on.

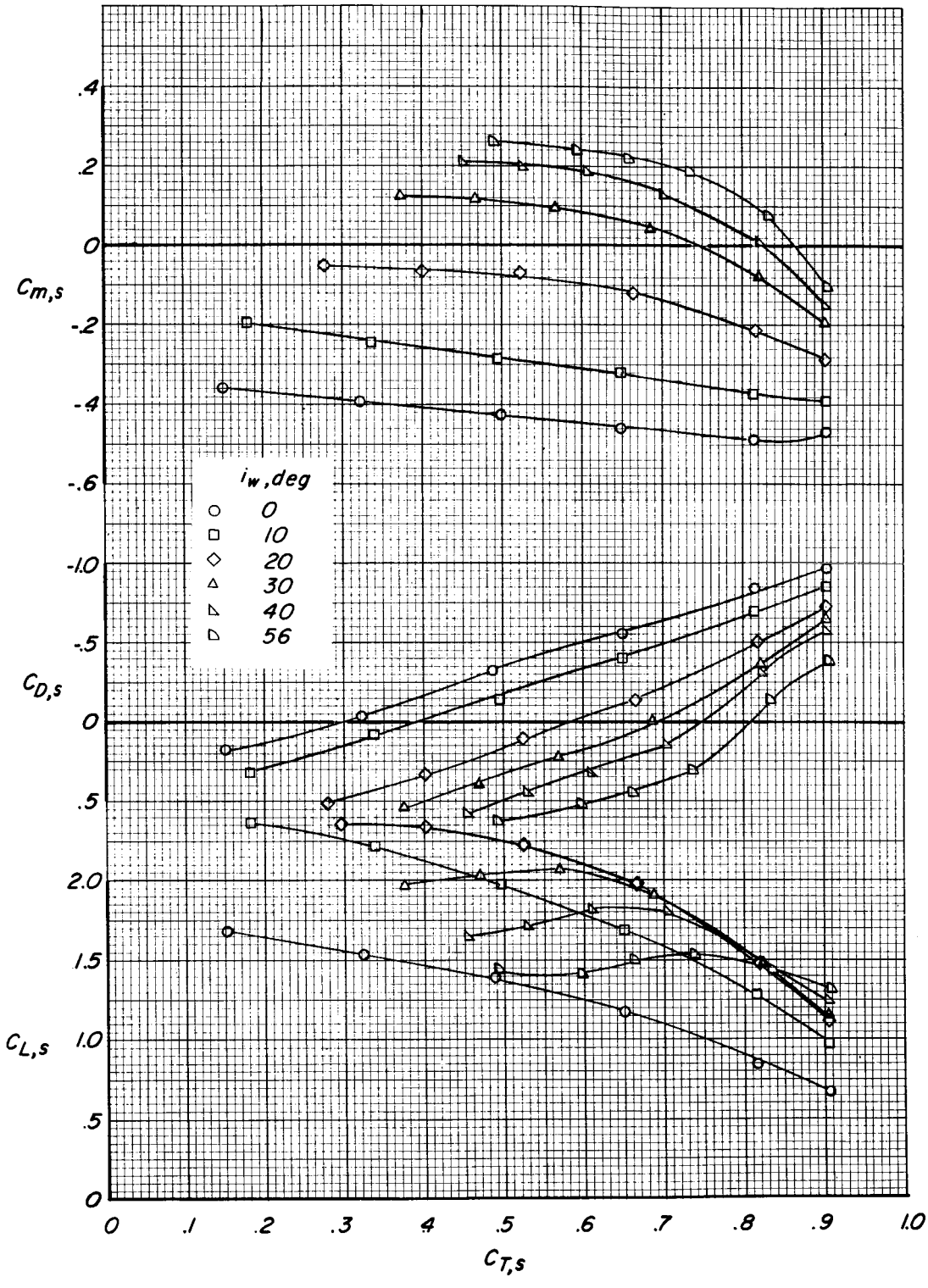

(b) $h/\bar{c}$ = 0.40; ground belt stopped.

Figure 20.- Continued.

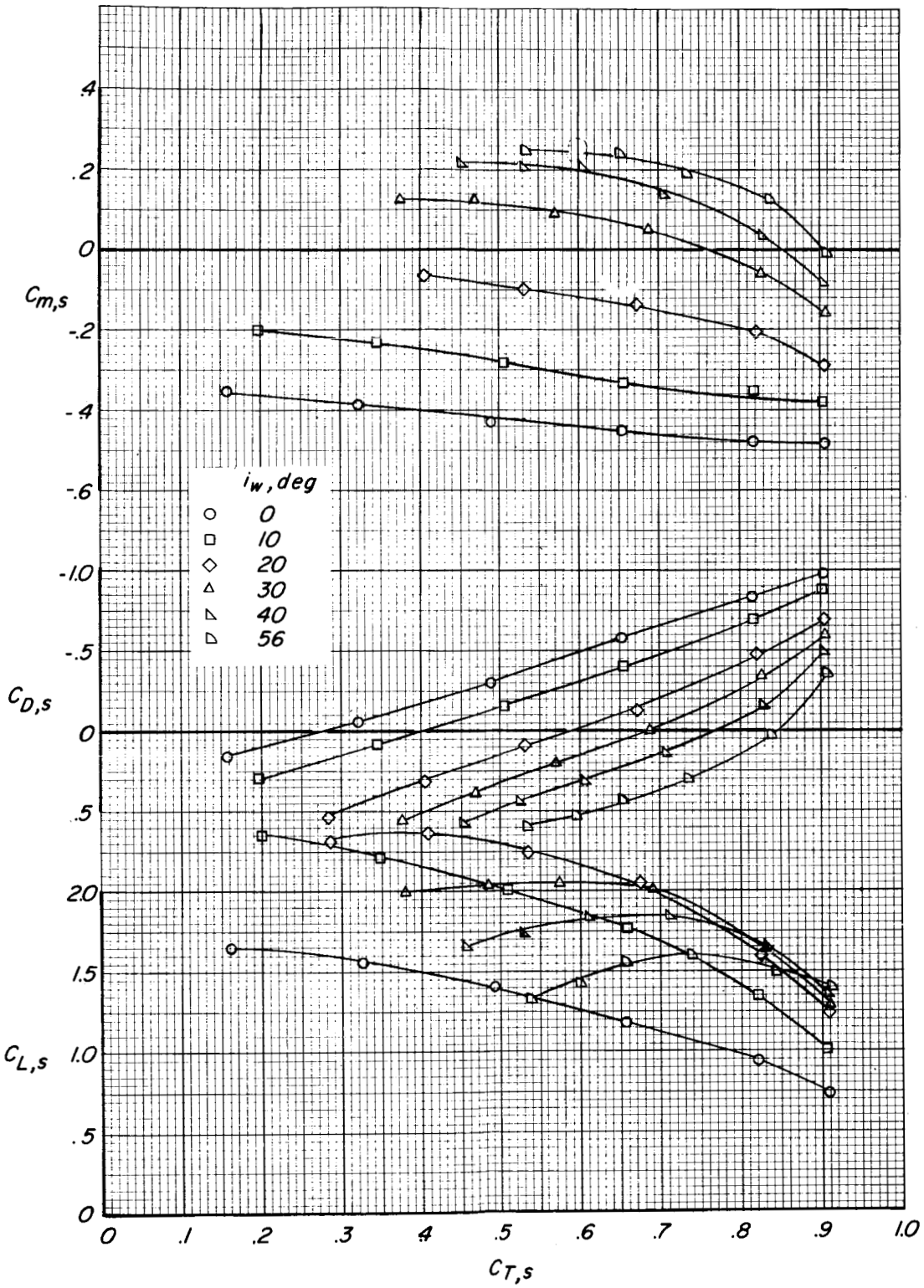

(c) $h/\bar{c} = 0.40$; ground belt moving.

Figure 20.- Concluded.

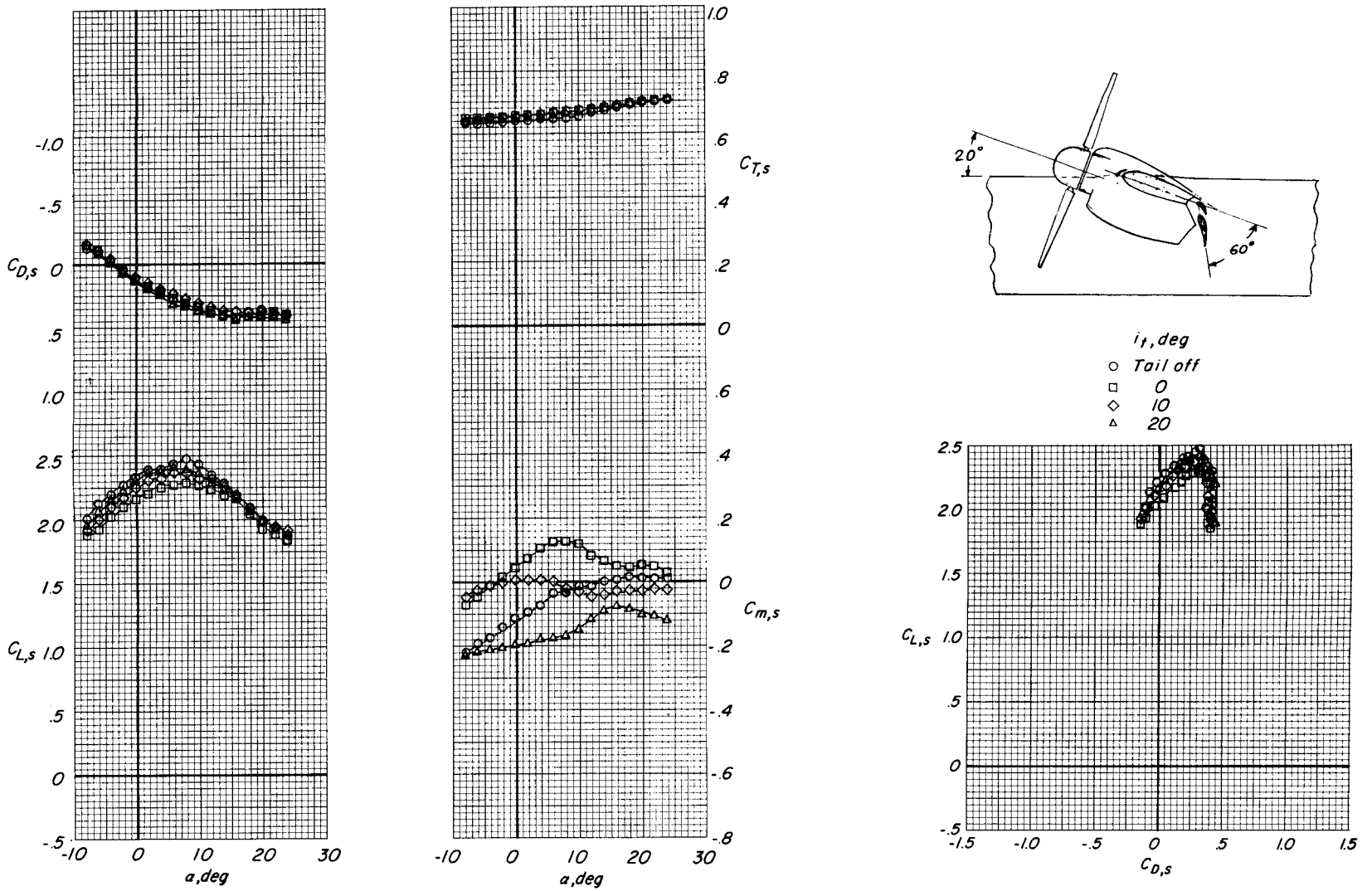

(a) $(C_{T,s})_{nominal} \approx 0.65$.

Figure 21.- Effect of horizontal-tail incidence on the aerodynamic characteristics. Ground belt stopped; $h/\bar{c} = 9.20 \approx \infty$; $i_w = 20^0$; $\delta_f = 60^0$; slat on.

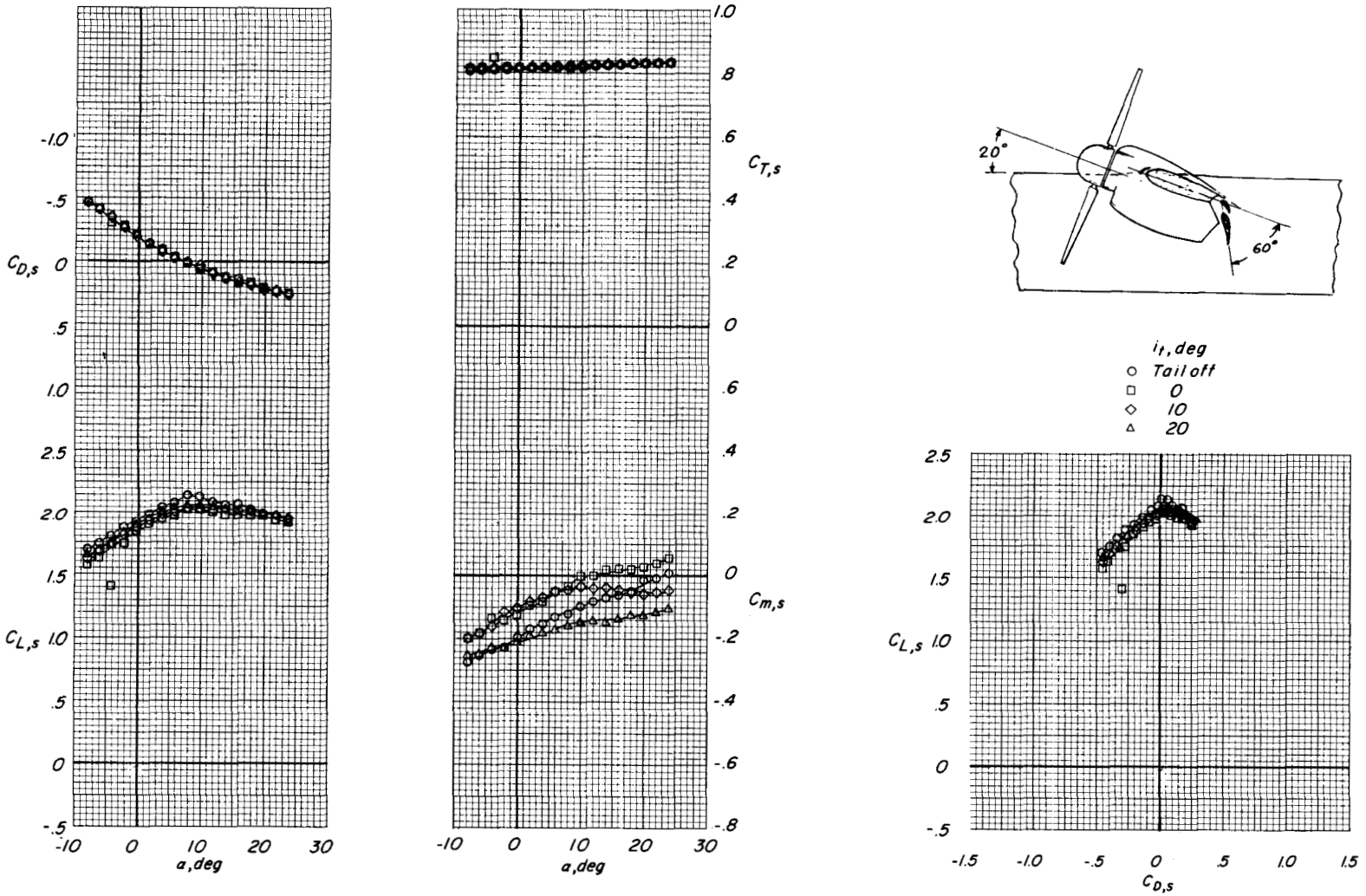

(b) $(C_{T,s})_{nominal} \approx 0.81$.

Figure 21.- Continued.

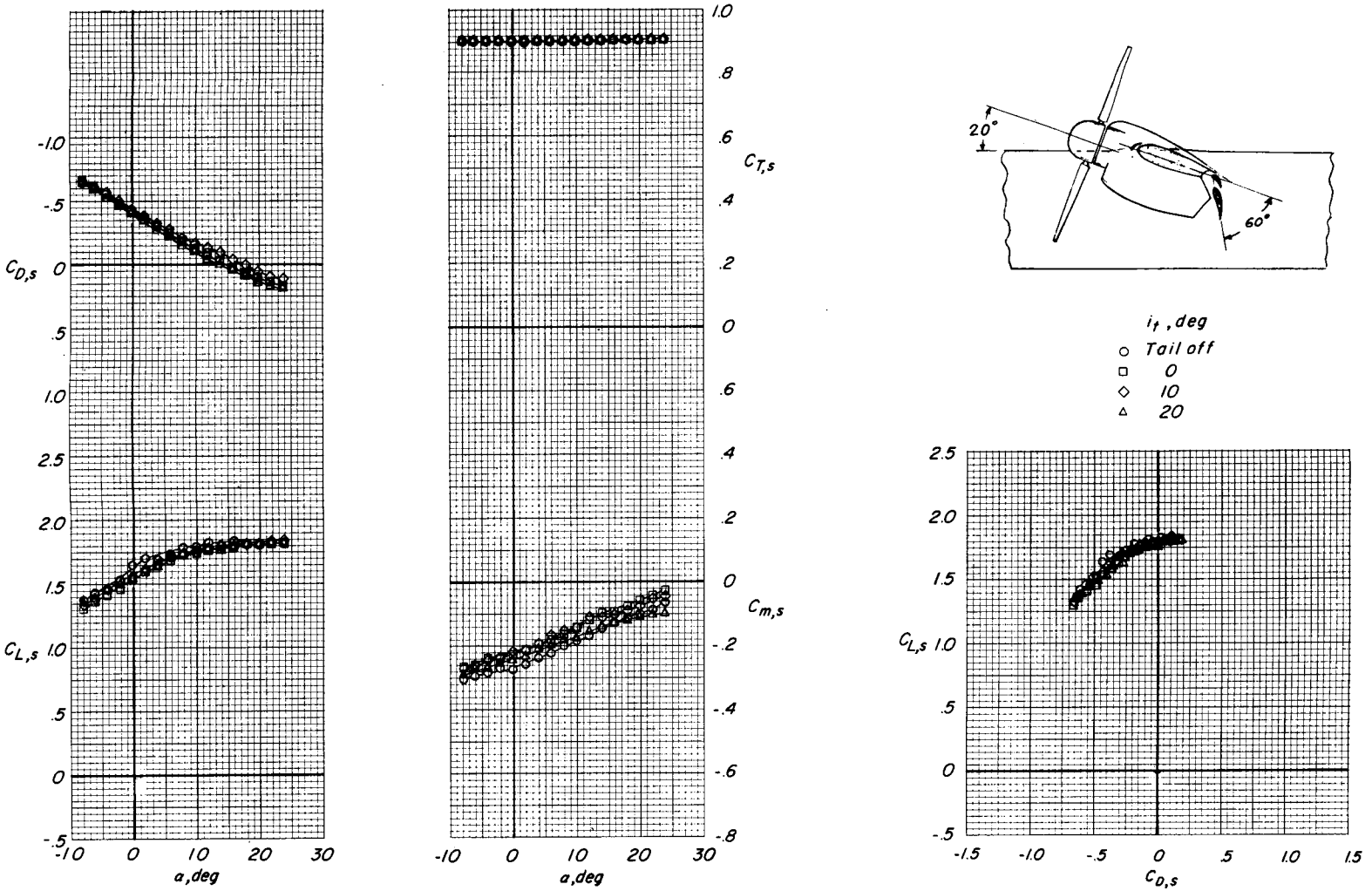

(c) $(C_{T,s})_{nominal} \approx 0.91$.

Figure 21.- Concluded.

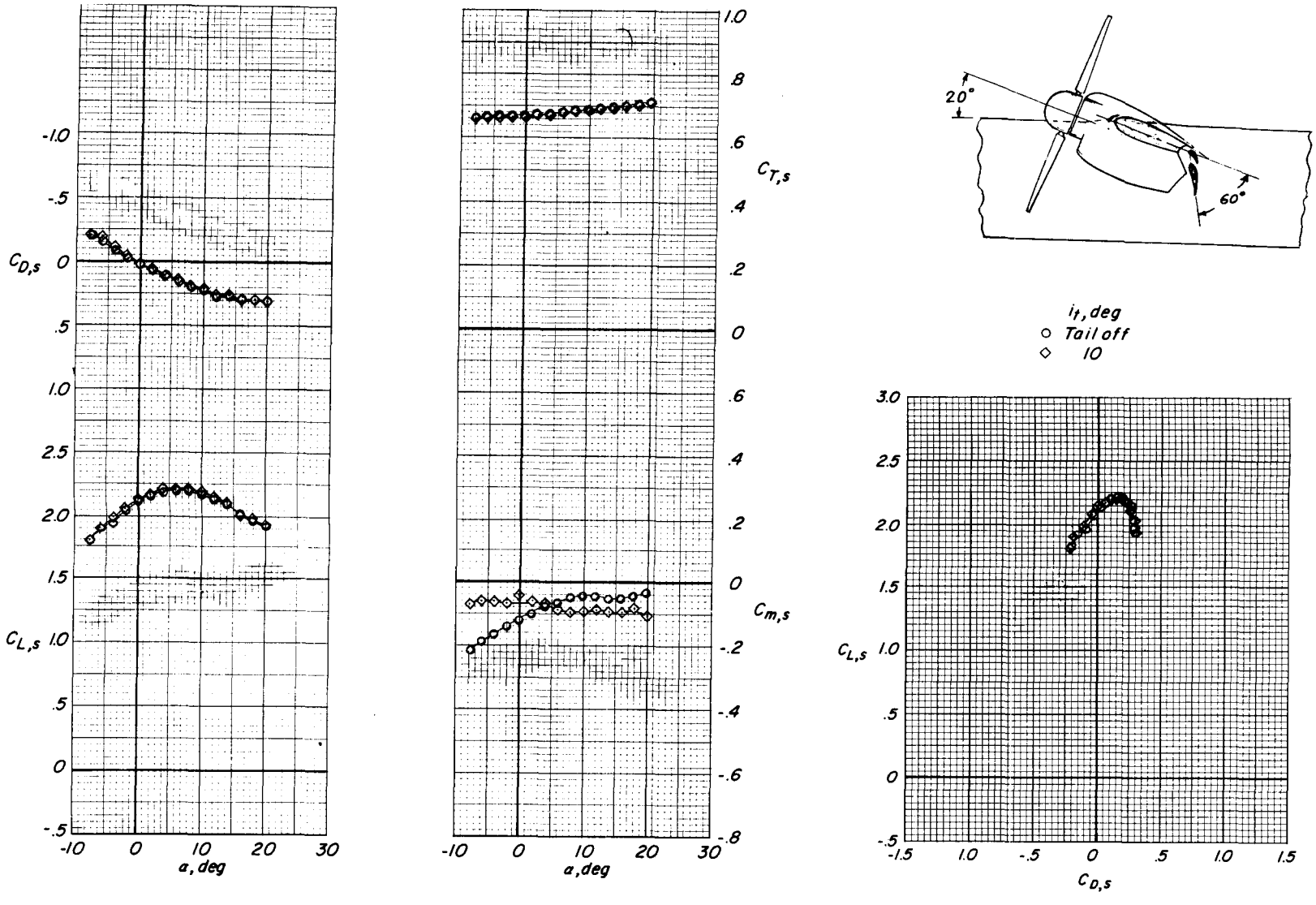

(a) $(C_{T,s})_{nominal} \approx 0.66$.

Figure 22.- Effect of horizontal-tail incidence on the aerodynamic characteristics. Ground belt stopped; $h/\bar{c} = 1.70$; $i_w = 20^0$; $\delta_f = 60^0$; slat on.

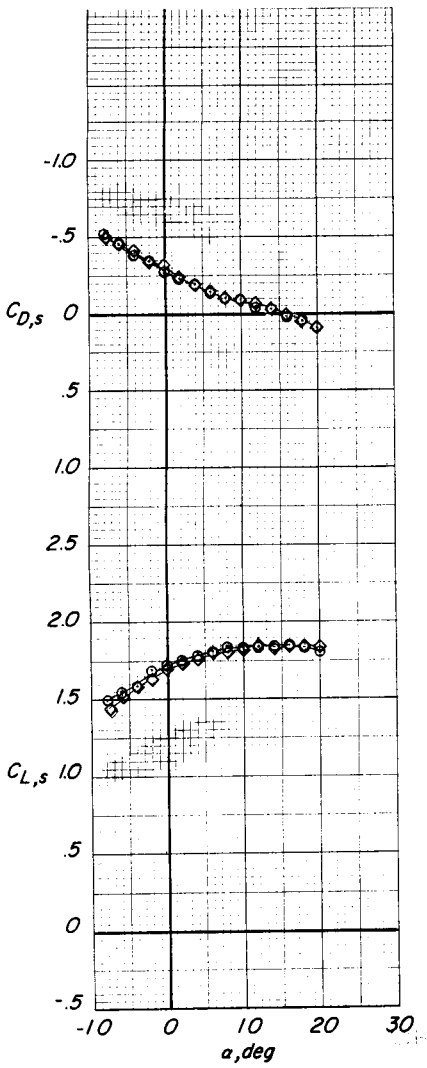

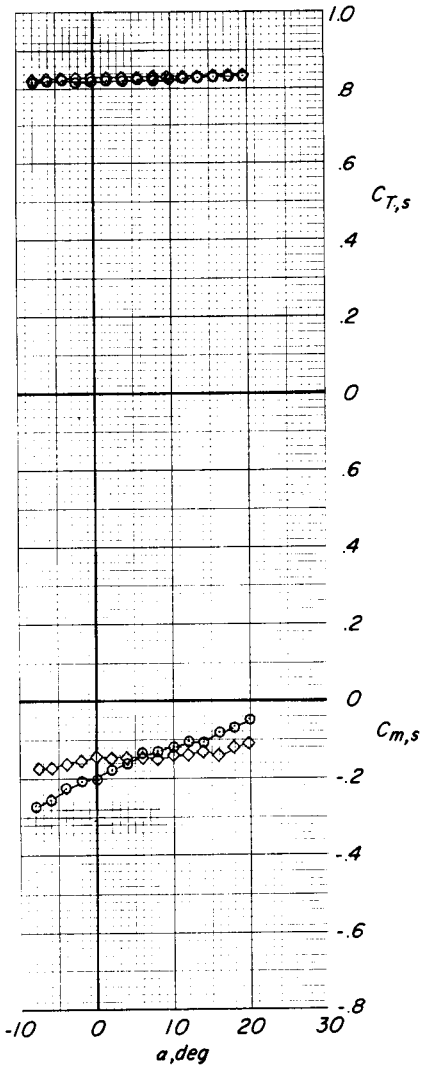

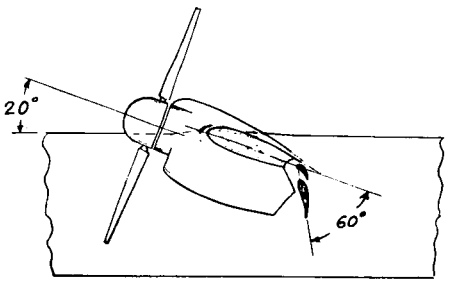

i_t, deg
○ Tail off
◇ 10

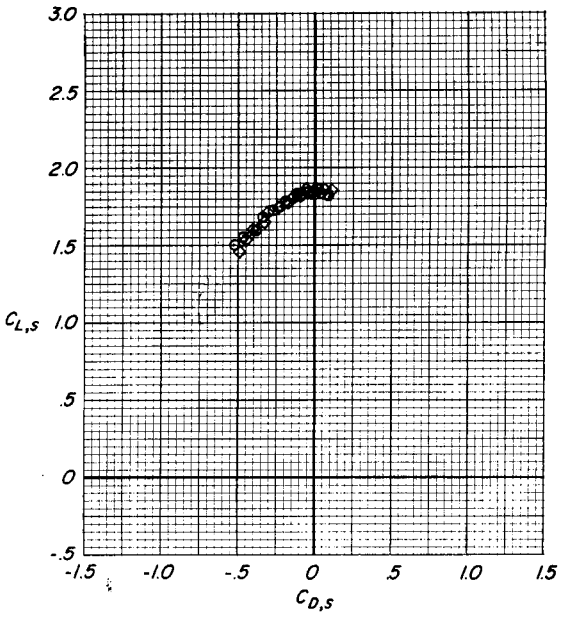

(b) $(C_{T,s})_{nominal} \approx 0.83$.

Figure 22.- Continued.

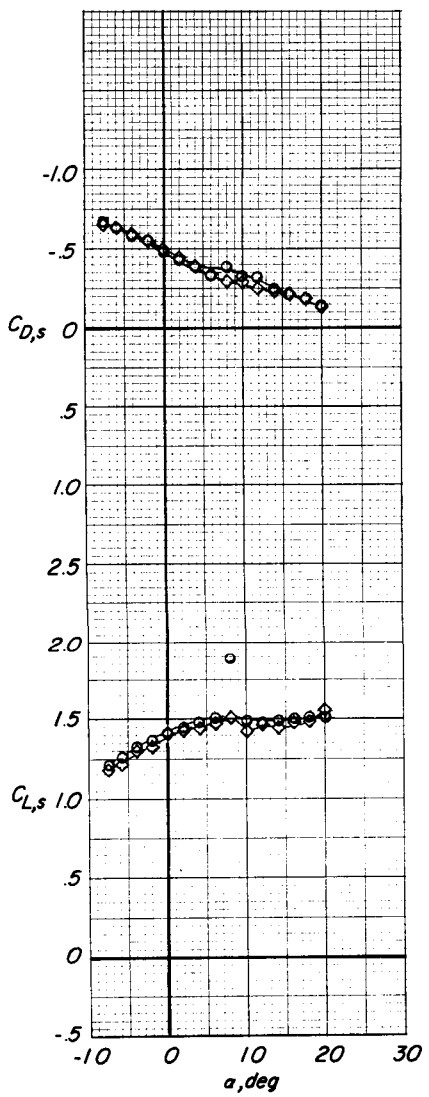

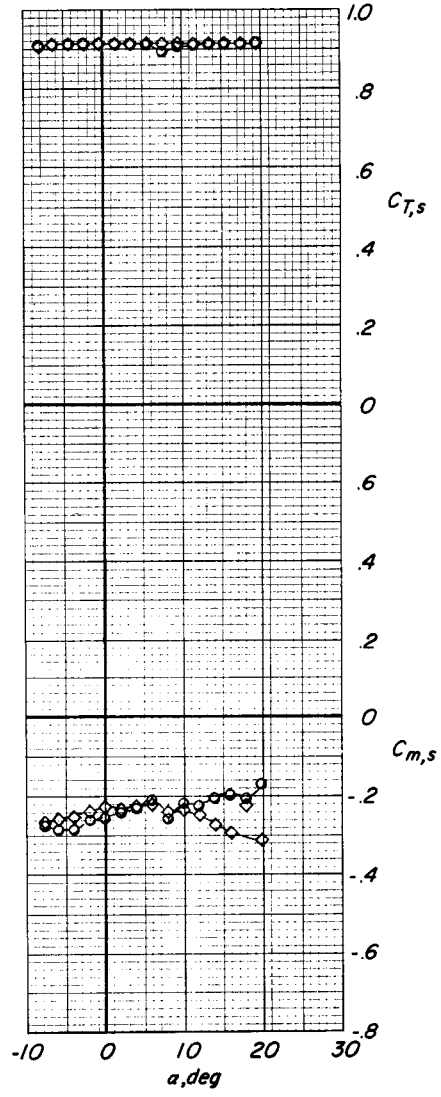

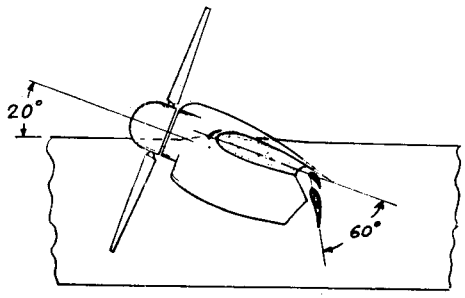

i_t, deg
○ Tail off
◇ 10

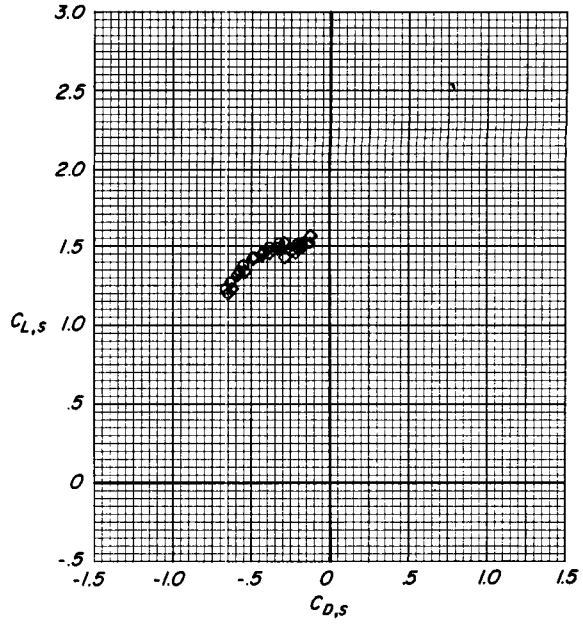

(c) $(C_{T,s})_{nominal} \approx 0.91$.

Figure 22.- Concluded.

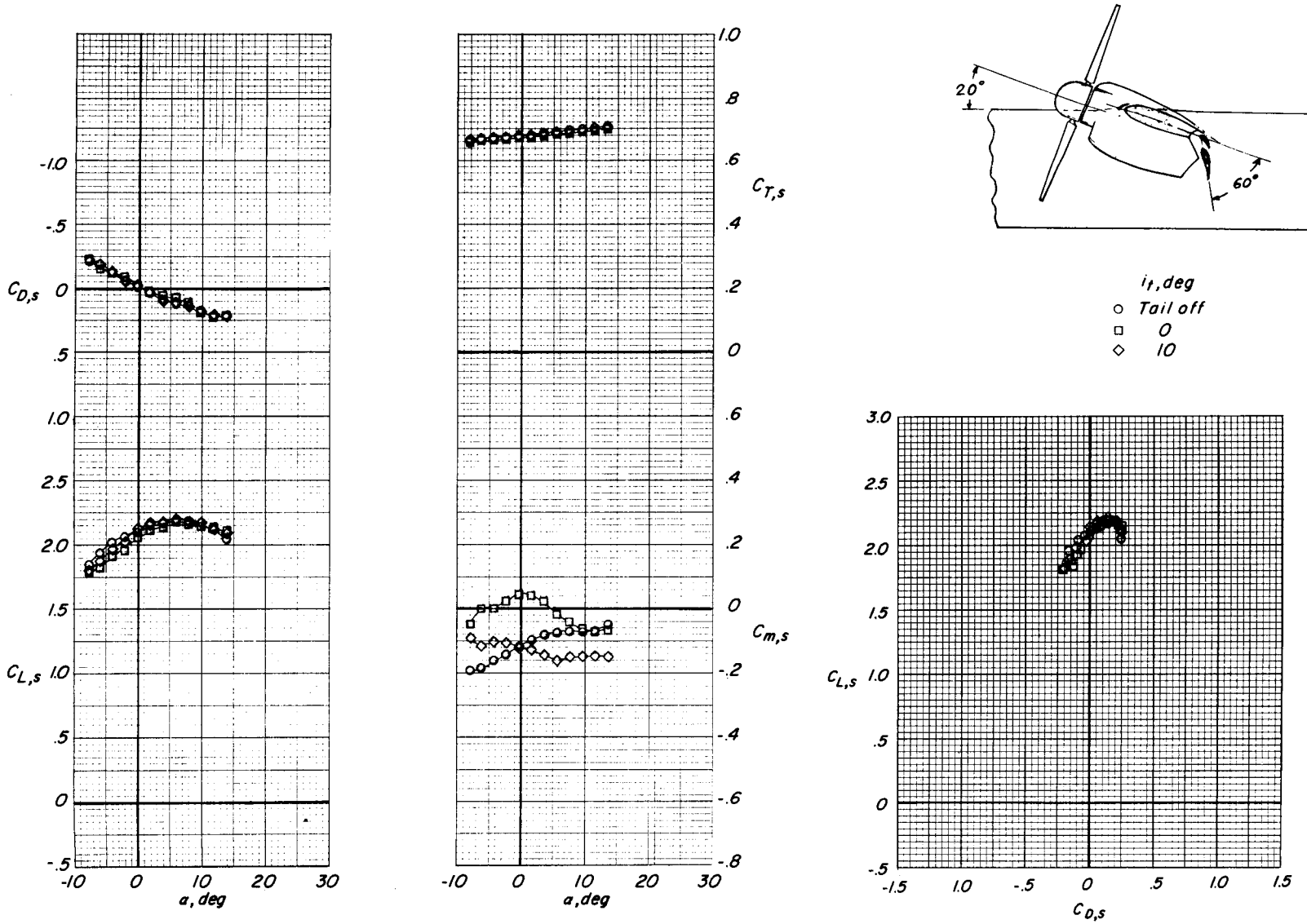

(a) $(C_{T,s})_{nominal} \approx 0.68$.

Figure 23.- Effect of horizontal-tail incidence on the aerodynamic characteristics. Ground belt stopped; $h/\bar{c} = 1.09$; $i_w = 20^0$; $\delta_f = 60^0$; slat on.

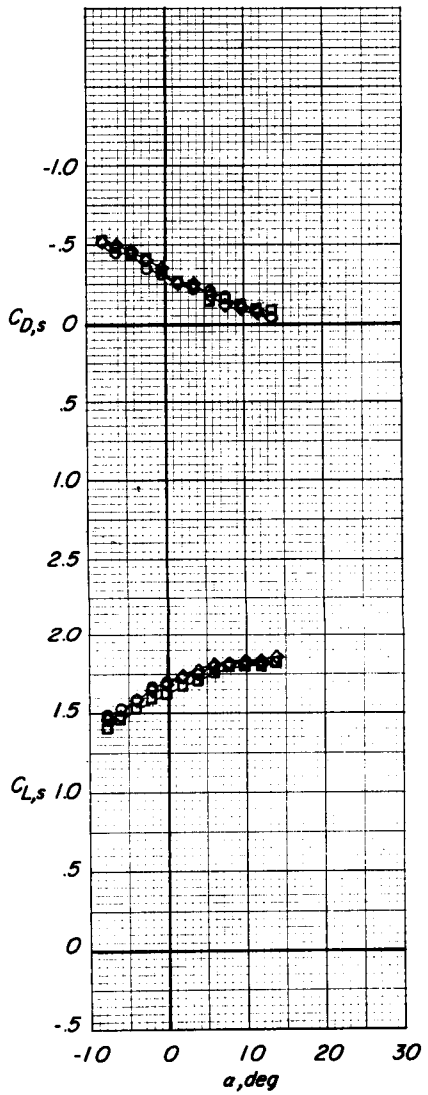

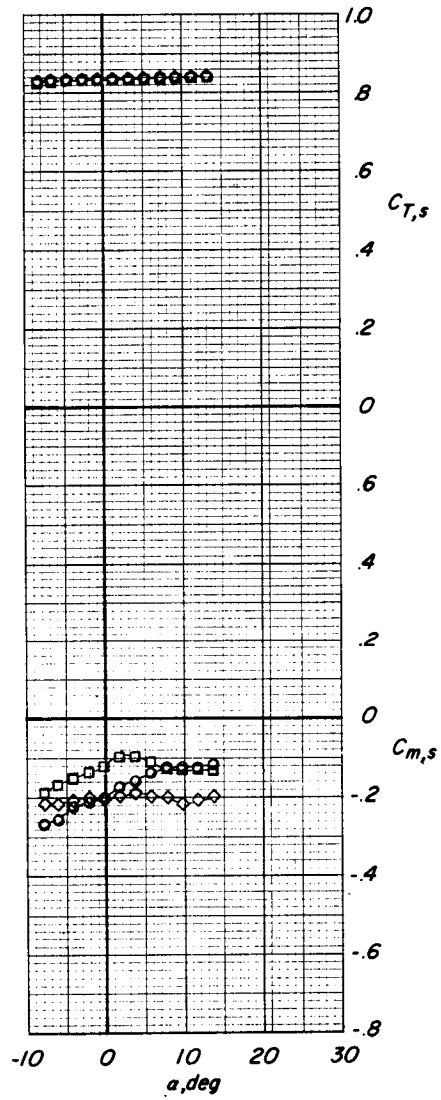

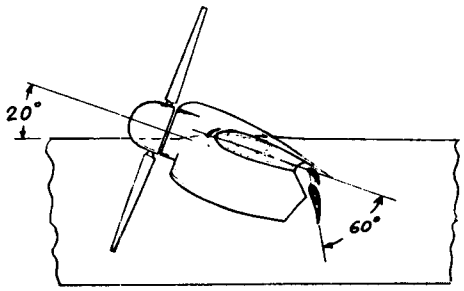

i_t, deg
○ Tail off
□ 0
◇ 10

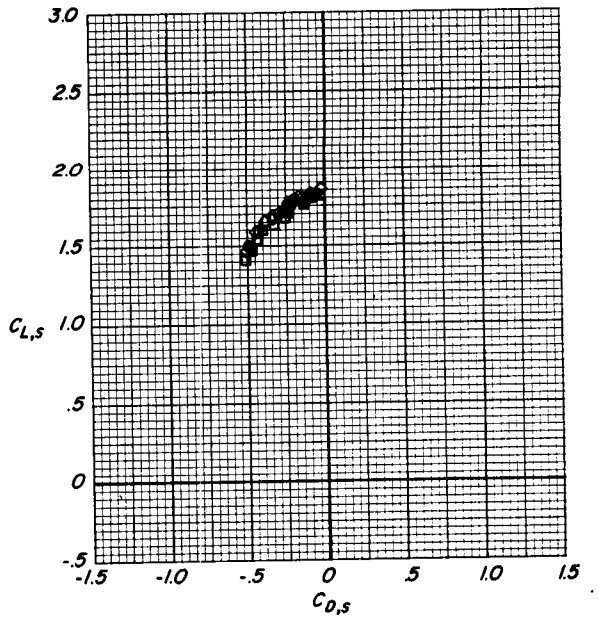

(b) $(C_{T,s})_{nominal} \approx 0.83$.

Figure 23.- Continued.

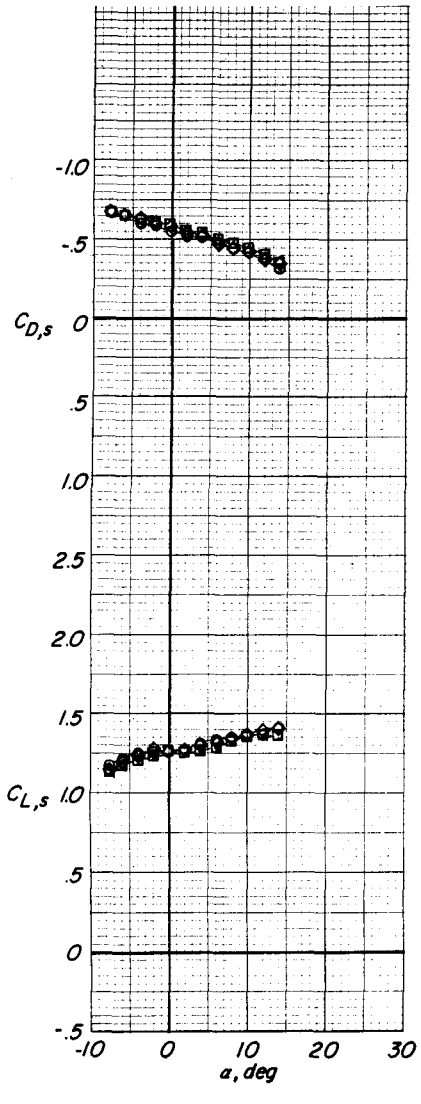

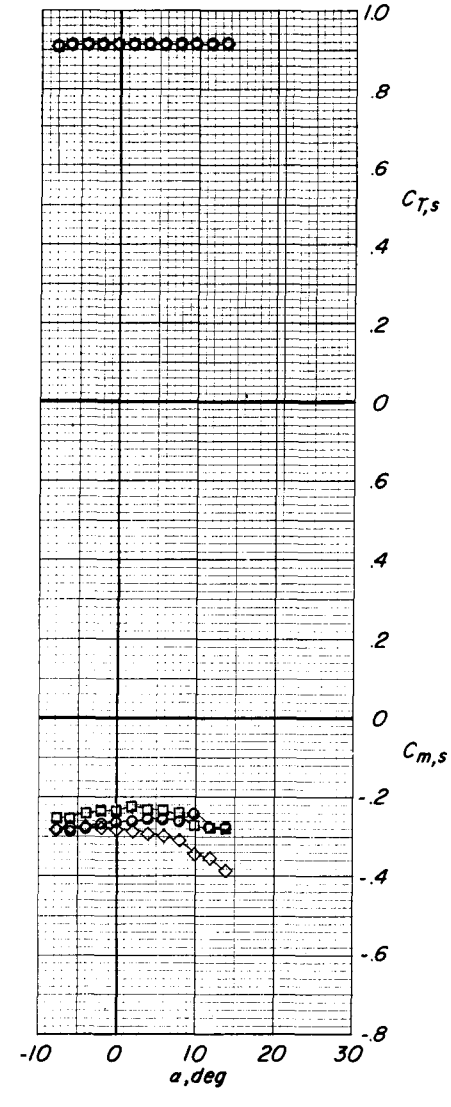

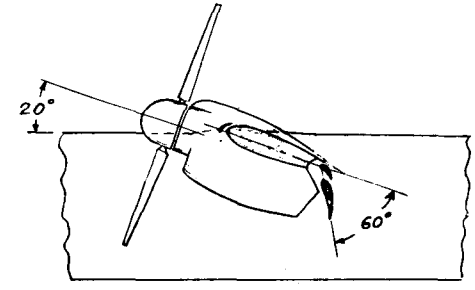

i_t, deg
○ Tail off
□ 0
◇ 10

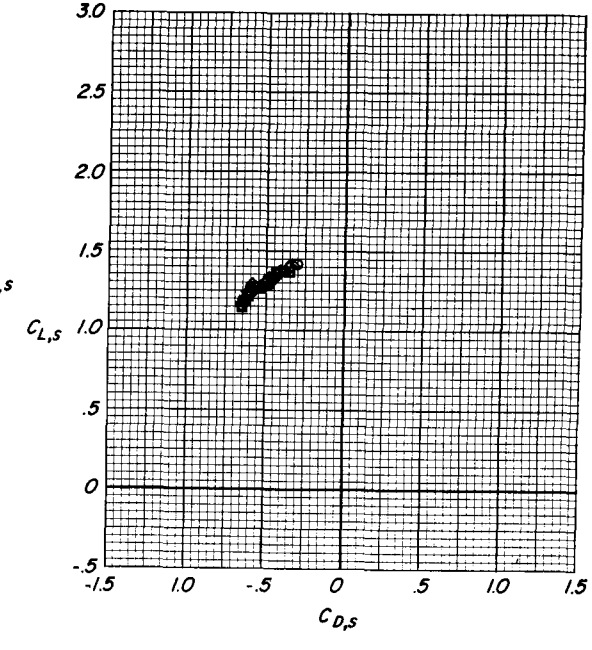

(c) $(C_{T,s})_{nominal} \approx 0.91$.

Figure 23.- Concluded.

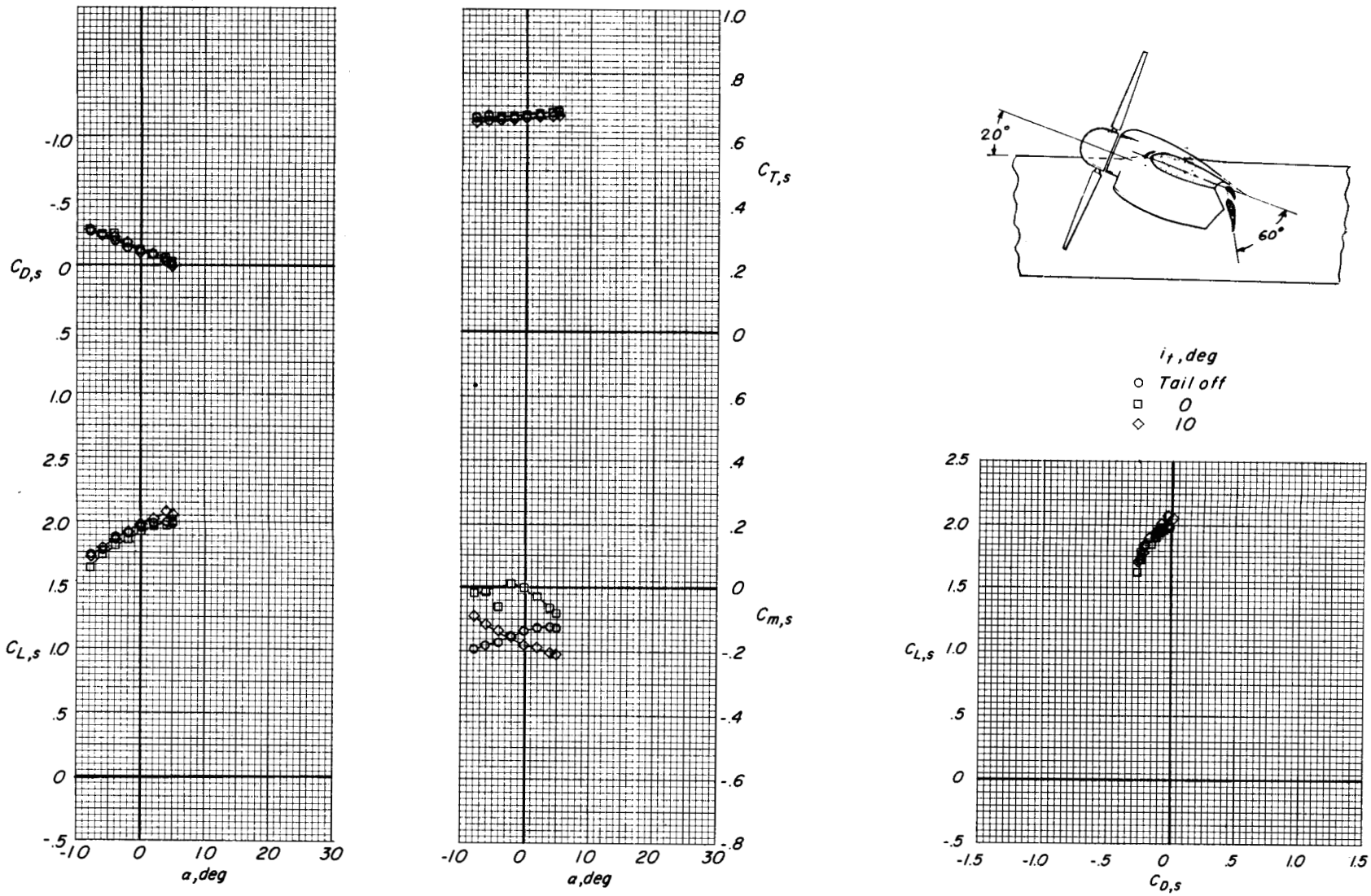

(a) $(C_{T,s})_{nominal} \approx 0.67$.

Figure 24.- Effect of horizontal-tail incidence on the aerodynamic characteristics. Ground belt stopped; $h/\bar{c} = 0.40$; $i_w = 20^0$; $\delta_f = 60^0$; slat on.

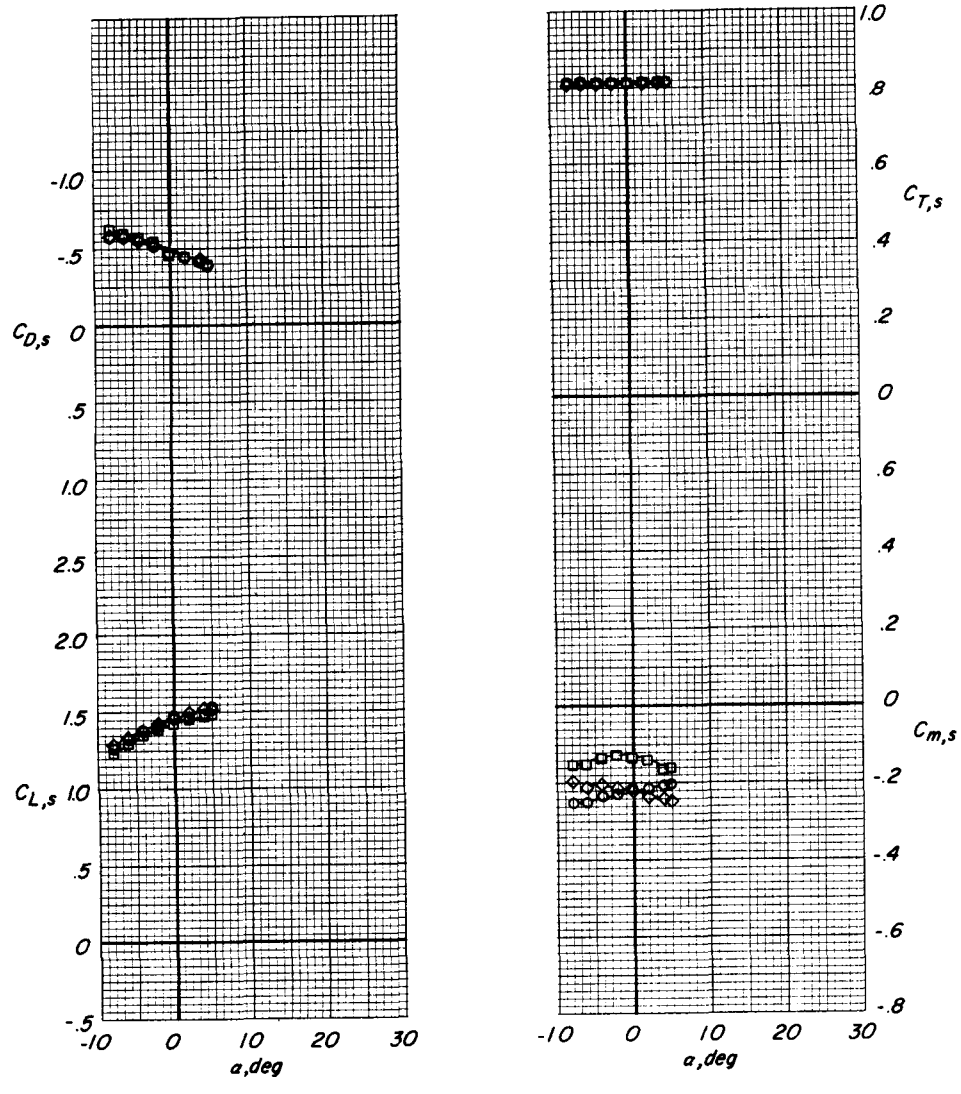

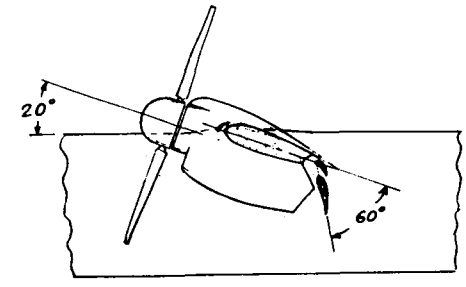

i_t, deg
○ Tail off
□ 0
◇ 10

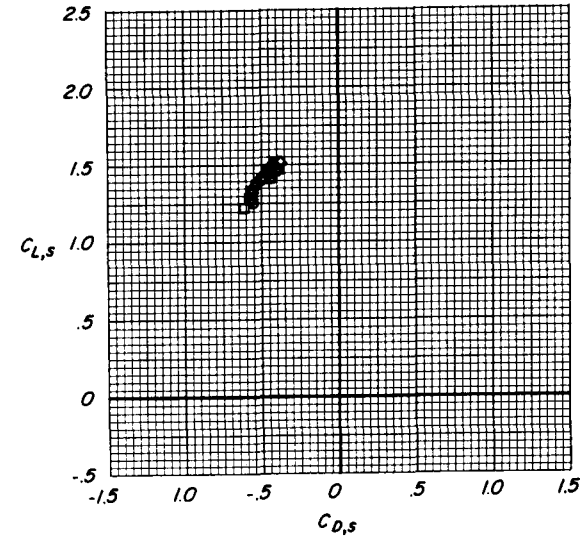

(b) $(C_{T,s})_{nominal} \approx 0.81$.

Figure 24.- Continued.

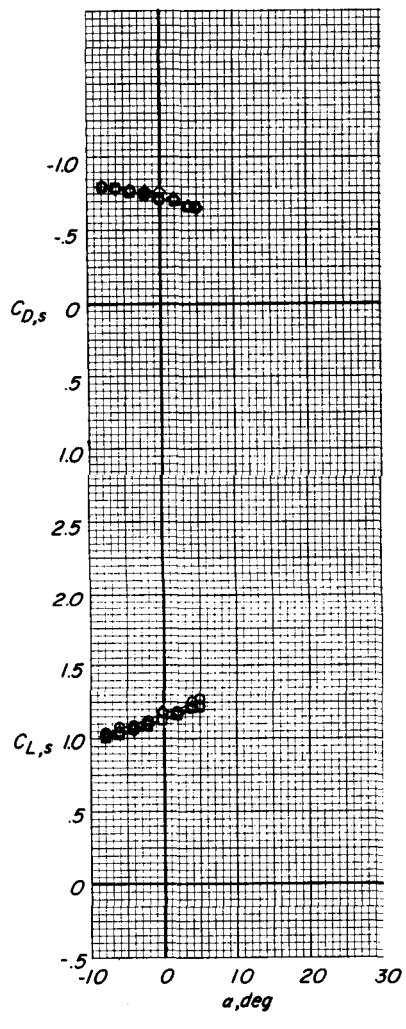

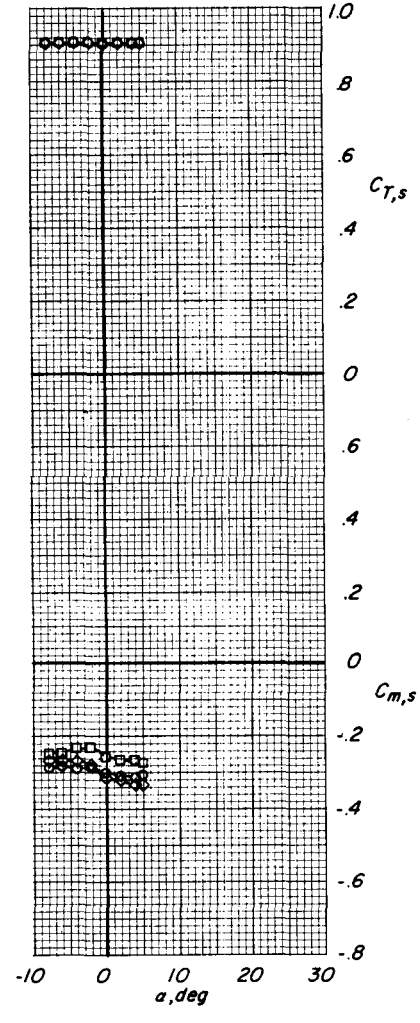

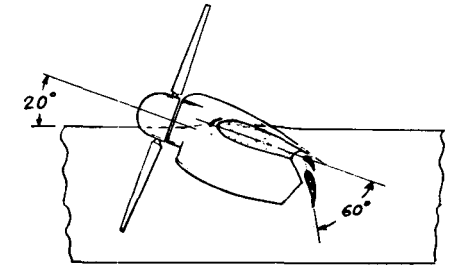

i_t, deg
○ Tail off
□ 0
◇ 10

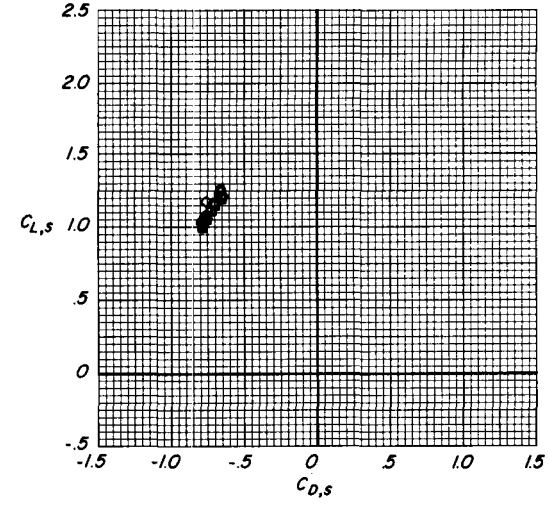

(c) $(C_{T,s})_{nominal} \approx 0.91$.

Figure 24.- Concluded.

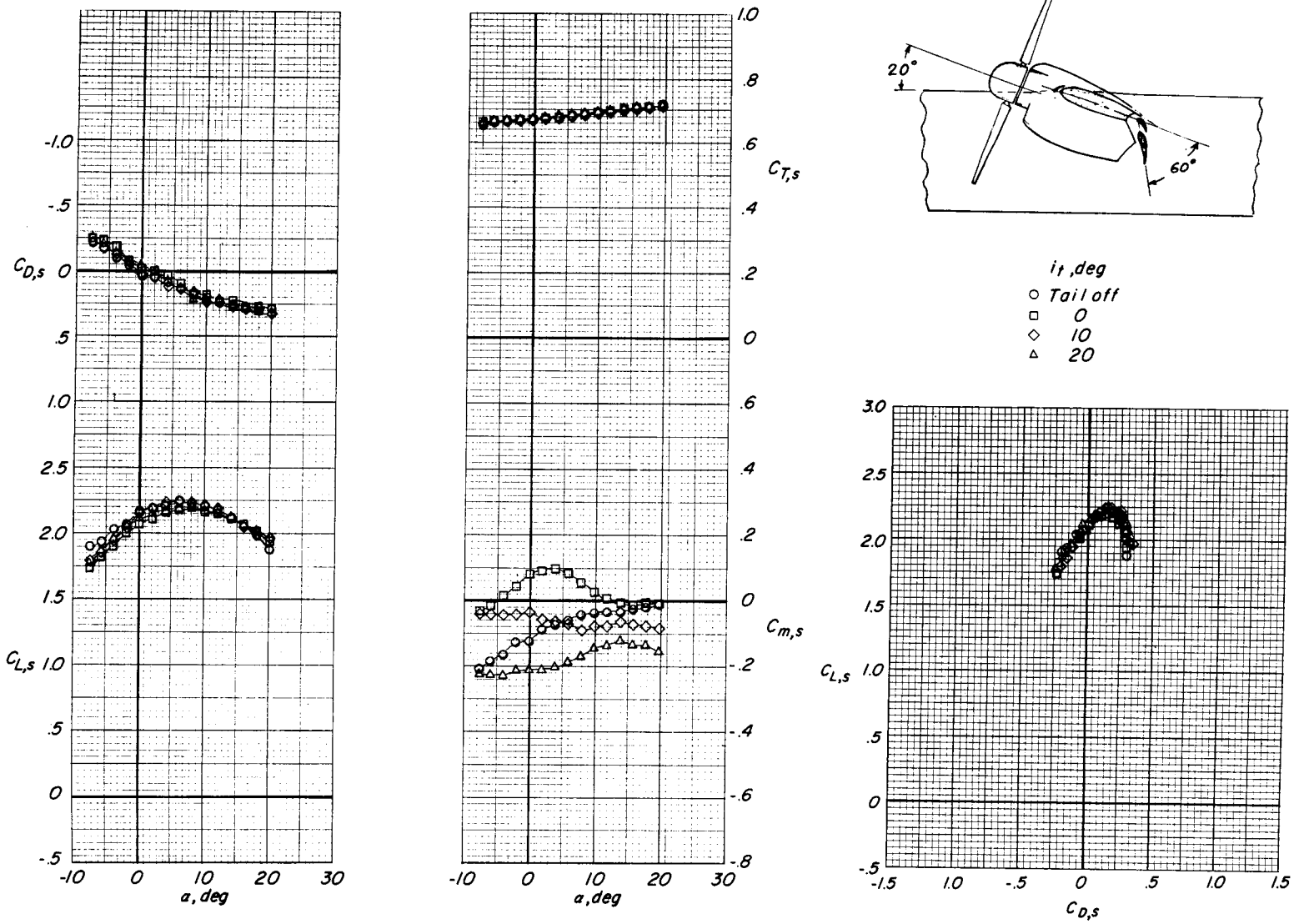

(a) $(C_{T,s})_{nominal} \approx 0.67$.

Figure 25.- Effect of horizontal-tail incidence on the aerodynamic characteristics. Ground belt moving; $h/\bar{c} = 1.70$; $i_w = 20^0$; $\delta_f = 60^0$; slat on.

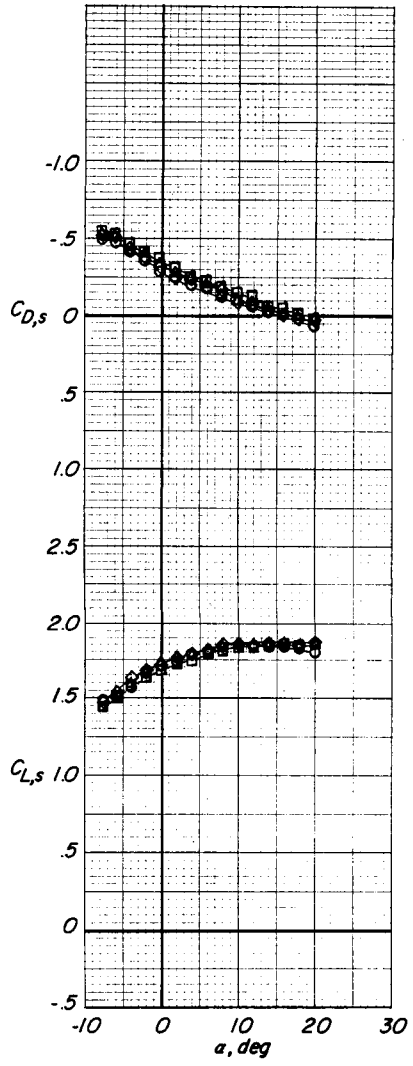

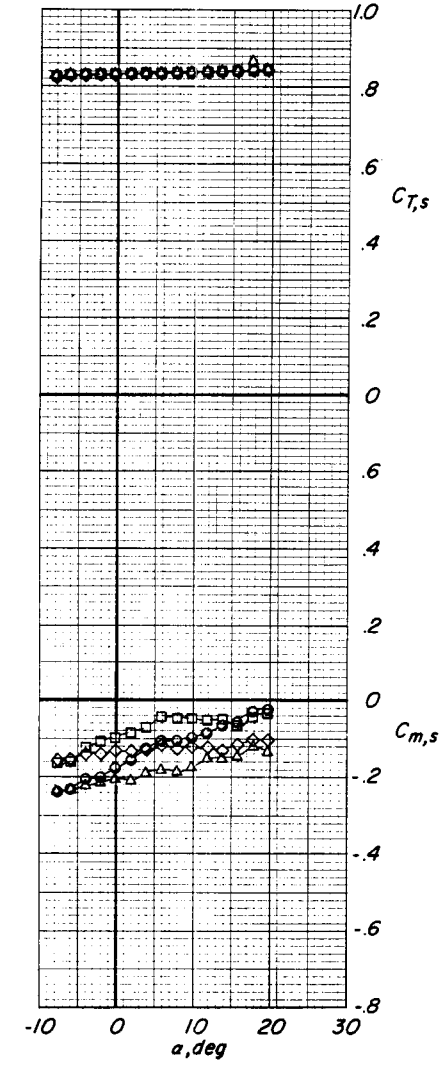

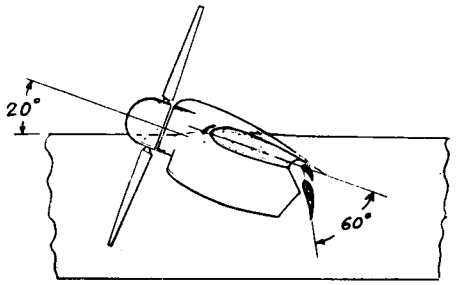

i_t, deg
- ○ Tail off
- □ 0
- ◇ 10
- △ 20

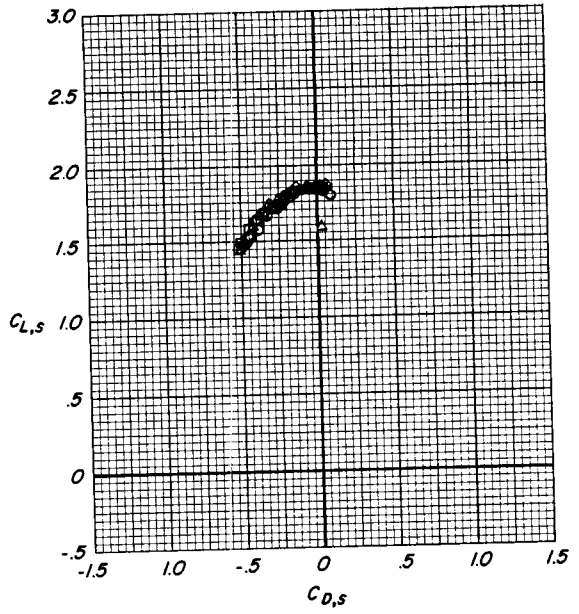

(b) $(C_{T,s})_{nominal} \approx 0.83$.

Figure 25.- Continued.

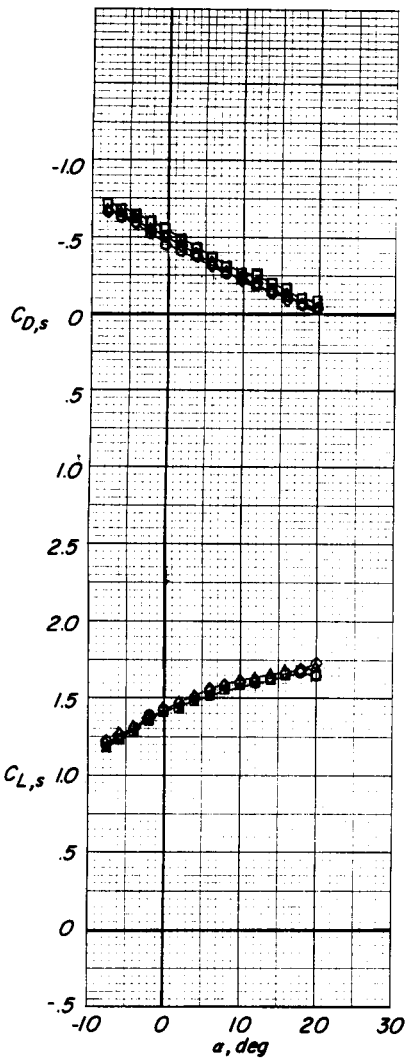

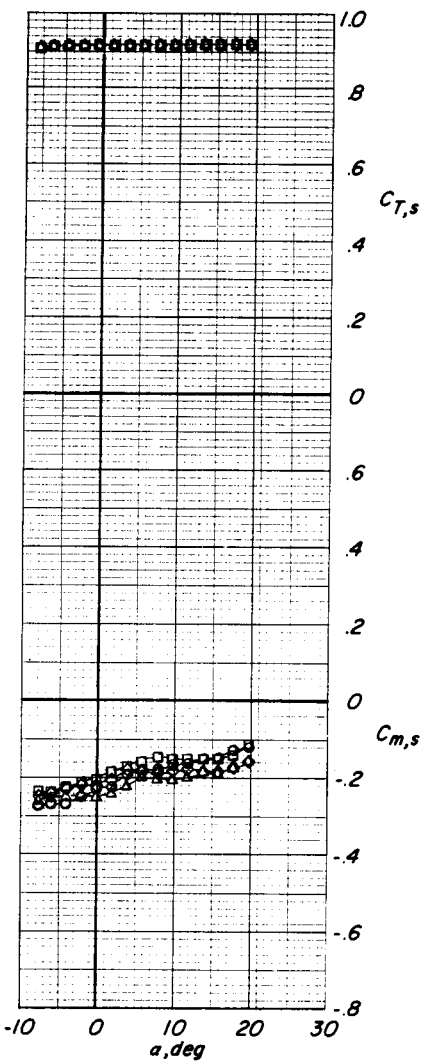

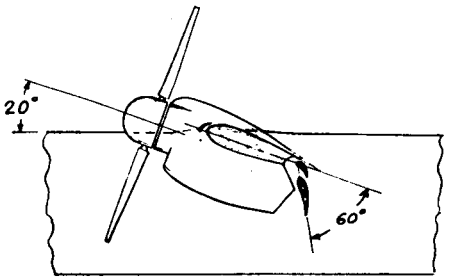

i_t, deg
○ Tail off
□ 0
◇ 10
△ 20

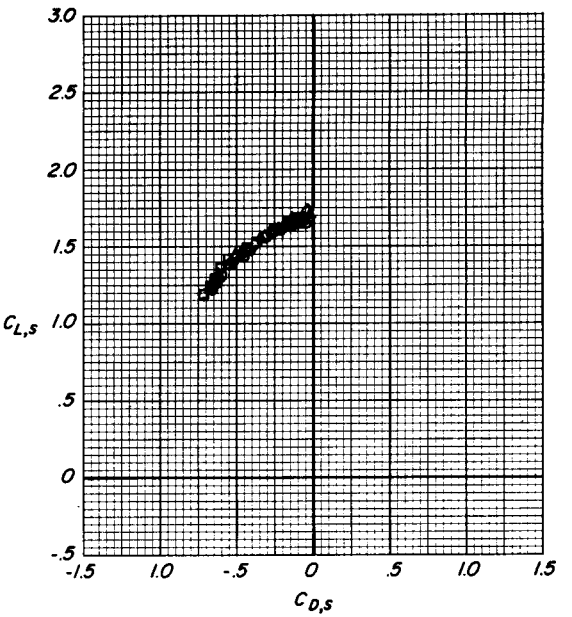

(c) $(C_{T,s})_{nominal} \approx 0.92$.

Figure 25.- Concluded.

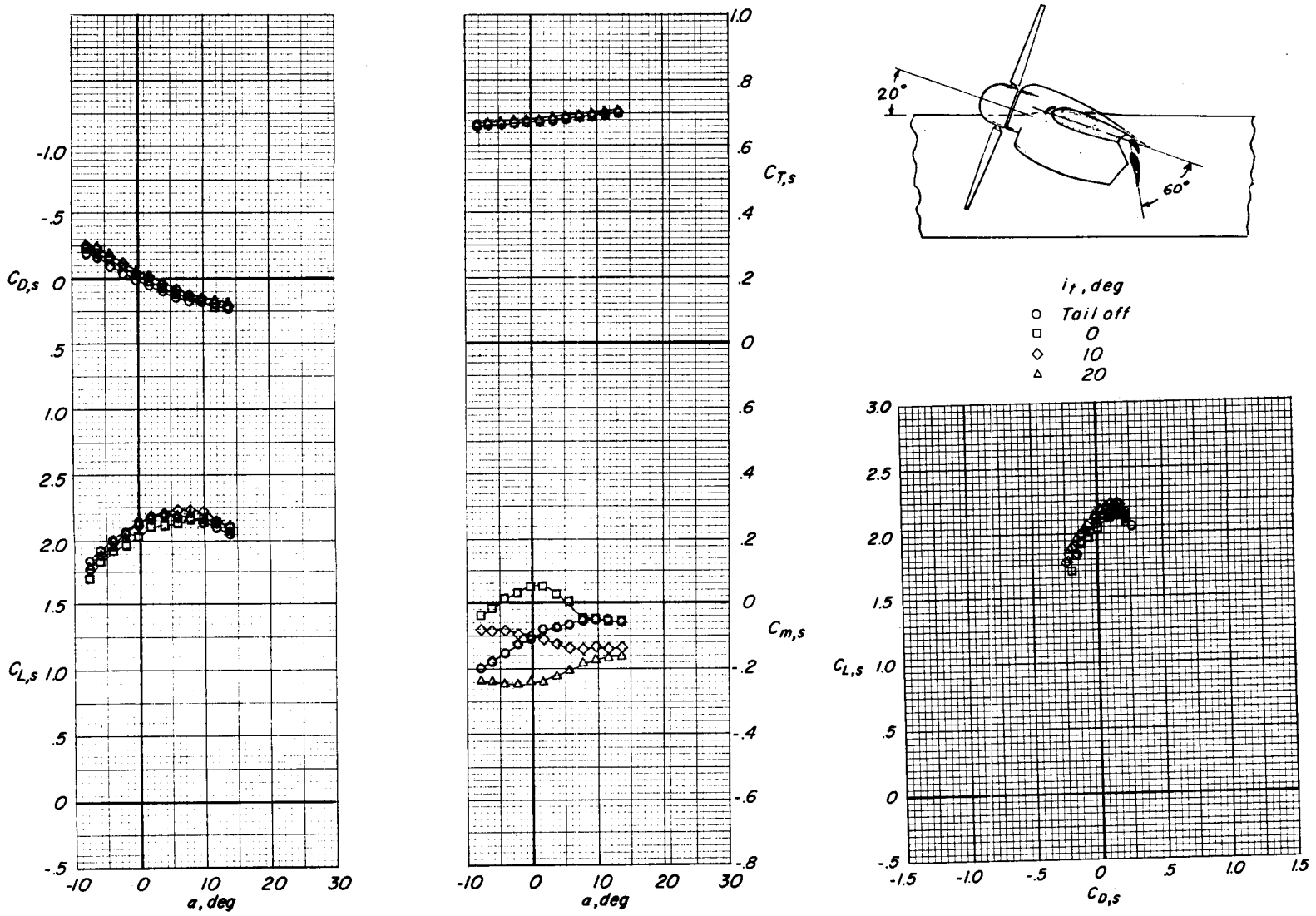

(a) $(C_{T,s})_{nominal} \approx 0.67$.

Figure 26.- Effect of horizontal-tail incidence on the aerodynamic characteristics. Ground belt moving; $h/\bar{c} = 1.09$; $i_w = 20^0$; $\delta_f = 60^0$; slat on.

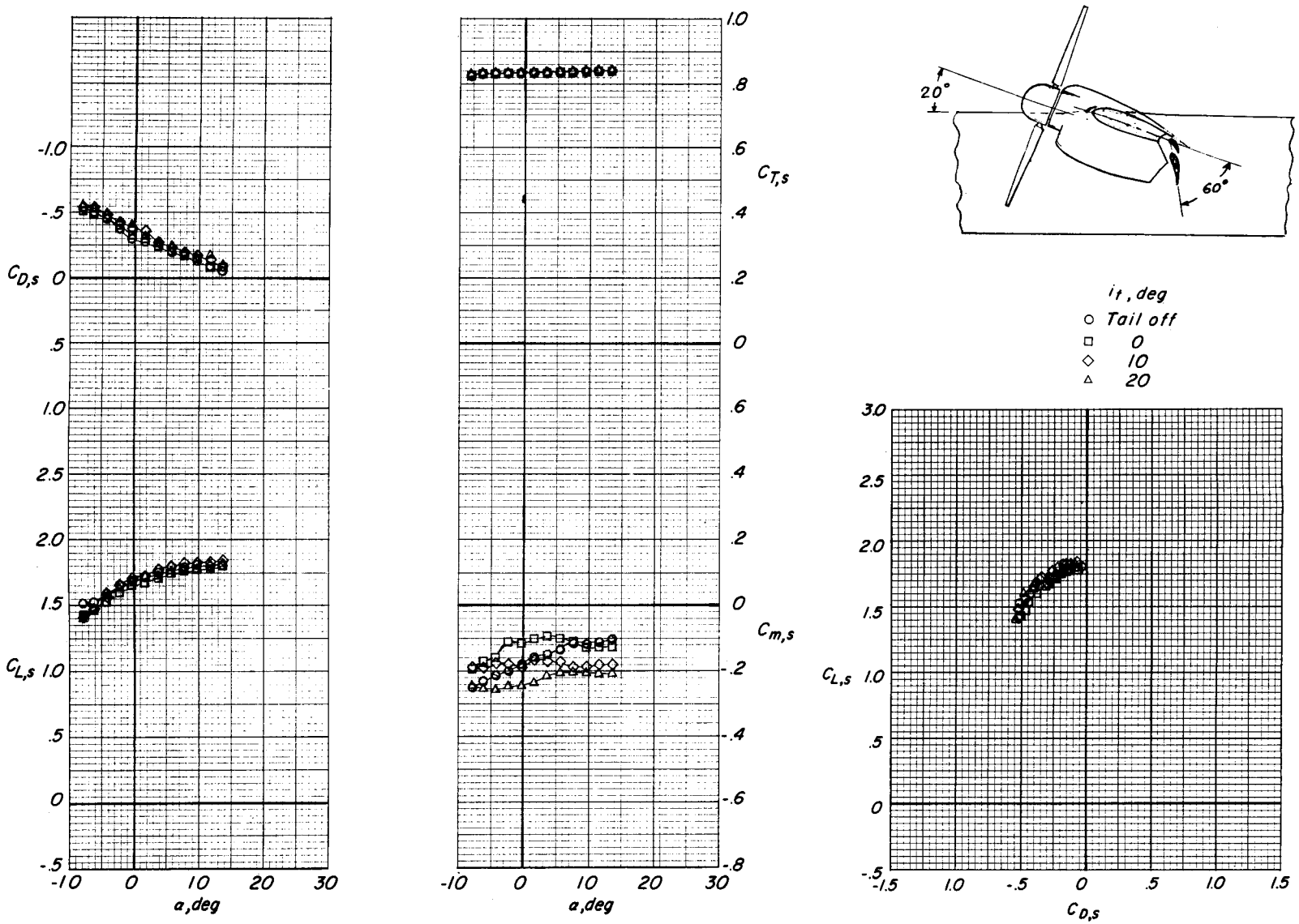

(b) $(C_{T,s})_{nominal} \approx 0.83$.

Figure 26.- Continued.

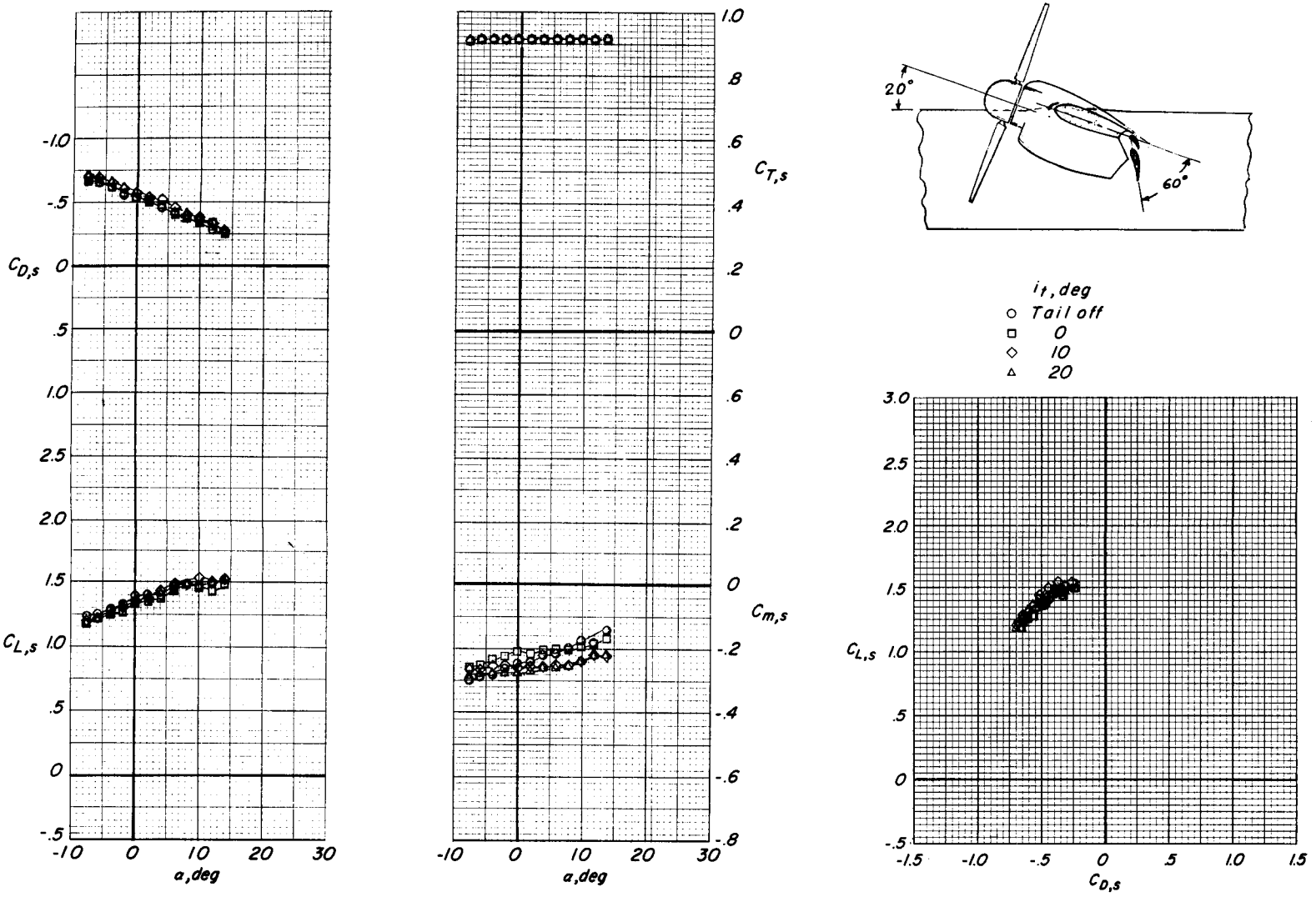

(c) $(C_{T,s})_{nominal} \approx 0.91$.

Figure 26.- Concluded.

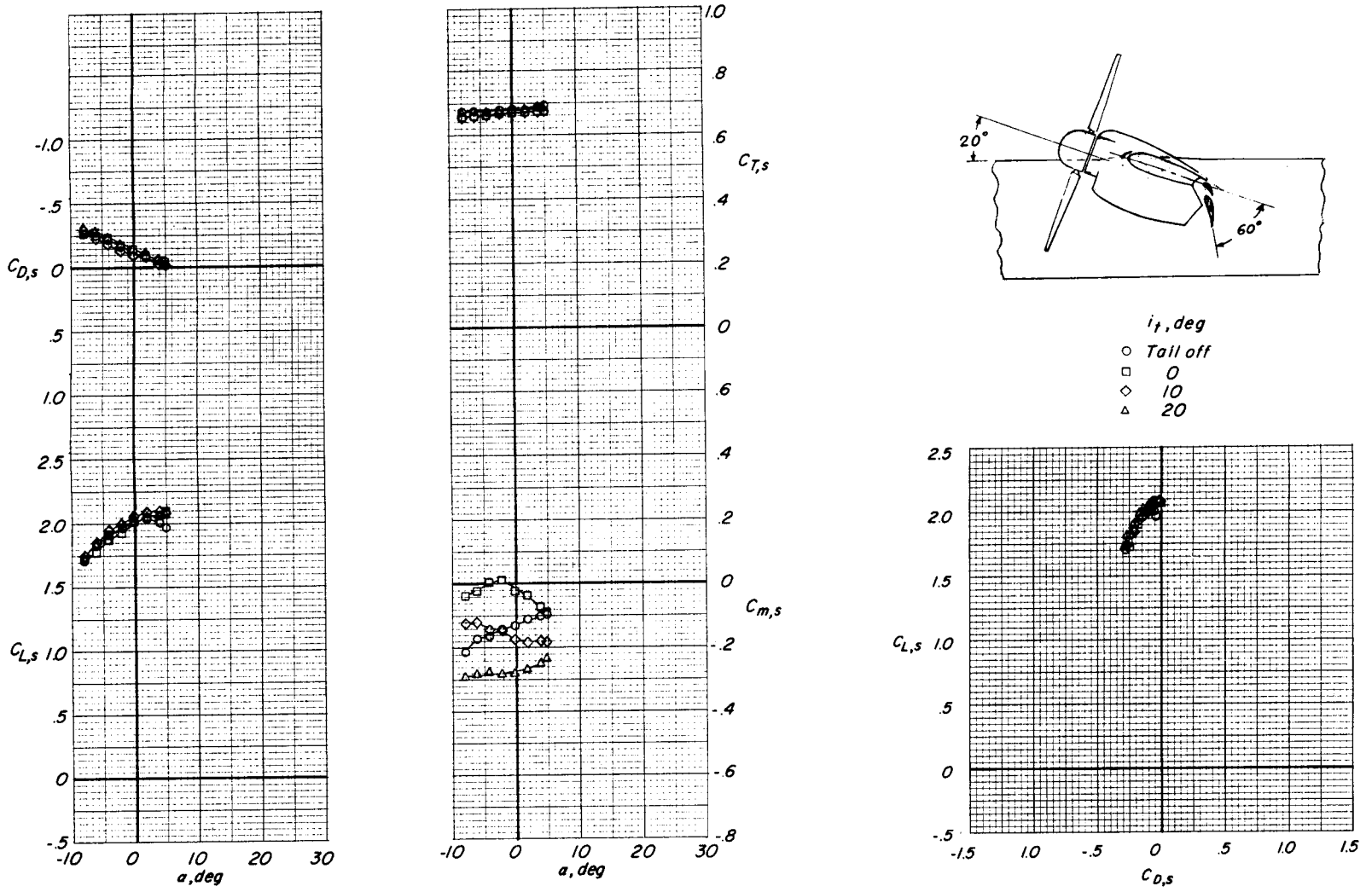

(a) $(C_{T,s})_{nominal} \approx 0.67$.

Figure 27.- Effect of horizontal-tail incidence on the aerodynamic characteristics. Ground belt moving; $h/\bar{c} = 0.40$; $i_w = 20^0$; $\delta_f = 60^0$; slat on.

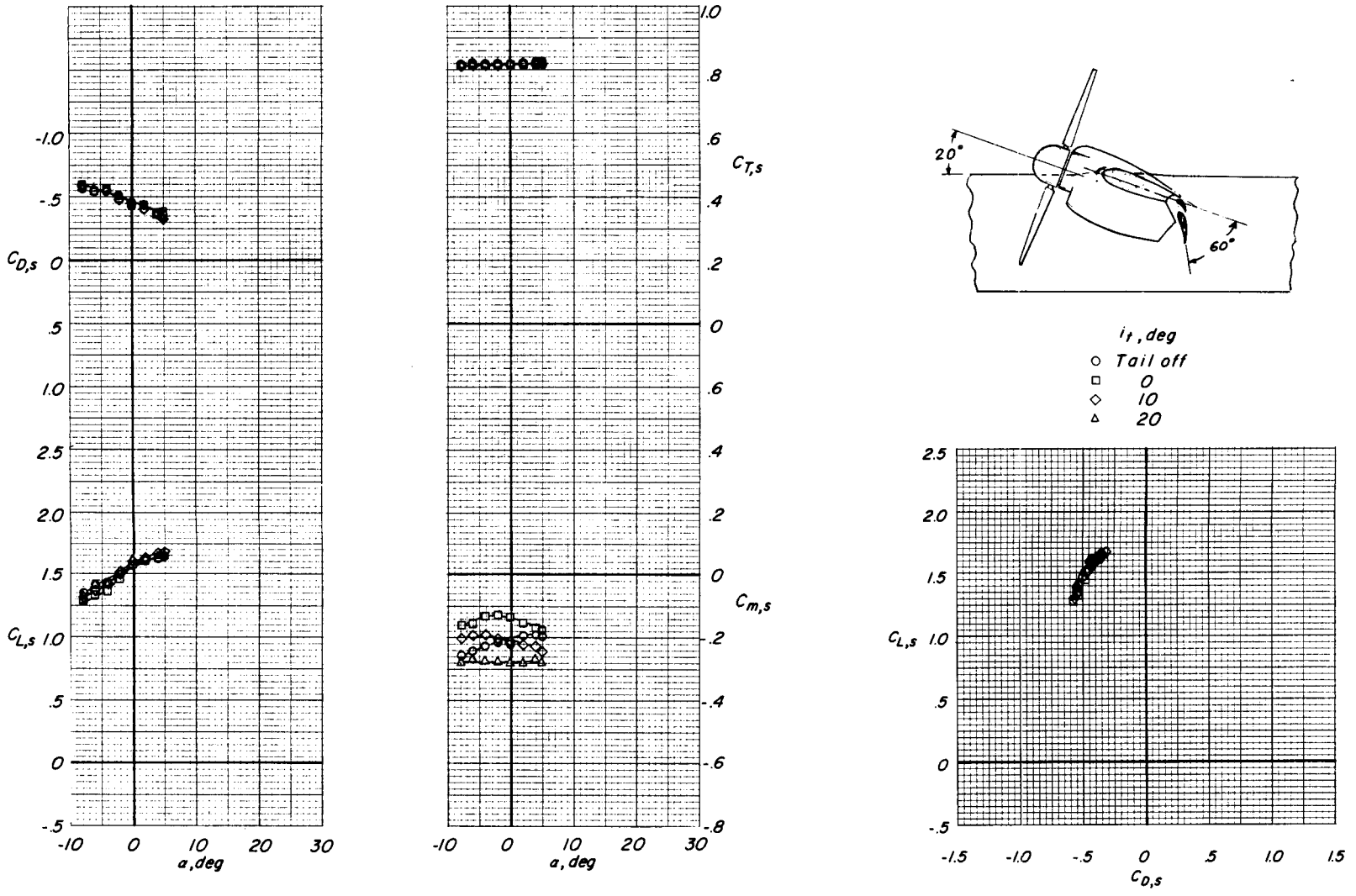

(b) $(C_{T,s})_{nominal} \approx 0.82$.

Figure 27.- Continued.

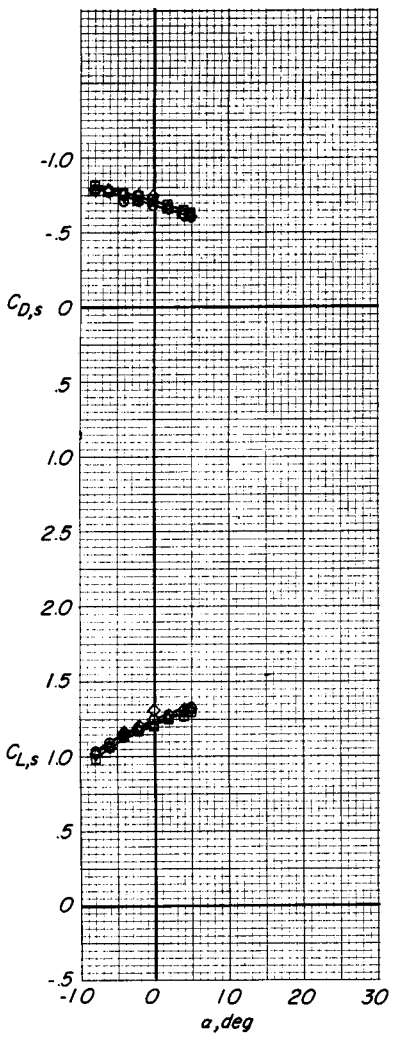

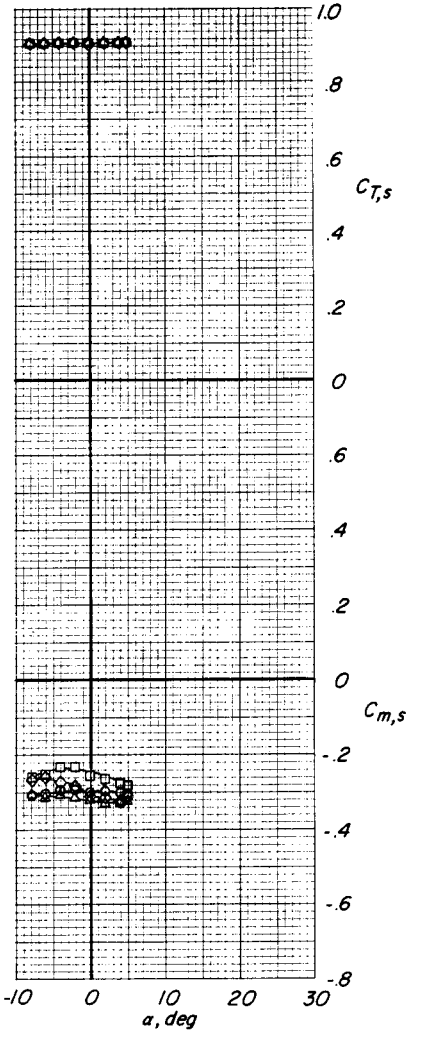

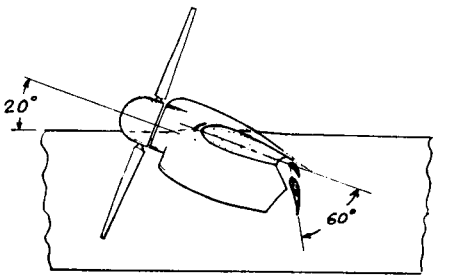

i_t, deg
- ○ Tail off
- □ 0
- ◇ 10
- △ 20

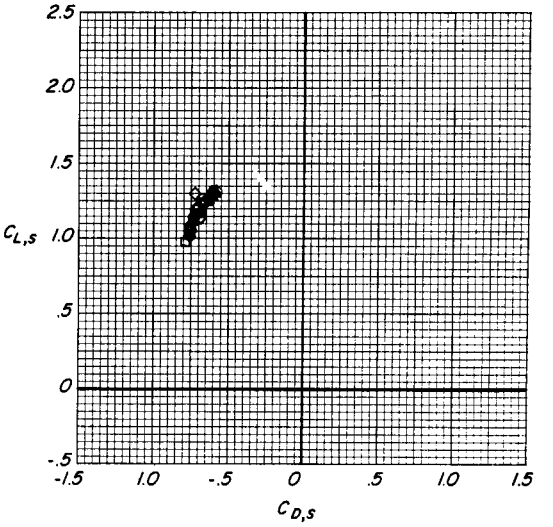

(c) $(C_{T,s})_{nominal} \approx 0.91$.

Figure 27.- Concluded.

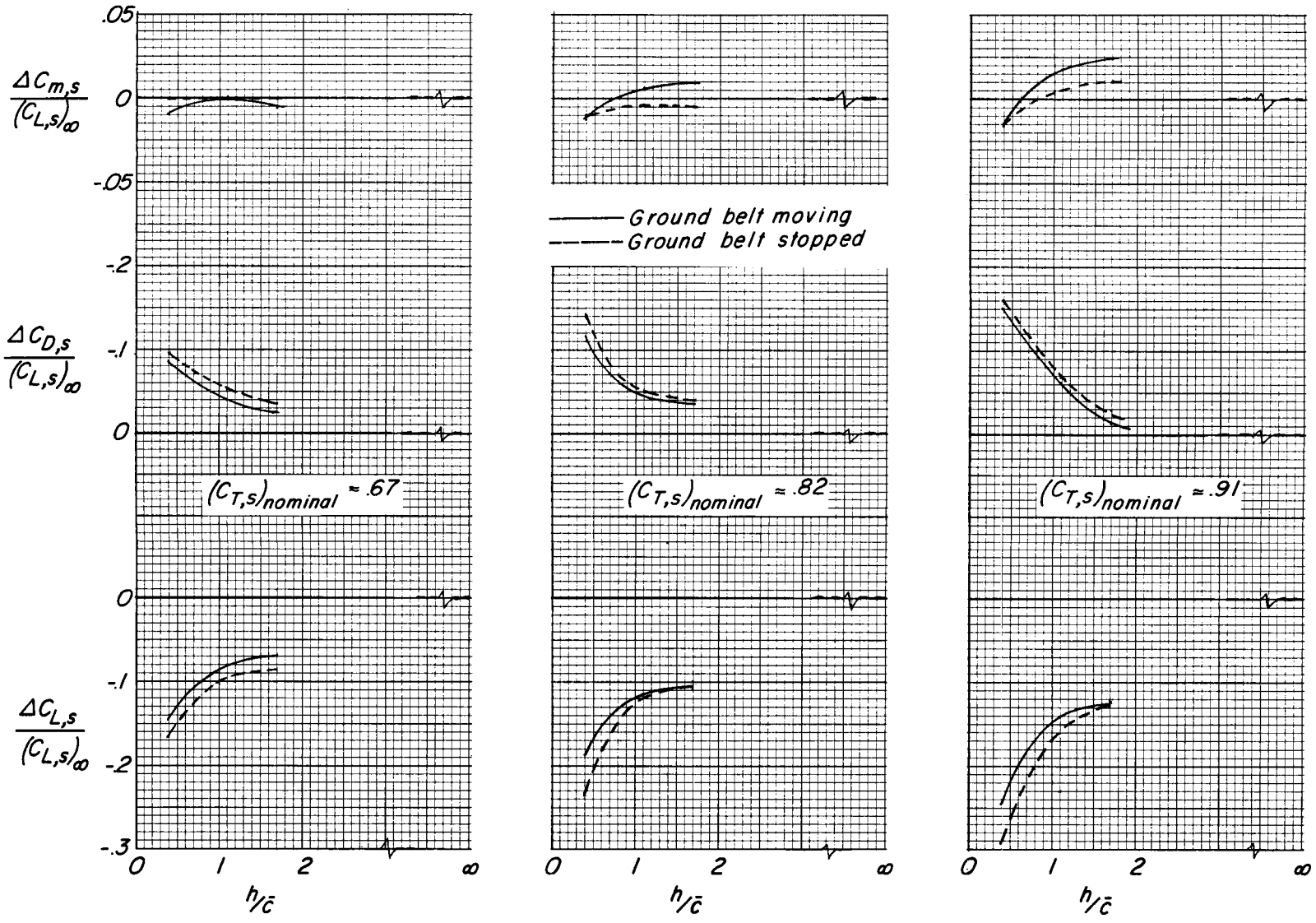

Figure 28.- Effect of ground-plane belt on the incremental aerodynamic changes due to ground proximity over a height range. $i_w = 20^0$; $\delta_f = 60^0$; slat on; horizontal tail off; $\alpha = 0^0$.

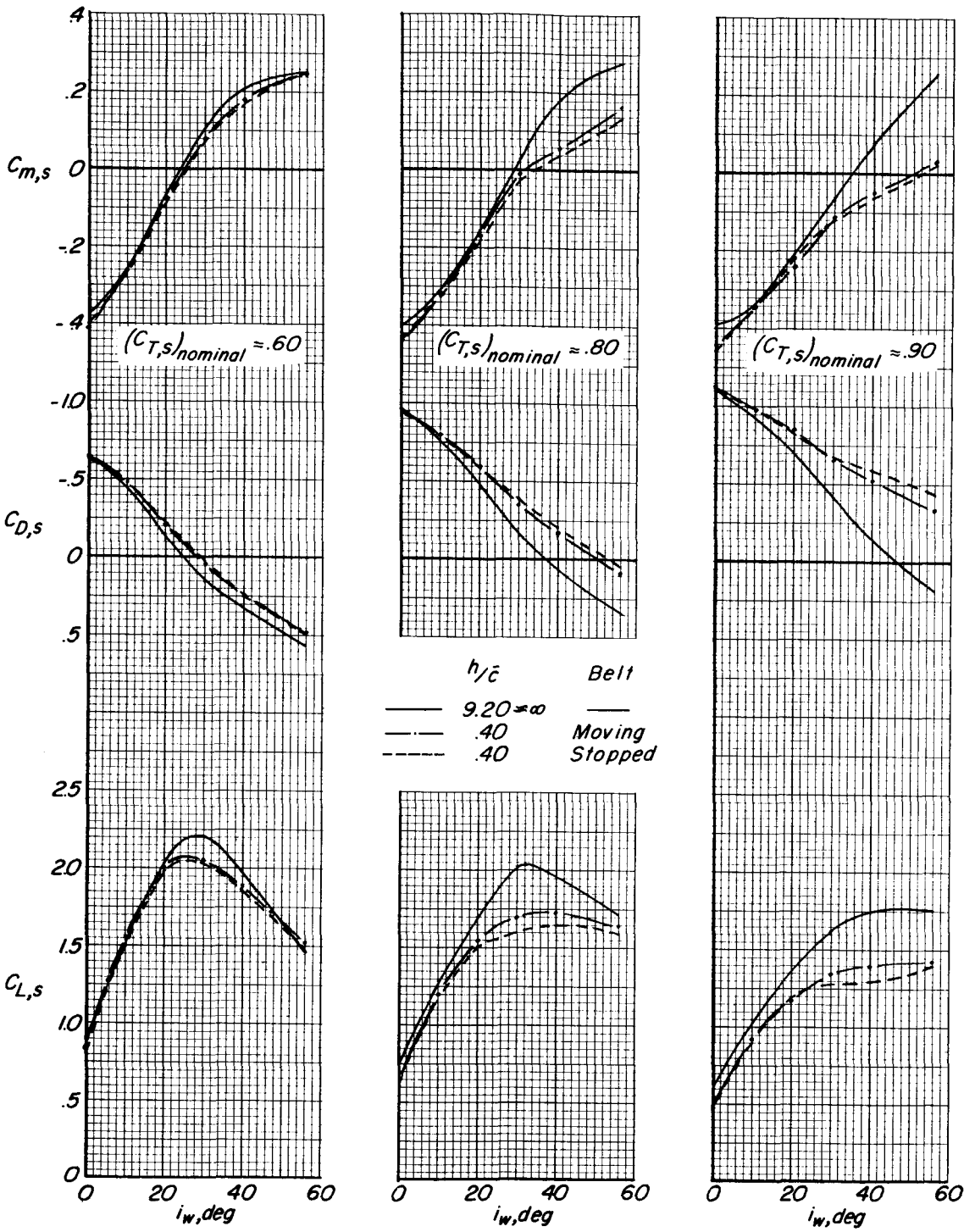

(a) $\delta_f = 40^0$.

Figure 29.- Ground effect and effect of ground-plane belt on the aerodynamic coefficients for a range of wing-incidence angles and thrust coefficients. Slat on; horizontal tail off; $\alpha = 0^0$.

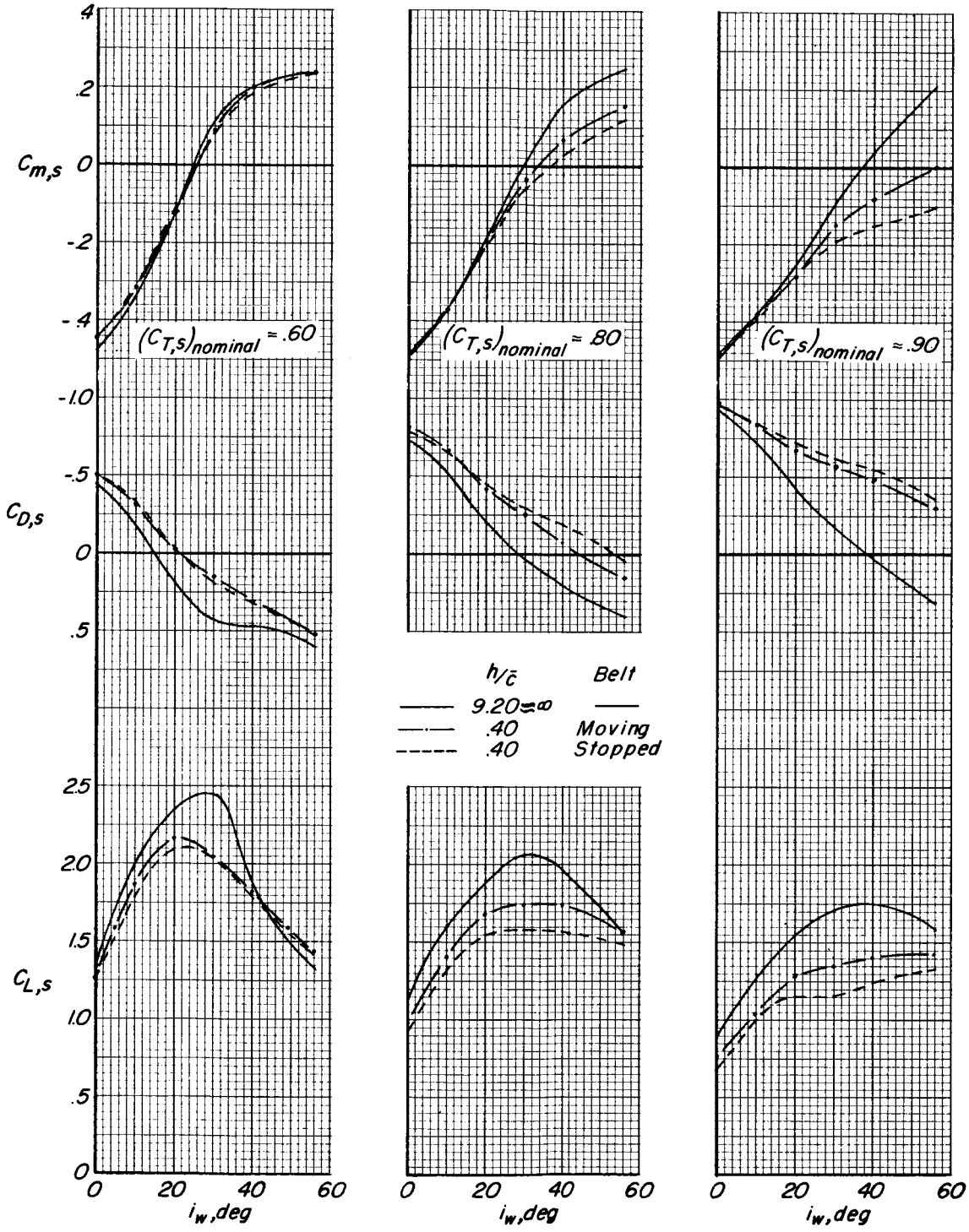

(b) $\delta_f = 60^0$.

Figure 29.- Concluded.

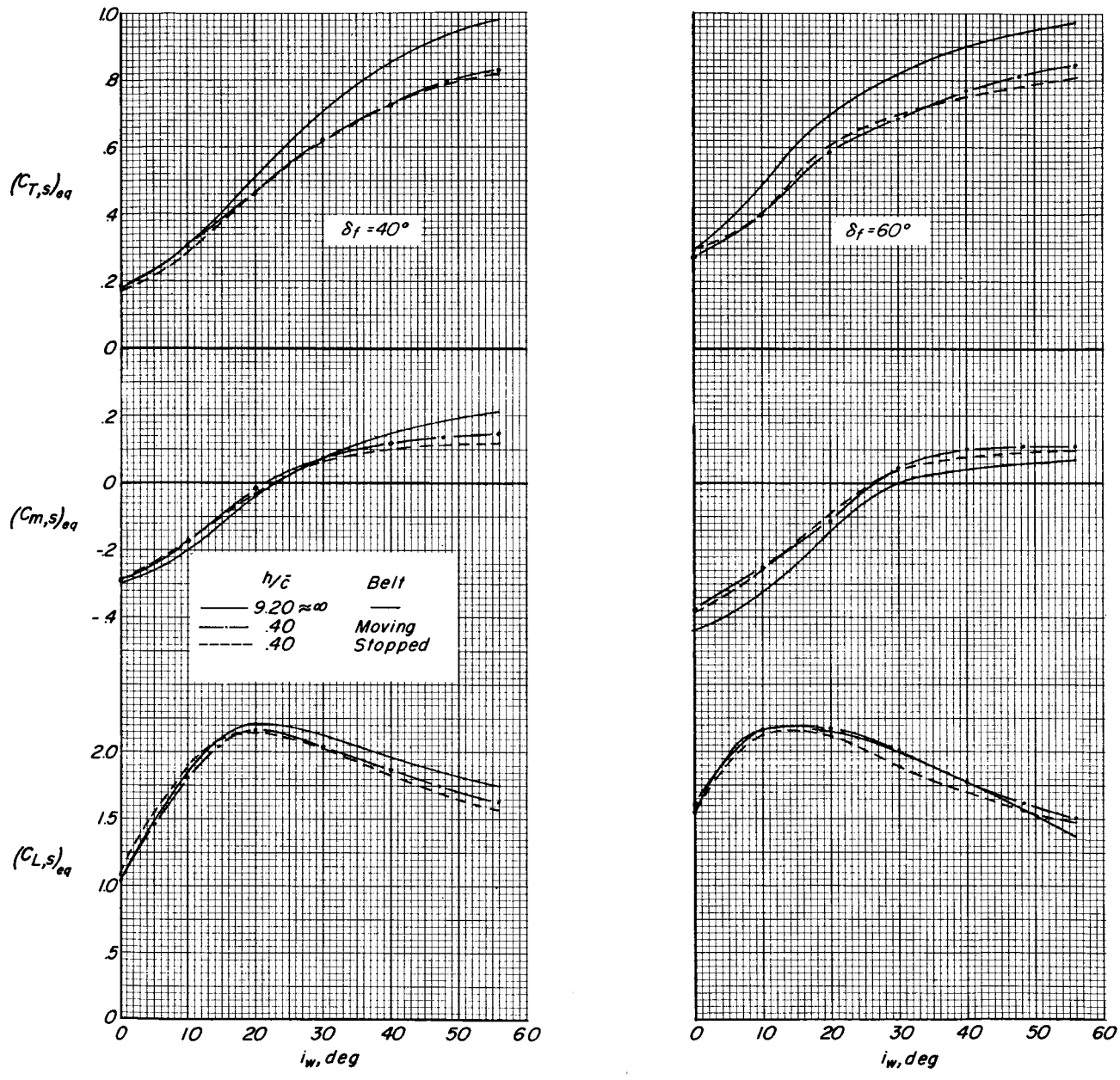

Figure 30.- Ground effect and effect of ground-plane belt on the equilibrium aerodynamic coefficients for a range of wing-incidence angles. Slat on; horizontal tail off; $\alpha = 0^0$; $C_{D,s} = 0$.

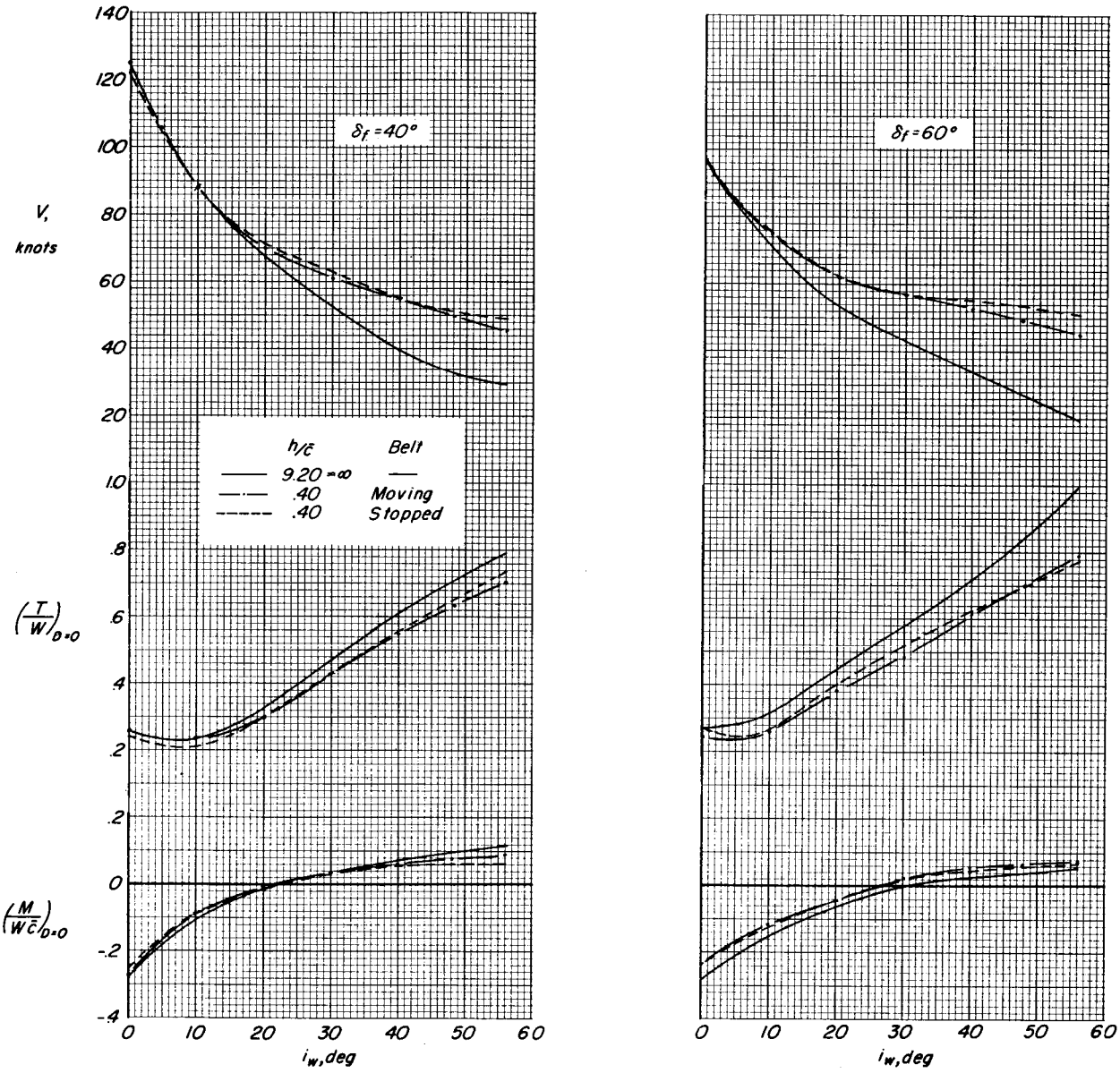

Figure 31.- Scaled-up equilibrium data for an assumed tilt-wing V/STOL airplane. W/S = 70 lbf/ft^2 (3350 N/m^2); $C_{D,S}$ = 0; α = 0^0; slat on.

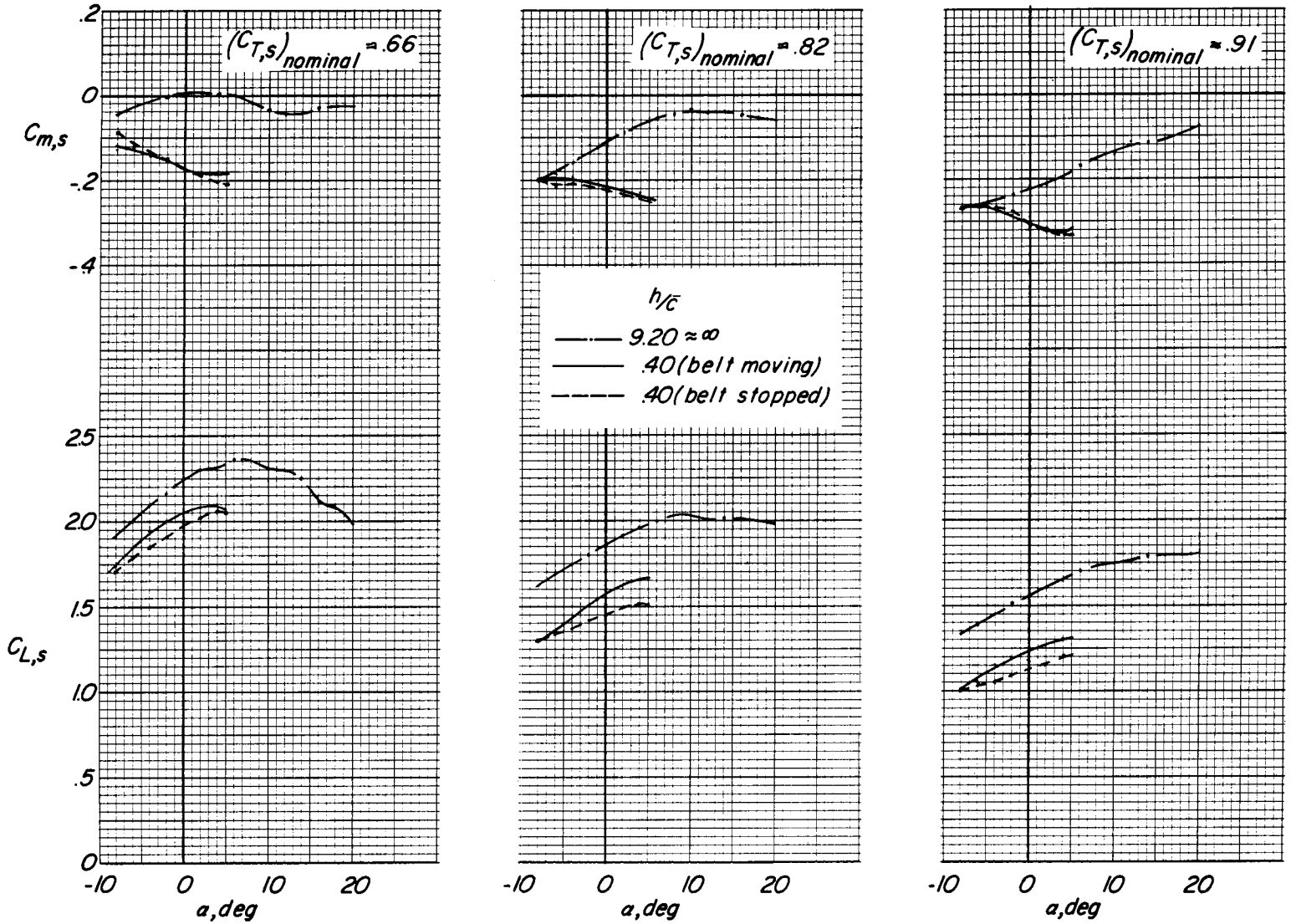

(a) $C_{L,s}$ and $C_{m,s}$ as functions of α.

Figure 32.- Effect of a moving and a stopped ground-plane belt on the aerodynamic characteristics both in and out of ground proximity. $i_w = 20^0$; $\delta_f = 60^0$; $i_t = 10^0$; slat on.

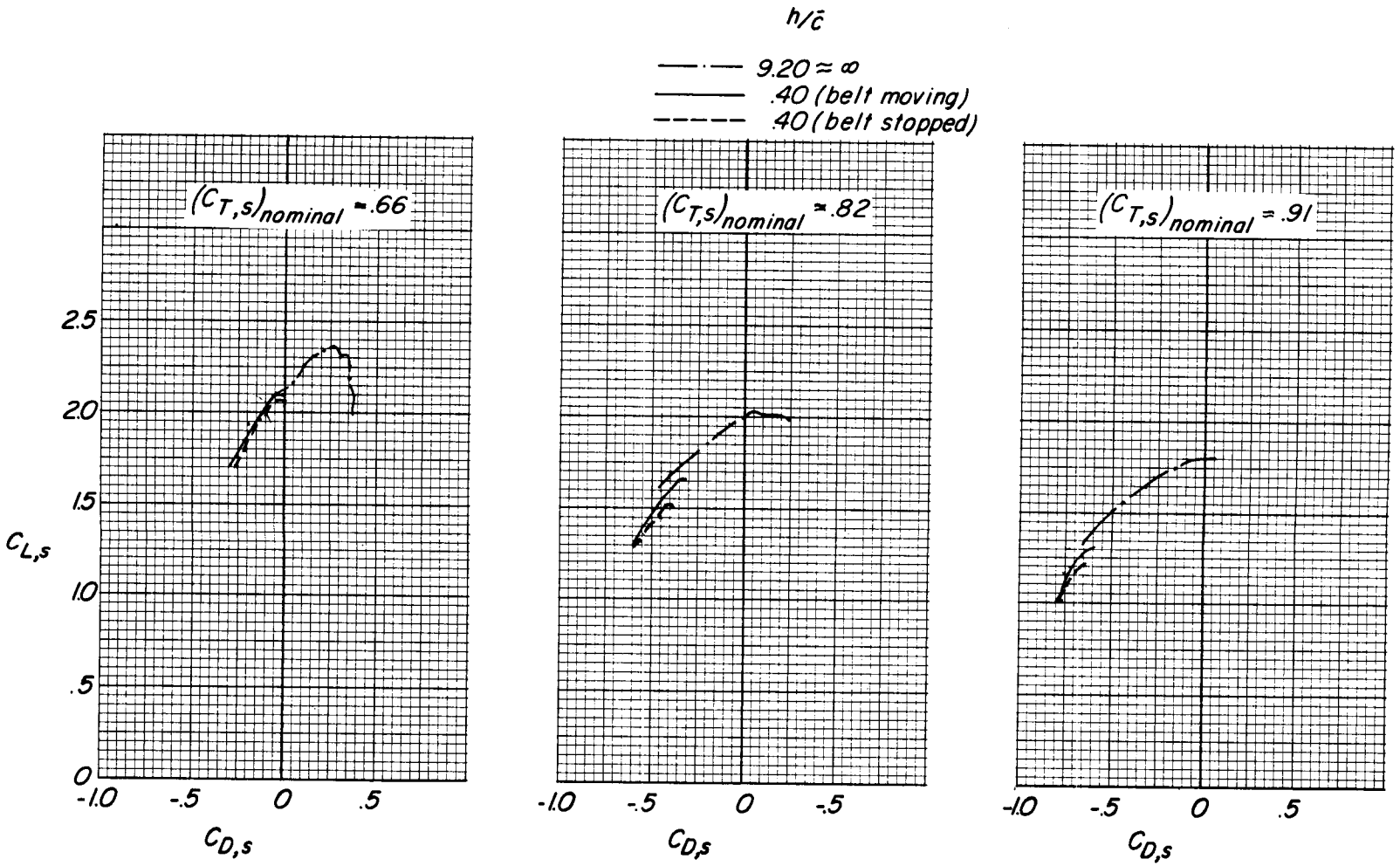

(b) $C_{L,s}$ as a function of $C_{D,s}$.

Figure 32.- Concluded.

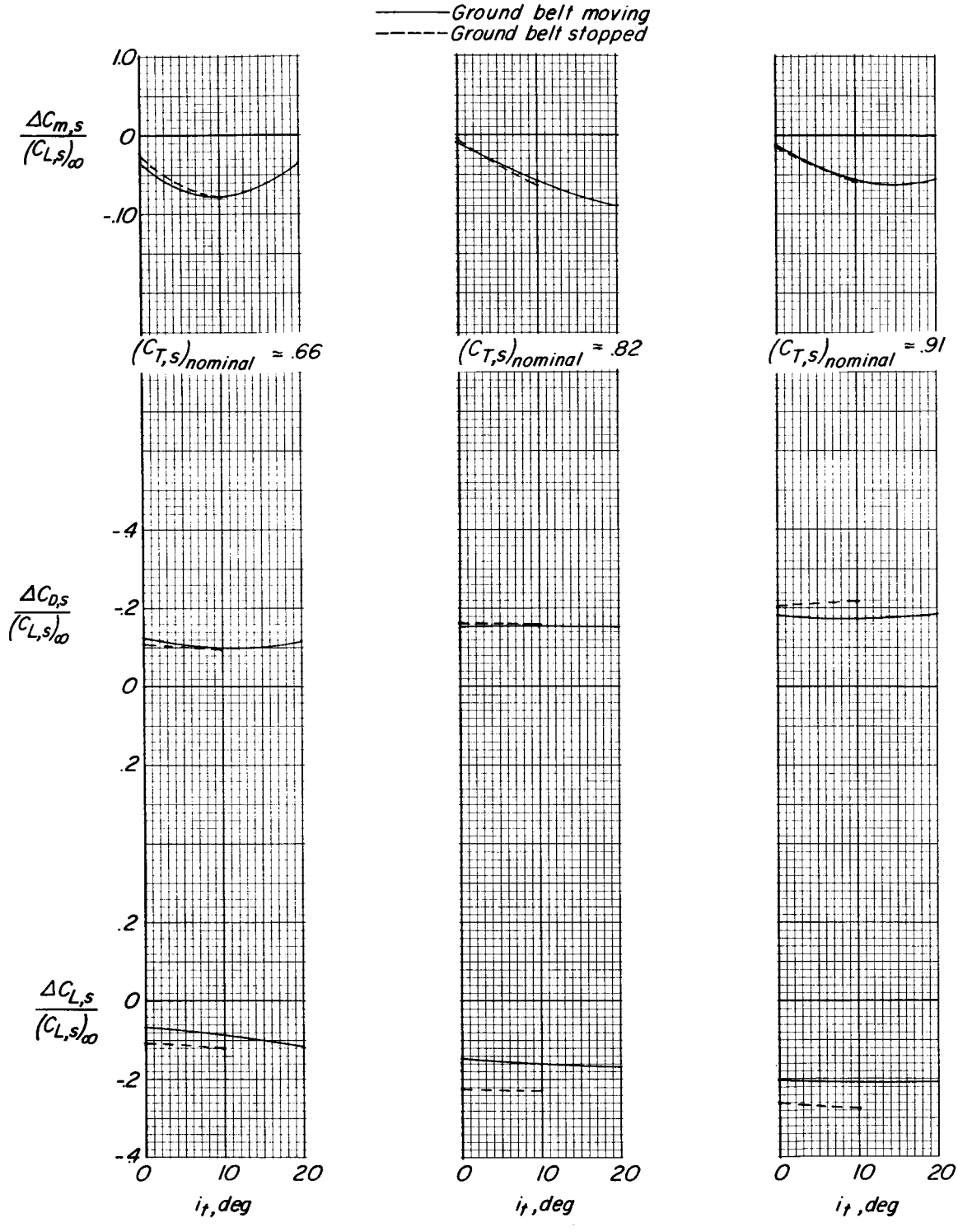

Figure 33.- Effect of a moving and a stopped ground-plane belt on the incremental aerodynamic changes due to ground proximity over a range of horizontal-tail incidence angles. $i_w = 20^0$; $\delta_f = 60^0$; $\alpha = 0^0$; slat on; $h/\bar{c} = 0.40$.

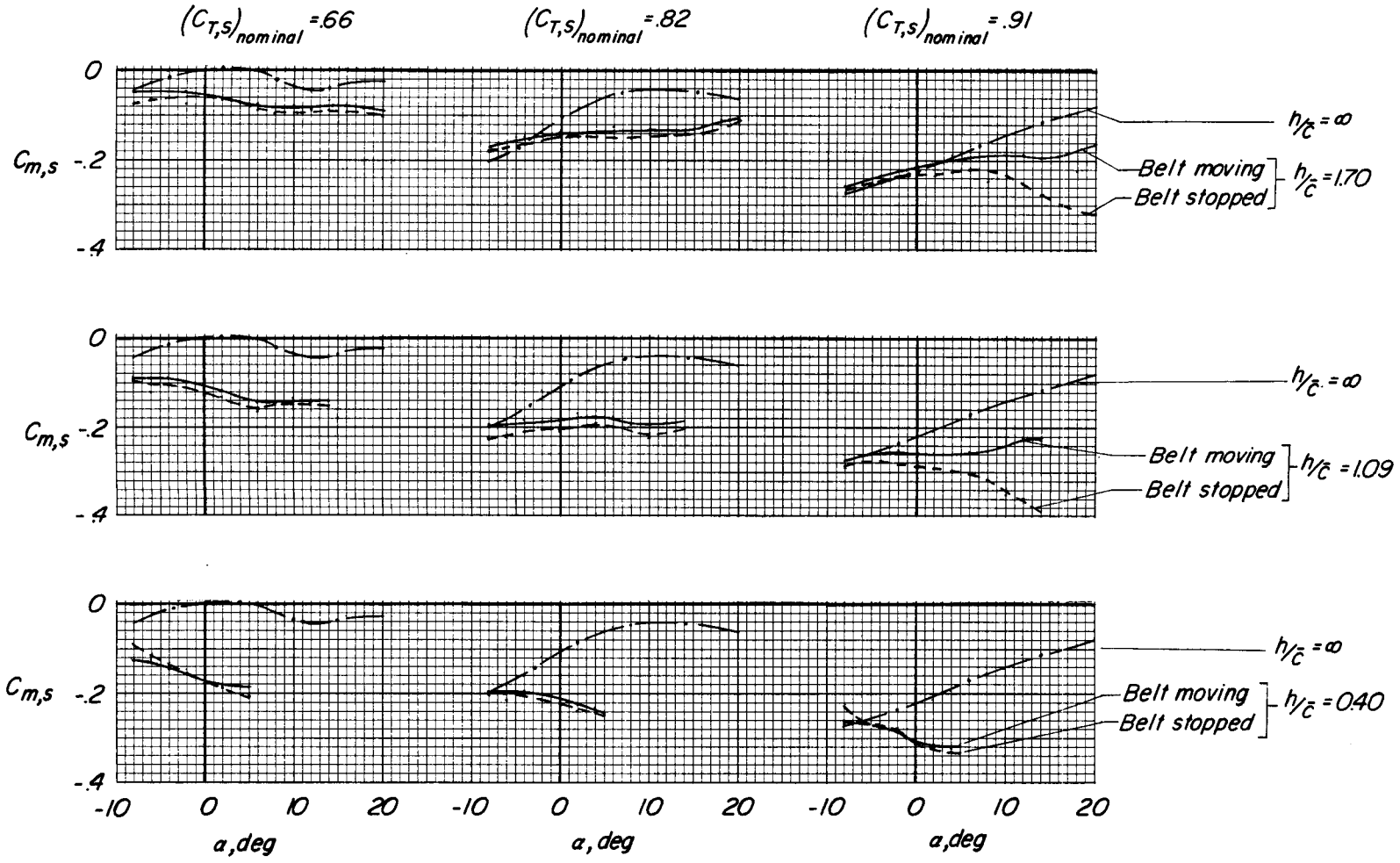

Figure 34.- Comparison of tail-on pitching-moment coefficients through a range of angles of attack for a stopped and a moving ground-plane belt for several ground heights. $i_w = 20^0$; $\delta_f = 60^0$; $i_t = 10^0$.

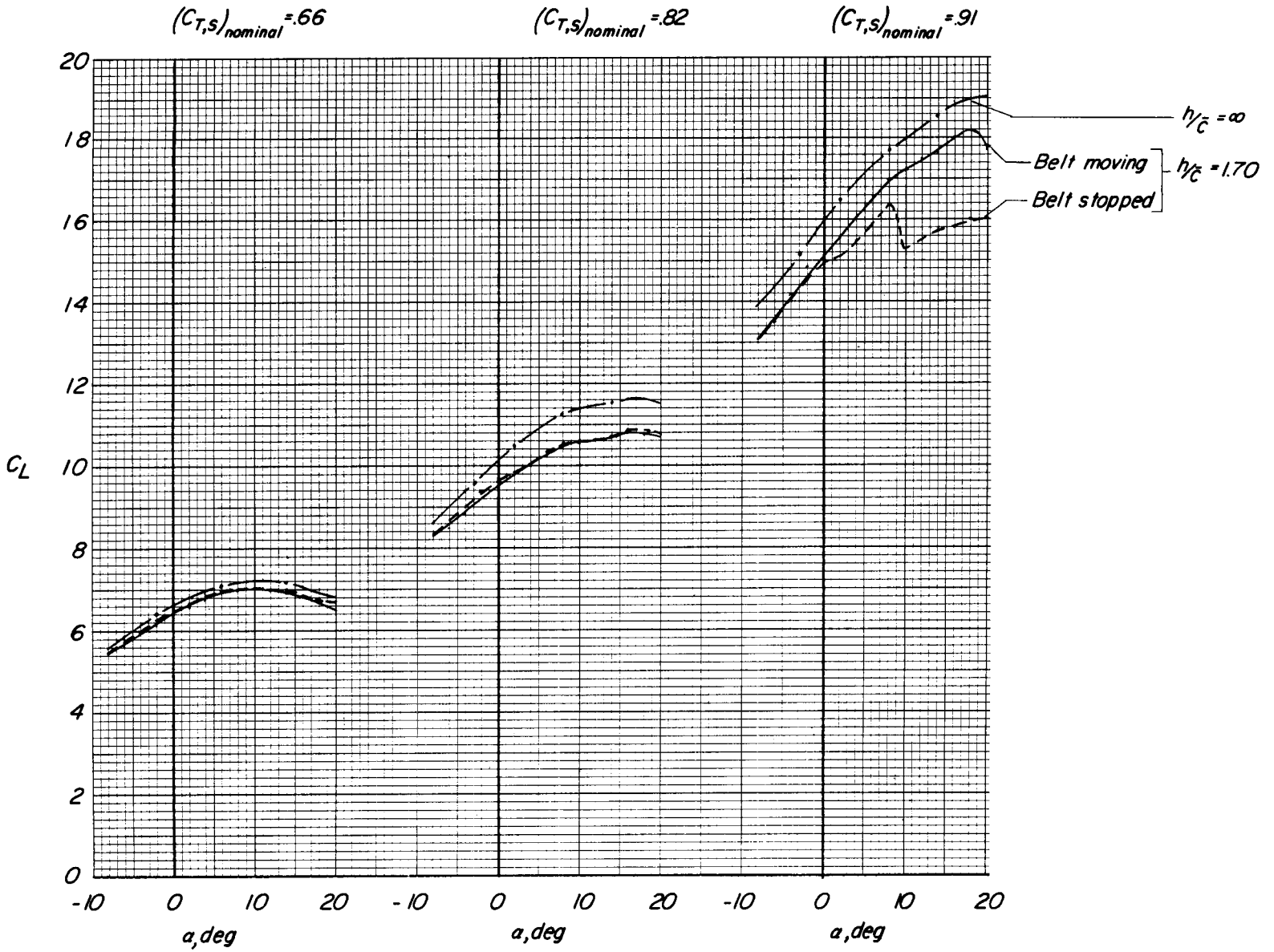

(a) $h/\bar{c}$ = 1.70.

Figure 35.- Comparison of conventional lift coefficients through a range of angles of attack for a stopped and a moving ground-plane belt for several ground heights. $i_w = 20^0$; $\delta_f = 60^0$; horizontal tail off.

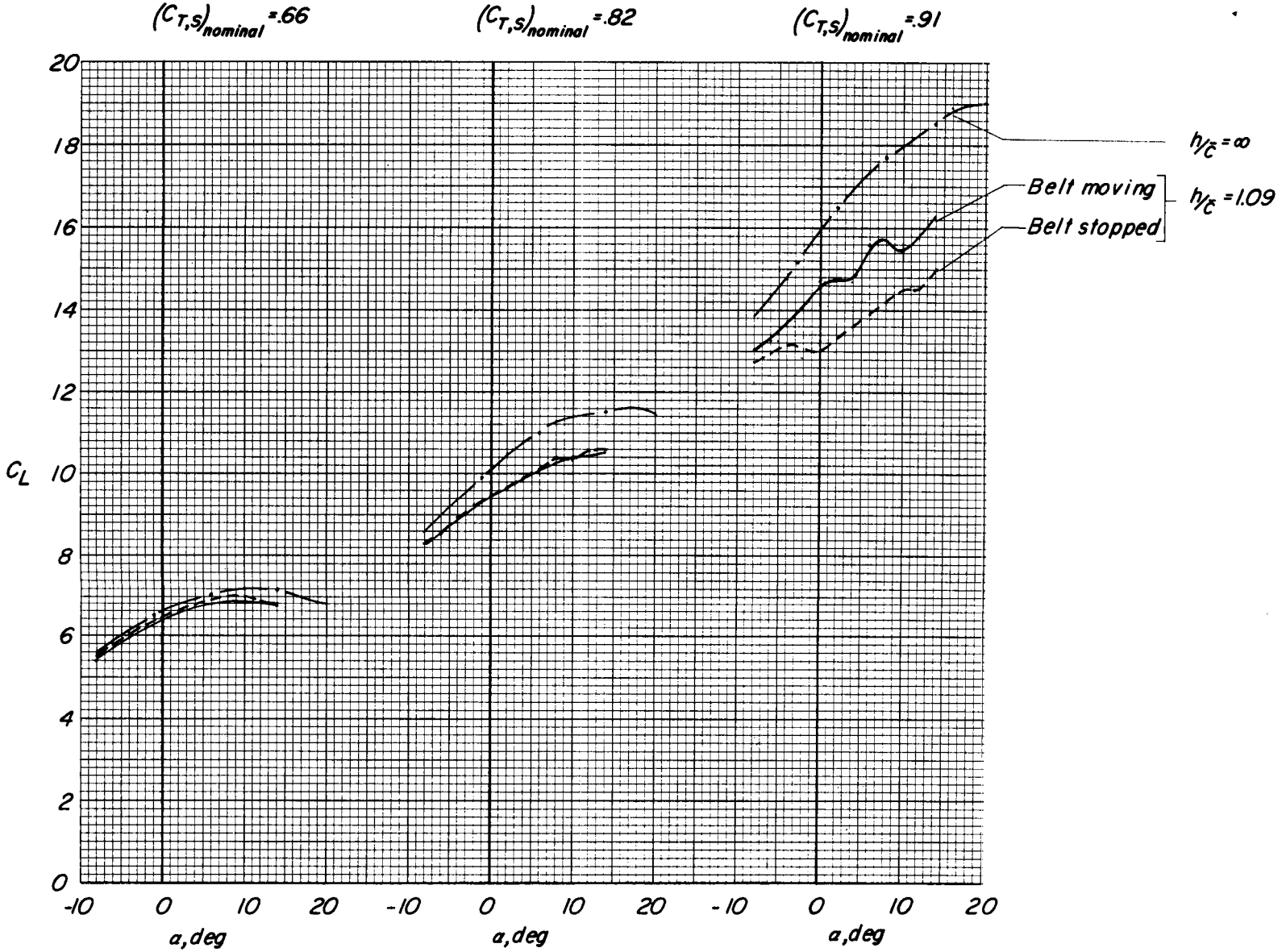

(b) $h/\bar{c}$ = 1.09.

Figure 35.- Continued.

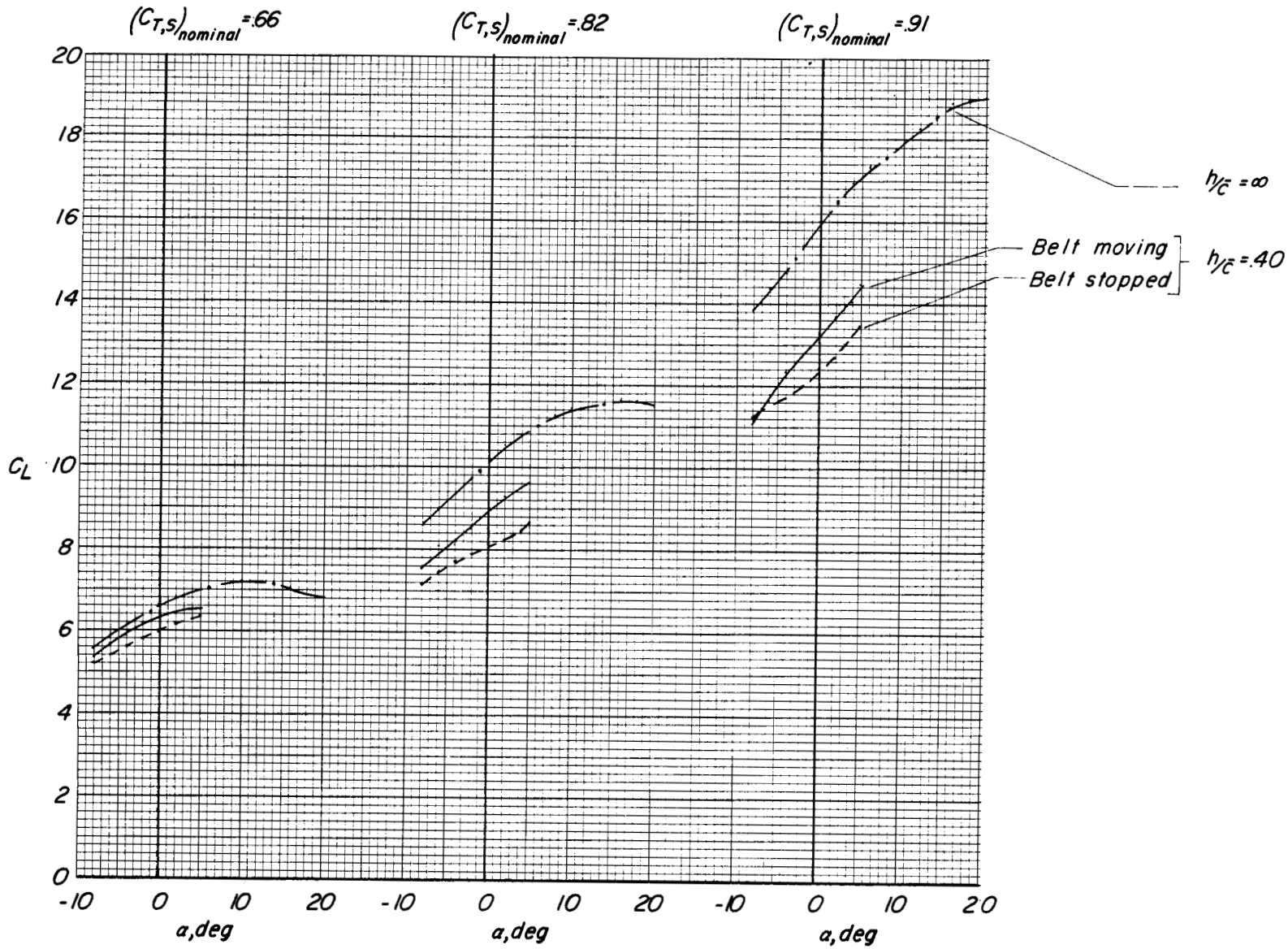

(c) $h/\bar{c}$ = 0.40.

Figure 35.- Concluded.